Rheology and Dynamics of Side-Group Liquid Crystalline Polymers in Nematic Solvents

Thesis by

Michael David Kempe

In Partial Fulfillment of the Requirements for the Degree of Doctor of Philosophy

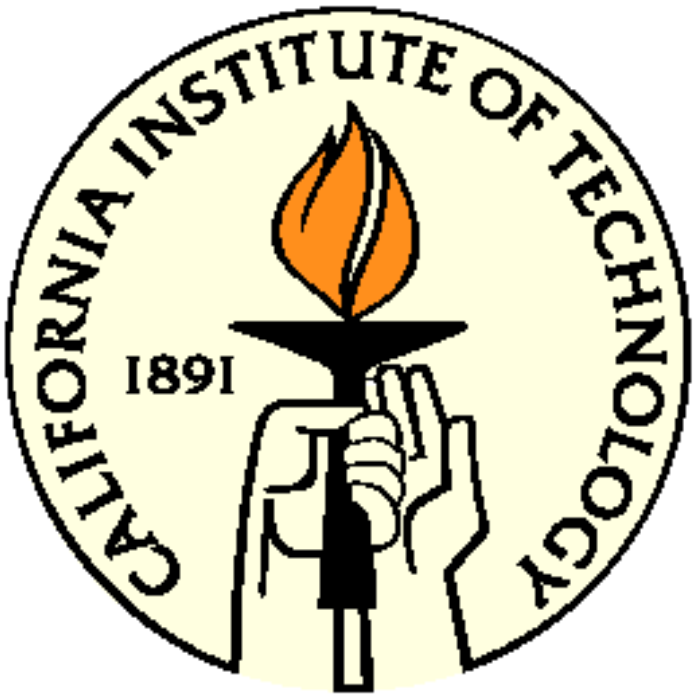

California Institute of Technology

Pasadena, California

2003

(Defended June 9, 2003)

Dedicated to

my wife, Andrea James Kempe,

for supporting me while earning my PhD.

Abstract

To form a liquid crystalline (LC) gel that retains the ability to respond rapidly to applied fields, it is necessary to work with low polymer concentrations. In turn, to form a dilute polymer network it is necessary to use very long polymers that are soluble in the small molecule LC. This research focuses on the synthesis of ultra-long side-group liquid crystalline polymers (SGLCPs), their properties when dissolved in nematic hosts, and the self-assembly of a nematic gel using an ABA triblock with an SGLCP midblock and LC-phobic end-blocks. Typically, LCs are made from small molecules that can be quickly reoriented. In applications such as artificial muscles, flexible displays, or compensating films, a more robust LC gel is desired. Prior routes to LC gels, typically using in situ polymerization, suffer from director misorientation, lack of control over cross-link density, polymer network inhomogeneity, undesired phase separation, and slow responses to applied fields. The present research (at the intersection of block copolymers, gels, and LCs) has demonstrated that an optically uniform LC gel with fast reorientational response can be achieved using a self-assembling ABA triblock copolymer.

To provide the fundamental underpinning for the design of a self-assembling gel, we first advanced the synthesis of model SGLCPs that have well-defined length even at high degrees of polymerization. The polymerization method must provide narrow length distribution, be applicable to block copolymers, and preferably enable chains of varied side-group structure to be prepared. These requirements were met by starting from an anionically produced prepolymer and attaching the mesogen in a second step (a “polymer analogous” approach). Homopolymers were made and characterized to determine how polymer structure affects solubility, rheological response, electro-optic response and

chain conformation. This showed that cyanobiphenyl (CB) side-groups provide excellent solubility in CB-based small molecule LCs even for SGLCPs an order of magnitude longer than those investigated in solution previously; that ultra-long SGLCPs have unprecedented effects on the flow behavior of LC solutions, and that the anisotropy $(R_{\perp}/R_{//}\approx 1.6)$ is insensitive to spacer length and degree of polymerization.

The size of a polymer is related to the concentration necessary to form a gel network; however, there have been few studies of SGLCP dimensions in LC solvents. Since it is the polymer backbone conformation that is of interest, researchers use polymers labeled on the backbone to avoid scattering from the side groups. Unfortunately in a dilute solution this provides unacceptably low scattered intensity. Therefore, we demonstrate a method for measuring the dimensions of an unlabeled SGLCP in a perdeuterated nematic solvent, in which scattering originates from both the backbone and the pendant side groups. Since it is the backbone conformation that is of interest, we developed a method to mathematically account for scattering due to the side groups.

Information gained from homopolymer studies guided the design of ABA block copolymers for nematic gels. We demonstrated that an optically uniform nematic gel can form in a small molecule LC even at low polymer concentrations using a triblock composed of an SGLCP center block and end-blocks that microphase separate to form physical cross-links. The key to making a dilute gel was using well-solvated, very long SGLCP midblocks. The necessity of cross-linking very dilute chain ends is prohibitive using covalent linking, but facile using end-blocks that spontaneously aggregate. In contrast to prior LC gels, these dilute gels maintain both the optical uniformity and fast reorientational responses of the small molecule LC host.

Acknowledgements

I would like to thank all those people who have supported me and helped me get where I am now. I thank Julie Kornfield for giving me the chance to be part of her research group where I have learned many things, and for giving me the freedom to let my research go where it needed to go. I am grateful to my committee members, Professors David Tirrell, Robert Grubbs, and Zhen Gang Wang, for reviewing my thesis.

It has been a privilege to work with the past and present members of the Kornfield group Maria Lujan Auad, Neal Scruggs, Rafael Verduzco, Derek Thurman, Eric Pape, Lucia Fernandez-Ballester, Wei Shen, Mike Mackel, Charles Nickerson, Erica Thompson, Giyoong Tae, Rob Lammertink, Weijun Zhou, Christine Adams, Chris Sanstedt, Jagdish Jethmalani, Bhavna Hirani, Ani Issaian, and Ravi Verma. They made this research more enjoyable by helping me through long months where nothing seemed to work.

I have been fortunate to have the opportunity to work with many great people. I would like to thank Neal Scruggs and Rafael Verduzco for deciding to continue my research when I leave Caltech. It is a great project which will surely yield interesting results over the next few years. Weijun Zhou was helpful with instrumentation and with teaching me some of the basics of liquid crystals. I enjoyed working with Maria Lujan Auad on the liquid crystalline polymer rheology project and am grateful that she was able to do some experiments that I had wanted to see done but could not find the time to get to myself. I would like to thank Guruswamy Kamaraswamy for help with general scientific questions. Rob Lammertink helped to convince me to revisit hydrosilylation techniques for making polymers. Without this help it would have been much more difficult for my

project to progress as far as it did. Jagdish Jethmalani, Christopher Ober, and Chi-yang Chao were instrumental in helping me learn chemical synthesis techniques and in helping me overcome the many synthetic problems that plagued my project. I would also like to thank the undergraduates who have worked with me, Zhendi Su and Abelardo Bourbois, for help with some synthesis and refractive index measurements.

I am grateful to the Air Force Office of Scientific Research (AFOSR) for providing the bulk of the money necessary for my research through a Liquid Crystal Multidisciplinary University Research Initiative (AFOSR LC-MURI) (f4962-97-1-0014) program. I acknowledge funding through the Corcoran fellowship for my first year of study. Most importantly, I am greatly indebted to the Achievement Rewards for College Scientists (ARCS) foundation for a very generous fellowship. Without this financial aid my life would have been monetarily extremely difficult throughout my stay at Caltech.

Through the LC-MURI program I was able to meet with many professors from other schools and would like to personally thank Professors Dave Walba, Peter Palffy-Muhoray, Chris Ober, Wesley Burghardt, Seth Marder, and especially Shin Tson Wu. Shin Tson taught me how to conduct reorientational response time measurements and was helpful in my search for a job.

The staff members here at Caltech are excellent people. Suresh Gupta was instrumental in helping me keep the computers running here in the lab and at home. Anne Horman has always been there to help me get through all the administrative work.

I would like to thank Steve Smith from Proctor and Gamble for letting me use his laboratory to make polymers. I would like to thank Edward Lang and Jyotsana Lal from Argonne National Laboratory for helping with small-angle neutron experiments. Without

the many e-mails and interest from Jyotsana I might not have put in the necessary time to do those experiments.

My undergraduate professors Lamont Tyler, Edward Trujillo, Noel DeNevers, and J. D. Seader were always good examples showing enthusiasm and concern for me as a student. A special thanks to J. D. Seader for telling me I needed to go to graduate school and for helping me through the application process. His classes were always tough but well focused on the practical aspects of chemical engineering teaching me how to work through difficult problems. Thanks to Edward Trujillo and Catherine Rappaport for giving me a chance to work in their lab and to get a good idea of what research is like.

Finally, I would also like to thank my parents for encouraging and supporting me in my education. Thanks to Maxwell and Bethany for always being happy to see me come home and for being sad to see me leave. Most importantly I would like to thank my wife, Andrea, for supporting me as I earned my PhD. Thanks for putting up with all the long hours, for allowing me to pursue my graduate degree, and for giving me a great place to come home to after a long day.

Table of Contents:

List of Figures

List of Tables

Chapter 1 Background

1.1 Introduction to Liquid Crystals

With the proliferation of modern electronic devices in recent years, more demands have been placed on the materials making up these devices. For example, a portable computer requires a light-weight, energy-efficient, and robust monitor that functions under a wide range of temperatures and lighting conditions. Despite years of research into a variety of alternatives, twisted nematic liquid crystal displays (LCDs) remain the predominant solution for many applications [1].

In a typical LCD, a polyimide layer is spin coated on top of a transistor array and physically rubbed to confer macroscopic orientational order on the liquid crystal (LC). Although this is an excellent way to orient LCs, this rubbing process often harms the substrate thin film transistors used in a display. LCD manufacturing could be improved with a gentler method to control LC alignment.

The goal of this research is to develop the fundamental understanding needed to design LC materials that will be easier to incorporate into LCDs and to improve their electro-optic characteristics. This information has been used in the design of a nematic gel made from an ABA triblock side group liquid crystalline polymer (SGLCP). In a nematic solvent, the LC-phobic styrene ends of a poly(styrene-block-SGLCP-block styrene) triblock copolymer microphase separate to form physical cross-links. At a sufficiently high concentration, these cross-links produced a mechanically stable nematic matrix.

A triblock copolymer based gel can also be aligned by shear, surface treatment, or can be left unaligned for use in a light scattering display. A nematic gel of this type can be heated so that the polystyrene blocks can disengage from the end-block aggregates to form a viscous fluid. This arrangement produces a thermoreversible nematic gel. If the electro-optic device were based on a light scattering state, the gel could be heated up to the isotropic state and quenched into the nematic state to lock in a light scattering, polydomain structure.

A device that works in a light scattering mode would use ambient light reducing power requirements and would function under a greater variety of lighting conditions [2]. Furthermore, it would not have a viewing angle dependence like typical laptop displays [3], would not require polarizers, and could eliminate the need for a rubbed polyimide layer resulting in a simplified fabrication process.

1.1.1 What Is a Liquid Crystal?

An LC is a material that has properties intermediate between a liquid and a crystal [4]. It flows when subjected to a shear stress but also has some orientational, and often some translational, order similar to a solid. Amongst LC materials there are two main classes; lyotropic LCs, which go through phase transitions in response to concentration changes, and thermotropic LCs, whose phase transitions are determined by temperature. The presence of LC order is due to a delicate balance of specific molecular interactions and/or steric effects. In lyotropic systems, the dominant effect is often a steric interaction where increases in concentration cause the LC molecules to adopt some orientational to enable them to pack more closely together [5]. In thermotropic LCs, steric effects are

typically less important and often an interaction, such as a dipole moment across a long series of conjugated bonds, causes the molecules to align. Through these types of interactions, an LC material can adopt order but still maintain the ability to flow in response to an applied shear stress. This research will focus on the properties of thermotropic LCs.

There are many ways in which positional and orientational order can be organized into different phase structures. Some of the most common LC phases are shown in Fig. 1.1. Above a critical temperature, most thermotropic LC materials lose their translational and orientational order to form an isotropic phase, Fig. 1.1a. As the temperature is reduced, a first-order transition takes place as the material adopts some orientational, and often translational, order. A nematic LC has only orientational order, Fig. 1.1b, and a smectic LC has both orientational and translational order, Fig. 1.1c,d. Depending on the relationships between the orientational and positional order, smectic phases exhibit a number of different sub-classifications. Two of the simplest cases are the smectic A and C phases. In the smectic A phase, the molecules are arranged into layers and oriented near the layer normal. In the smectic C phase, the molecules tend to orient at an angle relative to the layer normal.

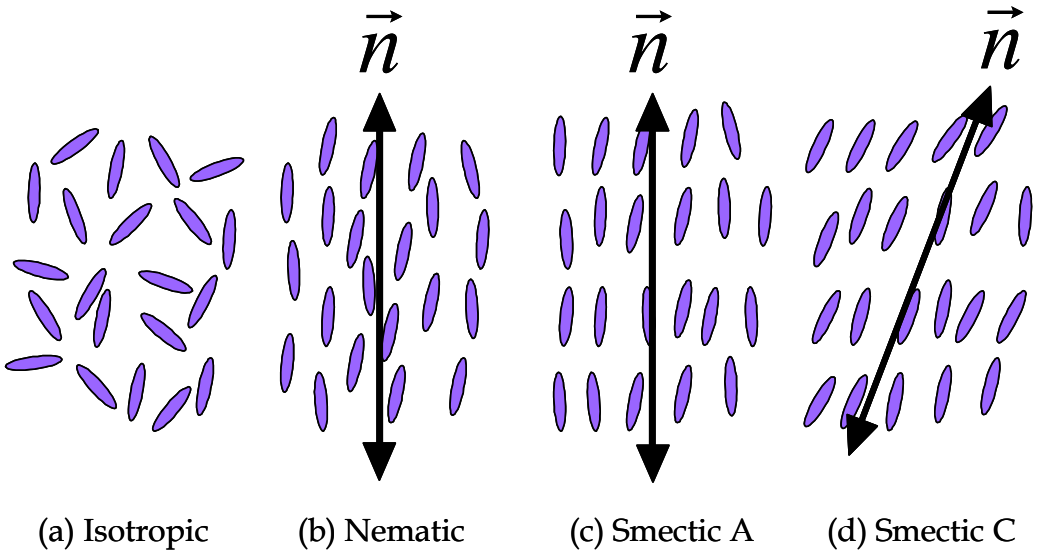

Figure 1.1. Common phases seen in liquid crystals.

In both nematic and smectic phases the molecules have significant mobility and are not aligned exactly in the same direction but on average align near a direction called the "director" $\vec{n}$, Fig. 1.1. The distribution of the molecular orientations around the director is characterized by the order parameter

$$S = \frac{1}{2}\left\langle 3\cos^2\theta_j - 1 \right\rangle, \quad (1.1)$$

where θ_j is the angle between the j^{th} molecule and the director and the brackets indicate an ensemble average. Typically values of S are 0.6 and 0.8 corresponding to an average angle of 31° or 21° for a nematic and smectic phase, respectively. In this study, we were primarily concerned with the properties of nematic LCs.

1.1.2 Anisotropic Properties

Because LCs exhibit orientational order, their properties are different when measured in different directions. In a nematic LC, the extraordinary refractive index (n_e), for light

polarized parallel to the molecular axis, is typically larger than the ordinary refractive index (n_o), for light polarized perpendicular to the molecular axis. This optical anisotropy, or birefringence, is defined as $\Delta n = n_e - n_o$. Along with the refractive index, the dielectric constant, diamagnetic susceptibility, thermal conductivity, diffusion constants, polarizability and many other properties are a function of director orientation. Similar to birefringence, dielectric and diamagnetic anisotropy are, respectively, defined as $\Delta\varepsilon = \varepsilon_{//} - \varepsilon_{\perp}$ and $\Delta\chi = \chi_{//} - \chi_{\perp}$.

In electro-optic devices, it is these anisotropies, combined with the ability of the director to reorient, that are exploited. Because of a non-zero $\Delta\varepsilon$, a liquid crystal can reorient in response to an electric field. An on/off light valve can be created for an electro-optic device by the proper control of light polarization and director orientation.

1.1.3 Viscous Response: The Leslie-Ericksen Theory

In a nematic liquid crystal the orientational order of the fluid makes the viscous response to an applied shear strain complex. The stress response is related both to the orientation of the director and to the rotational velocity of the director relative to an applied strain. F. M. Leslie [6, 7] and J. L. Ericksen [8, 9] developed a mathematical model describing the viscous response of a liquid crystal using six viscosity parameters. If one ignores the effects of distortional elasticity, the stress response, according to Ericksen's transversely isotropic fluid model (TIF), is

$$\tau_{ij} = \alpha_1 n_k n_p A_{kp} n_i n_j + \alpha_2 N_i n_j + \alpha_3 N_j n_i + \alpha_4 A_{ij} + \alpha_5 A_{ik} n_k n_j + \alpha_6 A_{jk} n_k n_i , \quad (1.2)$$

where the "n"s represent director components, A_{ij} is the symmetric part of the velocity gradient tensor [10]

$$A_{ij} = \frac{1}{2}\left(\upsilon_{ij} + \upsilon_{ji}\right), \quad (1.3)$$

N_i represents the angular velocity of the director relative to the fluid vorticity

$$N_i = \frac{dn_i}{dt} + n_j \frac{1}{2}\left(\upsilon_{ij} - \upsilon_{ji}\right), \quad (1.4)$$

and ν_{ij} is the fluid velocity. By considering the symmetry of the director, Parodi [11] found that

$$\alpha_6 - \alpha_5 = \alpha_3 + \alpha_2, \quad (1.5)$$

indicating that only five of the six parameters are independent.

According to Ericksen's TIF model, if one assumes the motion of the director is confined to the plane defined by the velocity and the velocity gradient directions, the viscous response is related to the strain rate, $\dot{\gamma}$, by [12]

$$\tau_{xy} = \dot{\gamma}\left[\left(\alpha_1 + \frac{(\alpha_2 + \alpha_3)^2}{\alpha_3 - \alpha_2}\right)\sin^2\theta\cos^2\theta + \frac{1}{2}(\alpha_3 + \alpha_4 + \alpha_6) - \frac{\alpha_3^2}{\alpha_3 - \alpha_2}\right]. \quad (1.6)$$

This shows that the transient response is a function of the angle θ relative to the velocity gradient direction and will have maxima at $\pm 45^o$ and minima at 0 or 90^o.

1.1.4 Miesowicz Viscosity Coefficients

Another method for describing the viscous response of a liquid crystal, that is experimentally simpler, was developed by Miesowicz [13]. The three coefficients η_a, η_b, and η_c describe the viscosity when the director is, respectively, held in the vorticity, velocity, and the velocity gradient directions by a magnetic or electric field, Fig. 1.2. The Miesowicz viscosities are related to the Leslie-Ericksen coefficients by [14,15]

$$\eta_a = \tfrac{1}{2}\alpha_4, \quad (1.7)$$

$$\eta_b = \tfrac{1}{2}(\alpha_3 + \alpha_4 + \alpha_6), \quad (1.8)$$

and

$$\eta_c = \tfrac{1}{2}(-\alpha_2 + \alpha_4 + \alpha_5). \quad (1.9)$$

These viscosities are sometimes used because they are often easier to measure and can give more physical insight than the Leslie-Ericksen parameters.

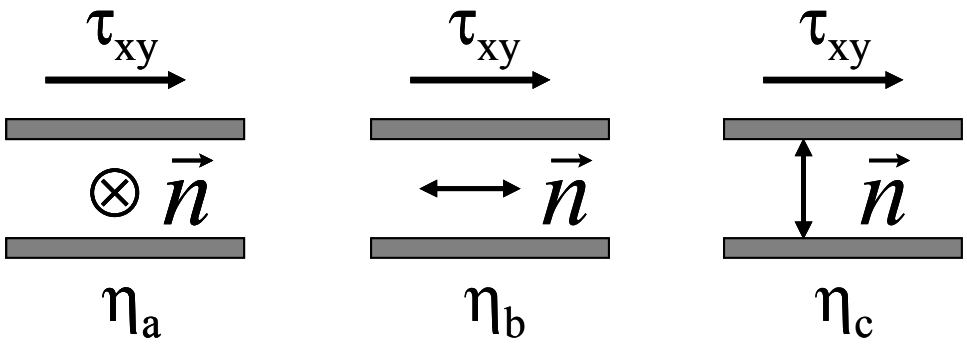

Figure 1.2. The Miesowicz viscosities are measurement with the director held stationary by either an electric or magnetic field.

1.1.5 Distortional Elasticity

Since LCs thermodynamically prefer to be macroscopically oriented, there is a free energy loss associated with deviations from a macroscopically aligned state. For a nematic LC, the possible distortions can be grouped into three types: splay, twist, and bend, Fig. 1.3. Each of these distortions can be related to a free energy loss by

$$F = \frac{1}{2}K_{11}\left[\nabla \cdot \vec{n}\right]^2 + \frac{1}{2}K_{22}\left[\vec{n} \cdot \left(\nabla \times \vec{n}\right)\right]^2 + \frac{1}{2}K_{33}\left[\vec{n} \times \left(\nabla \times \vec{n}\right)\right]^2, \quad (1.11)$$

The three constants in this equation are referred to as the Frank [16, 17, 18] elastic constants. These elastic constants are a measure of the restoring force experienced by a nematic liquid crystal when subjected to director distortions; therefore, larger constants result in faster director relaxation dynamics.

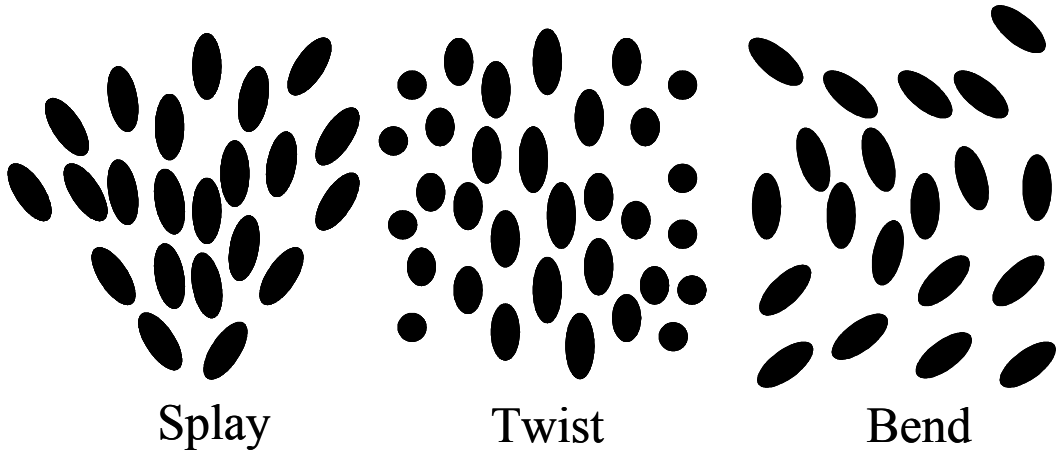

Figure 1.3. Possible distortions for a nematic LC. Each of these distortions is associated with an elastic constant K_{11} (splay), K_{22} (twist), and K_{33} (bend) in Eq. 1.11.

1.1.6 Liquid Crystal Director Reorientation

If the motions of the director are confined to the plane defined by the velocity and the velocity gradient directions, similar to Eq. 1.6, and one considers the evolution of the

director in response to an applied electric or magnetic field, or to a shear stress, one obtains [1]

$$\left(\alpha_2 \sin^2\theta - \alpha_3 \cos^2\theta\right)\frac{\partial v}{\partial y} + \varepsilon_o \Delta\varepsilon E^2 \sin\theta\cos\theta + \frac{\Delta\chi B^2}{\mu_o}\sin\theta\cos\theta$$
$$+ \frac{\partial}{\partial y}\left[\left(K_{11}\cos^2\theta + K_{33}\sin^2\theta\right)\frac{\partial\theta}{\partial y}\right] + \left(K_{33} - K_{11}\right)\sin\theta\cos\theta\left(\frac{\partial\theta}{\partial y}\right)^2 = I\frac{\partial^2\theta}{\partial y^2} + \gamma_1\frac{\partial\theta}{\partial t}, \quad (1.12).$$

where θ is defined as the angle of the director relative to the velocity gradient direction. The first term corresponds to hydrodynamic forces on the director in response to a shear stress and is obtained by a hydrodynamic torque balance on the director using Eq. 1.2. The next two terms correspond to the torque due to an external electric, *E*, and magnetic, *B*, field acting on the director. The fourth and fifth terms, derived from Eq. 1.11, are Frank elastic stresses that function to restore macroscopic alignment to the sample. On the other side of the equality, the first term describes an inertial force on the director which is almost always negligible. The last term describes viscous dissipation due to director rotation where the constant $\gamma_1=(\alpha_3-\alpha_2)$ is called the twist viscosity.

While at first Eq. 1.12 is quite complicated, when it is applied to an electro-optic system, conditions are usually obtained where there is typically one force in opposition to the twist viscosity. If small perturbations are considered (i.e., θ is small) the equations can often be simplified even further.

1.1.7 Tumbling Parameter

If one assumes that director elasticity is unimportant, that the director is confined to the plane defined by the velocity and velocity gradient directions, and that there are no external fields, a torque balance on the director using the Leslie-Ericksen theory [12], Eq.

1.12 or 1.2, can be used to obtain a relationship between the rate of change of the director and the shear strain (γ)

$$(\alpha_3 - \alpha_2)\frac{\partial \theta}{\partial t} = \left(\alpha_3 \sin^2 \theta - \alpha_2 \cos^2 \theta\right)\frac{\partial \gamma}{\partial t}. \qquad (1.13)$$

Here it can be seen that the hydrodynamic torque depends on the coefficients α_2 and α_3. If the director is oriented along the velocity gradient direction ($\cos\theta=1$, $\sin\theta=0$), the hydrodynamic torque tends to make the director rotate with the vorticity for $\alpha_2<0$ and against the vorticity if $\alpha_2>0$, Fig. 1.4. Similarly, α_3 dictates the sense and magnitude of the rotation of the director when it is oriented along the flow direction, ($\cos\theta=0$, $\sin\theta=1$). If $\alpha_3>0$ the director will rotate with the vorticity and if $\alpha_3<0$, it will rotate counter to the vorticity.

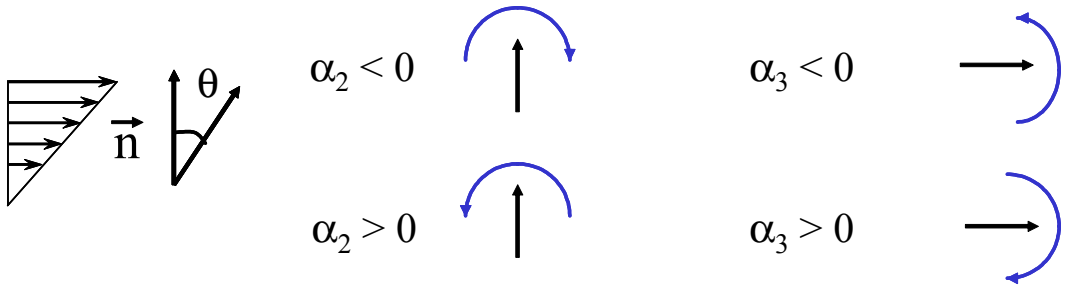

Figure 1.4. In the 2-D Leslie-Ericksen transversely isotropic fluid model, the rotation of the director in response to a shear stress is governed by the viscous coefficients α_2 and α_3.

For a typical LC material, like 4'-pentyl-4-cyanobiphenyl (5CB), both α_2 and α_3 are negative [19]. This means that the director will rotate with the vorticity when $\theta=0$ and counter to the vorticity when $\theta=\pi/2$; therefore under shear, the director will find a steady-state angle that is typically near the velocity direction. For many LCs [20, 21, 22, 23, 24], such as 4'-octyl-4-cyanobiphenyl (8CB) in the nematic phase near a smectic transition temperature, $\alpha_2<0$ and $\alpha_3>0$ causing the director to rotate with the vorticity for

all θ. Since the director will continuously rotate around 360^o this behavior is called flow tumbling. For discotic LCs [25, 26, 27, 28] or concentrated solutions of oblate polymers in a nematic solution [29] (see Chapter 4) both α_2 and α_3 are positive and the director will find a steady-state angle near θ=0. The last case for α_2>0 and α_3<0 is by definition not possible since it would result in $\gamma_1=(\alpha_3-\alpha_2)<0$. If this were the case then, according to Eq. 1.12, rotation of the director would not dissipate energy.

To characterize the response of the director to an applied shear strain a tumbling parameter, λ, is defined as,

$$\lambda = \frac{\alpha_2 + \alpha_3}{\alpha_2 - \alpha_3} = \frac{\gamma_2}{-\gamma_1}. \quad (1.14)$$

If $|\lambda|$<1 then the nematic is flow tumbling and if $|\lambda|$>1 then it is flow-aligning with a steady-state angle of,

$$\theta_{ss} = \frac{1}{2}\cos^{-1}\left(\frac{-1}{\lambda}\right) = \tan^{-1}\left(\sqrt{\frac{1+\lambda}{\lambda-1}}\right). \quad (1.15)$$

For λ>1 the steady-state angle will be near the flow direction (45^o<θ_{ss}<90^o) and for λ<-1 the steady-state angle will be near the velocity gradient direction (-45^o<θ_{ss}<0^o). When the tumbling parameter is applied to Ericksen's TIF model it is the only viscous parameter necessary to describe the rotation rate of the director using

$$\frac{\mathbf{D}\vec{n}}{\mathbf{D}t} = \vec{n}\cdot\underline{\underline{\omega}} + \lambda\left(\vec{n}\cdot\underline{\underline{d}} - \vec{n}\vec{n}\vec{n}:\underline{\underline{d}}\right), \quad (1.16)$$

where $\underline{\underline{\omega}}$ is the vorticity tensor, $\underline{\underline{d}}$ is the symmetric part of the velocity gradient tensor, and $D\vec{n}/Dt = \partial n/\partial t + v\cdot\nabla n$ is the material derivative.

Starting with θ=0^o, integration of Eq. 1.13 and substitution of Eq. 1.14 yields

$$\tan(\theta) = \pm\left(\frac{1+\lambda}{\lambda-1}\right)^{1/2} \tanh\left(\frac{\gamma}{2}\sqrt{\lambda^2-1}\right) \quad (1.17)$$

for a flow-aligning LC ($|\lambda|>1$) and

$$\tan(\theta) = \left(\frac{1+\lambda}{1-\lambda}\right)^{1/2} \tan\left(\frac{\gamma}{2}\sqrt{1-\lambda^2}\right) \quad (1.18)$$

for a tumbling LC ($|\lambda|<1$). This demonstrates how λ determines the rotational response of the director to an applied shear strain.

1.2 Small Molecule and Polymeric Nematic Liquid Crystals

Polymeric materials can be made into LC materials having the same phase structures as small molecule LCs. In these materials a mesophase forming structure, called a mesogen, can be attached to a polymer either in the backbone to form a main chain LC polymer, Fig. 1.5a, or as a side group, Fig. 1.5b,c. In main chain liquid crystalline polymers (LCPs) such as Kevlar [30], the attractive forces between molecules are so strong that they only form lyotropic LC phases and decompose before they get hot enough to form an LC phase in bulk. If the mesogenic units are connected by a highly flexible spacer [31], liquid crystalline phases can be found in bulk. In SGLCPs the mesogen is attached at either the side, Fig. 1.5b, or the end, Fig. 1.5c, of the molecule by means of a flexible spacer. This acts to decouple the motions of the mesogen from the backbone giving greater entropy to the system and lowering the glass transition temperature (T_g) making the mesomorphic phases more thermally accessible. Another advantage of increased mobility is that the entropy of solvation is greater, typically

making them more soluble in small molecule LCs than analogous main chain LCPs. This is the reason why this research has focused on SGLCPs.

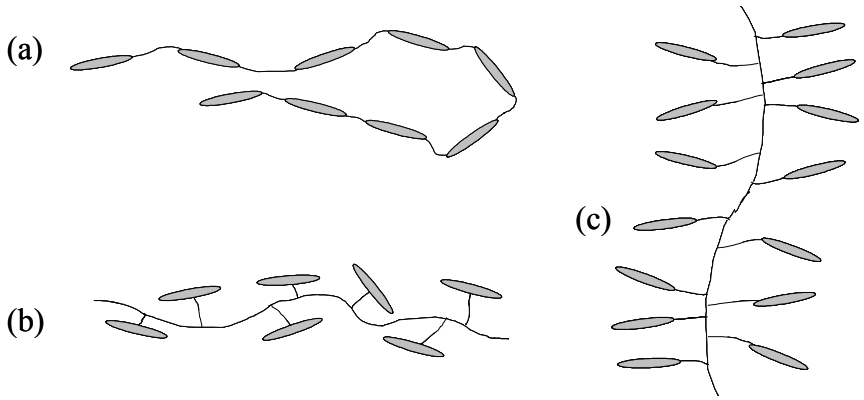

Figure 1.5. Schematic structures of typical liquid crystalline polymers. The ellipses represent rod-like mesogenic groups and the lines represent more flexible spacer or backbone segments.

1.2.1 Solution Anisotropy of Liquid Crystalline Polymers

When a polymer is dissolved in a nematic solvent, the flexibility of the chain segments is affected by the nematic order. For a main chain polymer, the mesogens are in the backbone forcing the polymer to become preferentially oriented along the director, Fig. 1.6a. Since a nematic fluid is symmetric with respect to rotations around the director, a polymer aligned along the director must also possess this symmetry; therefore a main-chain LCP will adopt a prolate ellipsoidal, or egg-shaped, conformation [32]. Similarly, most side-on, and some end-on SGLCPs, have mesogens that are parallel to the backbone and will also adopt a prolate conformation [33], Fig. 1.6b. Lastly, end-on SGLCPs often have mesogens that are perpendicular to the backbone. This causes the polymer to have a larger radius of gyration in the direction perpendicular to the director. This results in an oblate, or disc-like, spheroid conformation in the nematic state. The same arguments used here for solutions can also be applied to the melt.

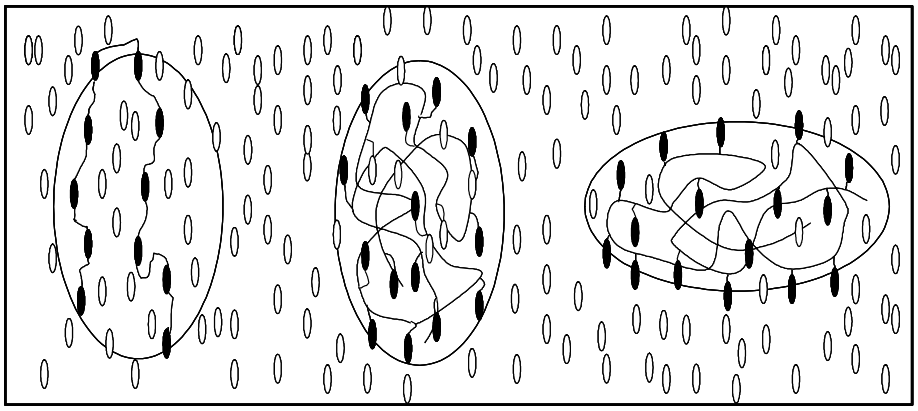

Figure 1.6. Schematic drawing of the conformations of liquid crystalline polymers in nematic solvents. (a) Prolate main chain LC. (b) Prolate SGLCP where the mesogenic groups are parallel to the backbone. (c) Oblate SGLCP where the mesogenic groups are perpendicular to the backbone.

1.2.2 Brochard Theory Consequences of Chain Anisotropy

The theory proposed by Brochard [34] concerns the effect of the addition of small amounts of an anisotropic polymer on the viscous response of a small molecule nematic LC. This theory uses an anisotropic bead-spring model [10, 35] for the polymer in which the radius of gyration of the polymer in the parallel direction is different from the perpendicular direction, $R_{//} \neq R_{\perp}$. This consideration, along with several other assumptions concerning relaxation processes and viscous dissipation, were evaluated in terms of the bead-spring model and applied to the Leslie-Ericksen theory to predict changes in the viscosity coefficients upon addition of polymer

$$\delta\gamma_1 = \frac{\left(R_{\perp}^{\,2} - R_{||}^{\,2}\right)^2}{R_{\perp}^{\,2} R_{||}^{\,2}} \left(\frac{ckT}{N}\right) \tau_R , \quad (1.19)$$

$$\delta\gamma_2 = \frac{R_{\perp}^{\,4} - R_{||}^{\,4}}{R_{\perp}^{\,2} R_{||}^{\,2}} \left(\frac{ckT}{N}\right) \tau_R . \quad (1.20)$$

Here, k is Boltzmann's constant, T is the absolute temperature, c is the monomer concentration, N is the degree of polymerization, and τ_R represents a characteristic polymer relaxation time. By inspection of Eq. 1.19 it can be seen that changes to γ_1 are always positive for the addition of polymer, but changes to γ_2 are positive for oblate, $R_{//}<R_{\perp}$, and negative for prolate, $R_{//}>R_{\perp}$, polymers. The parameters γ_1 and γ_2 are related to the tumbling parameter by

$$\lambda = -\frac{\gamma_2}{\gamma_1}; \quad (1.21)$$

therefore, a prolate polymer will increase the tumbling parameter and an oblate polymer will reduce the tumbling parameter [29, 36]. If enough oblate polymer is added to a nematic with $\lambda>1$, it will induce tumbling. As more polymer is added, λ will be reduced to less than -1 and the solution will become flow-aligning again.

The Brochard theory also predicts that the ratio of changes in the Miesowicz viscosities can be used to estimate the anisotropy of the polymer

$$\frac{R_{\perp}}{R_{||}} = \left(\frac{\delta\eta_b}{\delta\eta_c}\right)^{1/4}. \quad (1.22)$$

An alternative way to estimate chain anisotropy that is not explicitly stated by Brochard can be obtained by taking the ratio of Eqs. 1.19 and 1.20. After some algebraic manipulation and substitution of Eq. 1.21, one obtains

$$\frac{R_{\perp}}{R_{||}} = \left[\frac{\delta\gamma_1 + \delta\gamma_2}{\delta\gamma_2 - \delta\gamma_1}\right]^{\frac{1}{2}} = \left[\frac{(1-\lambda)\gamma_1 - (1-\lambda_o)\gamma_{1o}}{(1+\lambda_o)\gamma_{1o} - (1+\lambda)\gamma_1}\right]^{\frac{1}{2}}. \quad (1.23)$$

where the subscript "o" refers to values for bulk 5CB. Although there have been many studies that estimate polymer anisotropy based on changes in the Miesowicz viscosity [37], very little research has been done to measure the anisotropy of polymers in solution [38, 39, 40, 41]. The anisotropy of our polymers was measured using small-angle neutron scattering (SANS) along with detailed rheological studies. Therefore this is an ideal system for evaluating Eqs. 1.22 and 1.23.

1.2.3 The Importance of High Molecular Weight

Many researchers have studied the effects of polymers dissolved in LC materials. A typical example of this can be found in the work of Coles et al. [42, 43, 44, 45, 46]. They found that the viscosities γ_1, η_a, and η_b increased rapidly upon addition of polymer. All three viscosities seemed to vary exponentially, γ_1 by an order of magnitude, and η_a, and η_b by about two orders of magnitude, after the addition of about 20 wt % polymer. These findings demonstrate the main concern associated with the use of polymers in nematic solvents. In order to get fast reorientational responses, these viscosities need to be small. With such a large change in viscosity only a small amount, ~2 wt %, of polymer could more than double the reorientational response time of a display, making such a system useless.

Most experiments on nematic solutions have been done using homopolymers with molar masses around 20,000 to 50,000 g/mol [47]. Simply examining high molecular weight SGLCPs represents a new area of research and the use of triblock copolymers with long SGLCP blocks currently remains unexplored. Thus, this research into high

molecular weight block SGLCPs has produced results that were previously unattainable and has demonstrated new phenomena with the potential to improve electro-optic devices.

1.3 Synthesis and Characterization of Side Group Liquid Crystalline Polymers

1.3.1 Polymerization Techniques

The orientational order of an LC material reduces the entropy of dissolution making the dissolution of polymers in small molecule nematic LCs more difficult [48] as compared to an isotropic solvent. Finkelmann [49] suggested that the best way to get good solubility is to use polymers having a structure similar to the nematic solvent. Matching the mesogen of an SGLCP to a nematic solvent is relatively easy using radical polymerization or condensation polymerization techniques. The disadvantages of these techniques are that they produce polydisperse polymers, especially at high molecular weights, and cannot be used to make a homologous series of polymers with matched backbone lengths. These techniques also cannot be easily used to make well-defined block copolymers.

The preferred method for obtaining an SGLCP with a narrow molecular weight distribution is to use anionic polymerization. This technique provides a low polydispersity and can be used to create block copolymers. The main problem with this technique is that the types of monomers that can be used are limited. To avoid this problem, the polymer analogous approach is taken where the mesogen is attached to a previously synthesized polymer backbone having the desired polydispersity and degree of

polymerization, Fig. 1.7. This method allows one to use mesogens that would normally interfere with anionic polymerization.

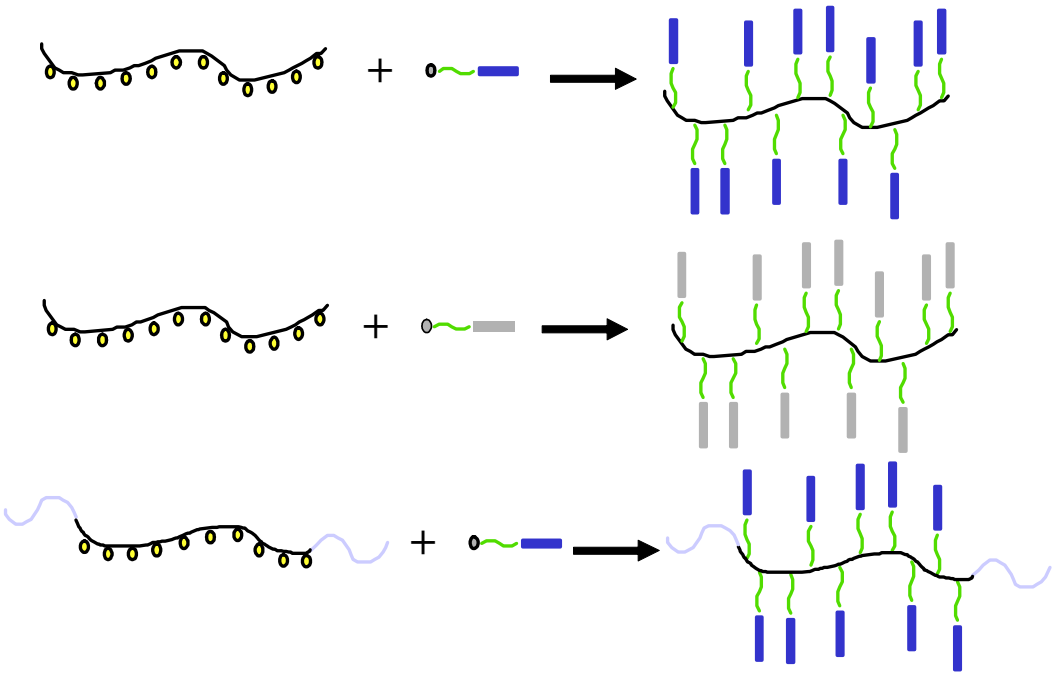

Figure 1.7. The polymer analogous approach. This method involves first making a functionalized polymer backbone and, in a second step, attaching the desired mesogen. This has the advantage of being able to attach a wide variety of mesogens and the ability to make well-defined block copolymers.

To pursue the polymer analogous approach to create the desired SGLCPs, a suitable functionalized polymer backbone had to be found. 1,2-Polybutadiene can be made with a functional pendant vinyl group on every other backbone carbon atom. Although there are many ways to attach a side group to a vinyl group, a method must be chosen which proceeds very close to completion and has few side reactions.

Two different methods for attaching the mesogen were used in this research. In the first method, the pendant vinyl groups were hydrolyzed to an alcohol using hydroboration with 9-borabicyclo[3.3.1]nonane (9-BBN) followed by oxidation under basic conditions (Appendix A2). Then, a mesogen with an acid chloride group was attached to the

pendant alcohol. Since this method contained three steps that involved the polymer, it was difficult to prevent cross-linking reactions from occurring. In the second method, a siloxane functionalized mesogen was attached directly to the pendant vinyl groups of 1,2-polybutadiene (Appendix A3). This attachment method did not go as far to completion as the acid chloride method, but since only one step involved the mesogen it was a more reliable method and, consequently, was used to create ABA triblock SGLCPs.

1.3.2 Objectives

Research into SGLCPs has been going on for years and there is a very large body of information on the subject. When one considers high molecular weight SGLCPs, the amount of research is much smaller. Furthermore, since creating high molecular SGLCPs with a small polydispersity index (PDI) requires either a living polymerization technique or a separation technique, such as fractionation, very little research has been done in this area. Consequently, there are still large gaps in the physical understanding of the interactions between polymers and LCs.

Furthermore, the primary goal of this research was to produce a new type of nematic gel using ABA triblock SGLCPs. By using a pre-formed self-assembling polymer network instead of a randomly cross-linked photo or thermally initiated system, excellent control over the physical characteristics of the gel can be maintained. These gels are intended for use in an electro-optic device requiring fast reorientations of the nematic director. Thus, we desire to use as little polymer as possible so that the reorientational response does not become too slow, as in a polymer melt [50]. The amount of polymer necessary to create a gel is dependent on the length of the center block. This distance can

be increased by choosing a mesogenic group that makes the backbone less flexible, or by simply making very high molecular weight polymers.

There were several obstacles that needed to be overcome to achieve the goal of an ABA SGLCP nematic gel. Firstly, we had to develop synthetic techniques that could be used to create telechelic block copolymers with a wide variety of mesogenic groups. This was accomplished by using a polymer analogous approach. Secondly, we had to extend these methods to very high molecular weight polymers so that a dilute gel could be formed. Thirdly, the polymers were characterized in a homopolymer form to see how the mesogen structure affected the polymer conformation, physical size, compatibility with nematic solvents, and electro-optic properties. Fourthly, since the director reorientation rate of an electro-optic device is usually slowed down by the addition of polymer, it was necessary to determine how a very high molecular weight polymer affected the viscosity of a nematic. This included studies of the effect of a polymer on director reorientation under an applied shear strain. Lastly, once a functional gel was obtained its properties were studied and compared with the results from the homopolymers to determine structure-property relationships.

Bibliography

[1] I. C. Khoo and S. T. Wu, *Optics and Nonlinear Optics of Liquid Crystals*, World Scientific, New Jersey (1993).
[2] H. E. A. Huitema, G. H. Gelinck, J. B. P. H. van der Putten, K. E. Kuijk, C. M. Hart, E. Cantatore, P. T. Herwig, A. J. J. M. van Breemen, and D. M. de Leeuw, *Nature* **414**, 599 (2001).
[3] H. Mori, Y Itoh, Y Nishiura, T. Nakamura, and Y. Shinagawa, *Jpn. J. Appl. Phys*. **36,** 143 (1997).
[4] P. G. de Gennes, *The Physics of Liquid Crystals*, Oxford University Press, New York (1974).
[5] M. Doi, *J. Polym. Sci*. **19**, 229 (1981).
[6] F. M. Leslie, *Arch. Ration. Mechan. Anal*. **28**, 265 (1968).
[7] F. M. Leslie, *Quart. J. Mech Appl. Math* **19**, 357 (1966).
[8] J. L. Ericksen, *Trans. Soc. Rheo*l. **5**, 23 (1961).

[9] J. L. Ericksen, *Arch, Rational Mech. Anal*. **4**, 231 (1960).
[10] J. D. Ferry, *Viscoelastic Properties of Polymers*, John Wiley and Sons, New York (1970).
[11] O. Parodi, *J. Phys.* **31**, 581, (1970).
[12] R. G. Larson, *The Structure and Rheology of Complex Fluids*, Oxford University Press, New York (1999).
[13] M. Miesowicz, Nature, **24**, 158 (1946).
[14] S. I. Kumar, *Liquid Crystals, Experimental Study of Physical Properties and Phase Transitions*, Cambridge University Press, New York (2001).
[15] A. Eich, B. A. Wolf, L. Bennett, and S. Hess, *J. Chem. Phys*. **113**, 3829 (2000).
[16] C. W. Oseen, *Trans. Faraday Soc*. **29**, 883 (1933).
[17] H. Zocher, *Trans. Faraday Soc*. **29**, 945 (1933).
[18] F. C. Frank, *Discuss. Faraday Soc*. **25**, 19 (1958).
[19] D. J. Ternet, R. G. Larson, L. G. Leal, *Rheol. Acta* **38**, 183 (1999).
[20] C. Gahwiller, *Phys. Rev. Lett*. **28**, 1554 (1972).
[21] K. Skarp, T. Carlsson, S. T. Langerwall, and B. Stebler, *Mol. Cryst. Liq. Cryst.* **66**, 199 (1981).
[22] P. E. Cladis and S. Torza, *Phys. Rev. Lett*. **35**, 1283 (1975).
[23] P. Pieranski and E. Guyon, Phys. Rev. Lett. **32**, 924 (1974).
[24] H. Siebert, P. Becker, I Quijada-Garrido, D. A. Grabowski, and C. Schmidt, *Solid State Nucl. Magn. Reson.* **22**, 311 (2002).
[25] J. T. Mang, S. Kumar, and B. Hammouda, *Mol. Cryst. Liq. Cryst*. **303**, 244 (1997).
[26] A. B. D. Brown and A. R. Rennie, *Chem. Eng. Sci.* **56**, 2999, (2001).
[27] G. E. Volovik, *JETP Lett*. **31**, 273 (1980).
[28] T. Carlsson, *Mol. Cryst. Liq. Cryst*. **89**, 57 (1982).
[29] M. D. Kempe and J. A. Kornfield, *Phys. Rev. Lett*. **90**, 115501 (2003).
[30] B. Jingsheng, Y. Anji, Z. Shengqing, Z. Shufan, H. Chang, *J. Appl. Polym. Sci*. **26**, 1211 (1981).
[31] W. Zhou, J. A. Kornfield, and W. R. Burghardt, *Macromolecules* **34**, 3654 (2001).
[32] J. P. Cotton, F. Hardouin, *Prog. Polym. Sci.* **22**, 795 (1997).
[33] S. Lecommandoux, M. F. Achard, F. Hardouin, A. Brulet, and J. P. Cotton, *Liquid Crystals* **22**, 549 (1997).
[34] F. Brochard, *J. Polym. Sci., Polym. Phys*. **17,** 1867 (1979).
[35] R. B. Bird, R. C. Armstrong, and O. Hassager, *Dynamics of Polymeric Liquids*, Wiley, New York (1977).
[36] D. F. Gu, A. M. Jamieson, and S. Q. Wang, *J. Rheol*. **37,** 985 (1993).
[37] Y. C. Chiang, A. M. Jamieson, Y. Zhao, A. M. Kasko, and C. Pugh, *Polymer* **42**, 4887 (2002).
[38] H. Mattoussi and R. Ober, *Macromolecules* **23**, 1809 (1990).
[39] H. Mattoussi, R. Ober, M. Veyssie, and H. Finkelmann, *Europhys. Lett*. **2**, 233 (1986).
[40] A. S. Cherodian, N. J. Hughes, R. M. Richardson, M. S. K. Lee, and G. W. Gray, *Liq. Cryst*. **14**, 1667 (1993).
[41] J. F. D'Allest, P. Maissa, A. T. Bosch, P. Sixou, A. Blumstein, R. Blumstein, J. Teixeira, and L. Noirez, *Phys. Rev. Lett.* **61**, 2562, (1988).
[42] M. S. Sefton, A. R. Bowdler, and H. J. Coles, H., *J. Mol. Cryst. Liq. Cryst.* **129**, 1 (1985).
[43] H. J. Coles and M. S. Bancroft, *Mol. Cryst. Liq. Cryst.* **237**, 97 (1993).
[44] H. J. Coles and A. I. Hopwood, *Mol. Cryst. Liq. Cryst. Lett.* **1,** 165 (1985).
[45] H. J. Coles and M. S. Sefton, *Mol. Cryst. Liq. Cryst. Lett.* **1**, 159 (1985).
[46] A. I. Hopwood and H. J. Coles, *Mol. Cryst. Liq. Cryst.* **130**, 281 (1985).
[47] A. M. Jamieson, D. F. Gu, F. L. Chen, and S. Smith, *Prog. Polym. Sci*. **21**, 981 (1996).
[48] P. Martinoty, A. Dubault, C. Casagrande, and M. Veyssie, *J. Physique. Lett.* **44** , 935 (1983).
[49] H. Finkelmann, H. J. Kock, and G. Rehage, *Mol. Cryst. Liq. Cryst*. **94**, 343 (1983).
[50] H. Ringsdorf and A. Schneller, *Makromol. Chem., Rapid Commun*. **3**, 557 (1982).

Chapter 2 Synthesis and Phase Behavior of Liquid Crystalline polymers

2.1 Introduction

Polymers are often used in electro-optic liquid crystalline materials, such as polymer-dispersed liquid crystals [1, 2], polymer-stabilized liquid crystals [3, 4], compensating films [5], and electro-mechanical actuators [6, 7]. The use of polymers in these systems depends upon such factors as their solubility, birefringence (Δn), electro-optic response, and rheological properties. Experiments performed by Gu et al. [8] found that the effect of side group liquid crystalline polymers (SGLCPs) on the twist viscosity of a liquid crystal solution was dependent on the spacer length between the backbone and the pendant mesogenic groups. The rheological response of an SGLCP in the melt or in a nematic solution also depends upon its conformation. If a polymer has a smectic phase, it is likely to have an oblate conformation in all its mesomorphic phases; however, Mattoussi and Ober [9] have shown that this does not necessarily apply to a mesomorphic solution, they found a prolate conformation in a nematic solvent for an SGLCP that had an oblate conformation in the melt [10]. The present precisely defined series of polymers is well suited for characterizing the effects of a dissolved polymer on an LC host and for studying the relationships between chemical structure, phase transition temperatures, and polymer conformation. The characterization of this polymer series will be essential for studies [11, 12] that test the predictions of the Brochard theory [13].

The theory proposed by Brochard [13] predicts how the addition of a polymer to a nematic liquid crystal will affect its orientational and rheological response to an applied shear stress. In these theories the anisotropy of a liquid crystalline polymer in a nematic solvent determines its effect [14, 15] on the Leslie-Ericksen [16, 17] viscosity coefficients. In Kempe et al. [11] (Chapter 4) we demonstrated that the addition of ~7.5 wt %, of the high molecular weight polymers used in this study, could change the viscosity coefficients sufficiently to cause a solution with calamitic, or rod-like, mesogenic units to align near the velocity gradient direction rather than near the velocity direction.

In this study a model series of large SGLCPs was synthesized. The backbone of the polymer was synthesized using living anionic polymerization, for low polydispersity [18, 19, 20, 21], and the mesogen was attached in a second step [22, 23, 24, 25]. This approach allowed the synthesis of high molecular weight, low polydispersity polymers with identical degrees of polymerization but different mesogens. Similarly, a single mesogen was attached to polymers with a length from DP=200 to 1150.

Prior to this study the longest 1,2-polybutadiene that had been reportedly converted to PBOH had DP≈900 [26]. Making high molecular weight polymers was difficult since the kinetics of the reaction were greatly reduced, the polymers were less soluble at all stages of the reaction, and most importantly, cross-linking reactions were not eliminated they were only minimized.

Pronounced odd-even effects associated with alternation between parallel and perpendicular mean orientations of the mesogens relative to the polymer backbone with increasing spacer length have been observed for certain backbone structures (especially

acrylates) [27, 28, 29]. In the present system, the melt and solution thermodynamics only exhibit weak odd-even effects as the spacer length was increased.

Along with melt studies, solution studies included the determination of solubility in nematic solvents and determination of the refractive indices (n_e and n_o) of the solutions. Since these polymers have cyanobiphenyl mesogens, excellent solubility was found in the nematic solvents 4-pentyl-4'-cyanobiphenyl (5CB), 4-pentoxy-4'-cyanobiphenyl (5OCB), and in the eutectic mixtures E7 and E44 [30]. In the 5CB solutions, the small changes in the refractive indices upon addition of polymer indicated that the order parameter of these solvents was not significantly affected.

Solubility of a polymer in a nematic solvent at high molecular weights was a significant achievement. The additional order of a nematic fluid reduces the entropy of solvation and often results in only slight solubility of low molecular weight polymers. In this system the similarity of structure resulted in the solubility of polymers an order of magnitude larger than those typically used by other researchers.

2.2 Polymer Characterization

The synthetic details for PBCBx, Fig. 2.1, series of polymers will be published in *Macromolecules* [31] and are given in appendices A1.2.1, A1.2.3 and A1.2.4.

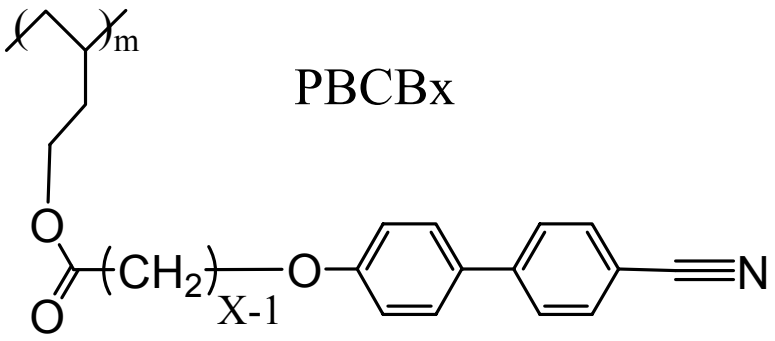

Figure 2.1. PBCBx denotes a 1,2-polybutadiene backbone, with a cyanobiphenyl mesogen. The "X" in the polymer name indicates the size of the spacer where X+4 is the number of atoms between the mesogen and the polymer backbone. In these experiments X=4 to 8.

The present development of a synthetic approach and examination of phase behavior (in the melt and in nematic solutions), provides a foundation for coordinated studies of chain conformation (showing the present polymers are oblate with $R_{\perp}/R_{//}$=1.6) [32] and rheology (showing that access to high polymers with DP>100 reveals unprecedented effects of dissolved SGLCPs on the flow behavior of LC solutions) [11, 12].

2.2.1 Multi-Angle Laser Light Scattering

Gel permeation chromatography (GPC) was carried out on two PLgel 5 mm mixed-C columns (Polymer Labs) connected in series with a DAWN EOS multi-angle laser light scattering (MALLS) detector and an Optilab DSP differential refractometer (both from Wyatt Technology). No calibration standards were used and *dn/dc* values were obtained for each injection assuming 100% mass elution from the columns. The molecular weight distribution of the final SGLCP verified that a final PDI≤1.16 could be achieved starting with prepolymer having PDI≤1.04, Table 2.1.

Polymer Sample	Predicted M_n (g/mol)[a]	Measured M_n (g/mol)	PDI	Butadiene Pre-Polymer M_n (g/mol)	Pre-Polymer PDI
PBCB4	388,000	540,000	1.16	63,000	1.04
PBCB6	78,000	92,000	1.14	11,500	1.03
PBCB6	364,000	427,000	1.13	54,000	1.04
PBCB6	420,000	504,000	1.09	63,000	1.04
PBCB7	437,000	525,000	1.09	63,000	1.04

Table 2.1. MALLS results. [a] The predicted molar masses were based on 100% attachment of the mesogen to the 1,2-polybutadiene pre-polymer backbone. Since multiple samples of each polymer were made and the physical properties measured were the same, the predicted molar masses were used throughout the text.

The predicted molar mass was based on 100% conversion of vinyl group to alcohol and 100% attachment of mesogenic groups with no cross-linking of the polymers. When compared with the actual molar mass determined by MALLS, the measured was always higher than the predicted molar mass. The higher this discrepancy the higher the PDI. If the primary cause of the increase in PDI was intermolecular cross-linking then the values of the measured molar masses were consistent with the measured PDIs of the samples.

2.2.2 Melt Properties

A series of polymers PBCBx (x=4,5,6,7,8) were made using a 1,2-polybutadiene prepolymer with a molar mass of M_n=63,000 g/mol. The transition temperatures and phases of these SGLCPs were determined using a Zeiss polarized optical microscope

(POM) with a Mettler FP82 hot stage and a differential scanning calorimeter (DSC) (Perkin Elmer DSC7). For the PBCBx polymers a characteristic nematic marbled texture was seen under POM. This present observation of a nematic phase is in accord with the phase behavior of PBCB5 reported by Sanger and Gronski [26].

In the PBCBx series, the nematic phase exists between a glass transition (T_g) and an isotropization transition (T_{ni}), Fig. 2.2. As the spacer length was increased (PBCB4 to PBCB8) the range of this nematic phase broadened as T_g decreased and T_{ni} increased. Longer spacers increase the mobility of the side chains, increasing their entropy and therefore causing T_g to decrease with increasing spacer length. Similarly to T_{ni}, the enthalpy of the nematic-isotropic transition (ΔH_{ni}) increased with spacer length. In contrast to ΔH_{ni}, the change in heat capacity at the glass transition temperature was insensitive to spacer length (ΔCp=0.30±0.02 J/g·^{o}C).

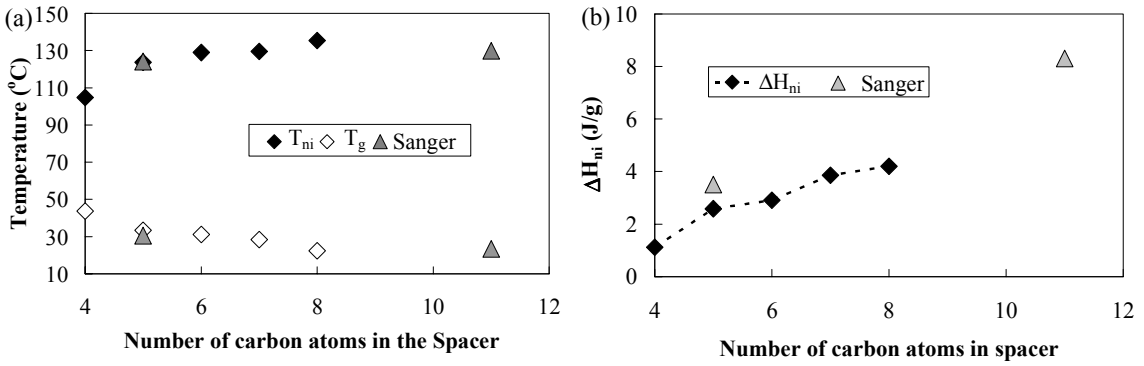

Figure 2.2. Effect of Spacer length for PBCBx polymers in comparison to Sanger [26] for similar polymers. (a) Transition Temperatures T_g and T_{ni}. (b) ΔH_{ni} showing a small odd-even effect.

The increases in both ΔH_{ni} and ΔT_{ni} with spacer length accord with known effects of increasing the spacer or alkyl tail length on SGLCPs [33, 34, 35]. In WAXS studies by Sanger and Gronski [26], an increased spacer length was found to promote the formation of a smectic phase in PBCB11. In our system a longer spacer increased the strength of

the nematic field increasing ΔH_{ni} and T_{ni}, but even for PBCB8 no smectic phases were seen.

For the largest spacer used, PBCB8, there were a total of 12 atoms between the polymer backbone and the biphenyl group, which makes it somewhat surprising that a smectic phase was not seen. Other researchers using cyanobiphenyl-based SGLCPs with silicon atoms on the backbone [36] or on the spacer [37] found smectic phases with 4 to 9 atoms and 7 atoms, respectively, in the spacer. Percec and Lee [38] synthesized a system of polymers where a cyanobiphenyl mesogen was attached using ether links connecting the methylene spacer to the backbone and to the mesogenic unit. They also found smectic phases for polymers with 7 or more atoms in the spacer. The presence of silicon atoms or ether links makes these spacers flexible decoupling the mesogen from the backbone which should favor the more disordered nematic phase. Therefore it must be the greater incompatibility of the spacers containing siloxane or ether groups and the cyanobiphenyl mesogen that favors the formation of smectic LCs relative to PBCBx.

Experiments by Shibaev et al. [34] using a cyanobiphenyl-based mesogenic group with a polymethacrylate and a polyacrylate backbone found smectic phases only at larger spacer lengths. They found smectic phases for spacers of 8 (but not 5) atoms in polymethacrylates and 14 (but not 8) atoms in acrylates. Since these systems use both an ether and an ester bond to link the mesogens, the flexibility of the spacer must be similar to our system. For the polymethacrylate system, smectic phases were formed with 8 atoms in the spacer; therefore, the cyanobiphenyl mesogen must be more incompatible with the polymethacrylate backbone than with the ethylene backbone of PBCBx.

In SGLCPs an odd-even effect is often seen as the length of the spacer is varied. In some acrylate [27] and methacrylate-based [28, 29] SGLCPs a strong odd-even effect results from the "hinge effect" where the mesogenic group alternates between a parallel and perpendicular orientation relative to the polymer backbone. In our SGLCP series, only one property, $\Delta H_{ni,}$ displayed an odd-even effect: the change in enthalpy was greater from x=4 to 5 and 6 to 7 than from 5 to 6 or 7 to 8, Fig. 2.2. Even though odd-even effects typically decrease with spacer length, work by Craig and Imrie [28, 29] saw them in T_{ni} and ΔS_{ni} for polymers with up to 15 atoms between the mesogen and the backbone and attributed it to the "hinge effect." In our systems the longest spacer had 12 atoms, therefore the absence of any strong odd-even effects suggests that these polymers had the same orientational relationship between the backbone and the mesogen. Neutron scattering results presented in Chapter 4 confirm that this is the case (the orientational tendency is transverse with $R_{\perp}/R_{//}\approx 1.6$ for the PBCBx series).

2.2.3 Solution Properties: Transition Temperatures and Solubility limits

The solubility of these polymers was checked in a number of common small molecule LCs. Samples of 5CB, E7, and E44 were purchased from Merck. All other small molecule LCs were purchased from Aldrich. Solutions were prepared by dissolving the polymer and LC in dichloromethane and then removing the dichloromethane under vacuum. The insolubility of our nematic polymer in the smectic LC 4'-octyl-4-cyanobiphenyl (8CB) was expected since smectic materials are most compatible with other smectic LCs having similar layer spacings [39]. Due to large differences in mesogen structure, the polymers were also insoluble in N-(4-methoxybenzylidene)-4-

butylaniline (MBBA). Once the phase and structure of the polymer and the solvent were matched more closely, good solubility was obtained. The polymer was found to be soluble in the cyanobiphenyl-based nematic LCs and in the eutectic mixtures, 5CB, 5OCB, E7, and E44 [30].

The ability of these polymers to dissolve in cyanobiphenyl-based nematic LCs at high molecular weights is a significant property. The additional order of a nematic fluid reduces the entropy of dissolution of the polymer reducing its solubility relative to isotropic solvents. Solubility issues often limit the choice of polymer and solvent, forcing experiments to be conducted at low molecular weights or at low concentration. The excellent solubility of our SGLCPs gives us the opportunity to extend research on SGLCPs in LC solvents to high polymers (DP>1000).

The effect of PBCB6 on the phase transition temperatures of the small molecule LC solvents was to increase T_{ni}, Fig. 2.3. In 5CB the polymer also caused the formation of a biphasic region in low concentration solutions (≤10 wt %); but at 50 wt % the LC transitioned directly from the nematic to the isotropic phase, Fig. 2.3a. In 5OCB, a small biphasic region, ~0.5 ^{o}C, smaller than the symbol size in Figure 2.3b, was visible only when heating the sample. Since the T_{ni} of 5OCB was closer to the T_{ni} of the polymers and possibly because of a slightly better matched in the structure, it transitioned into the isotropic state more quickly. In 5OCB the addition of polymer not only increased the T_{ni} but it also decreased the temperature of the melting point. When the solutions of 5OCB were cooled through the freezing point, small amounts of polymer phase-separated at the grain boundaries of the crystals.

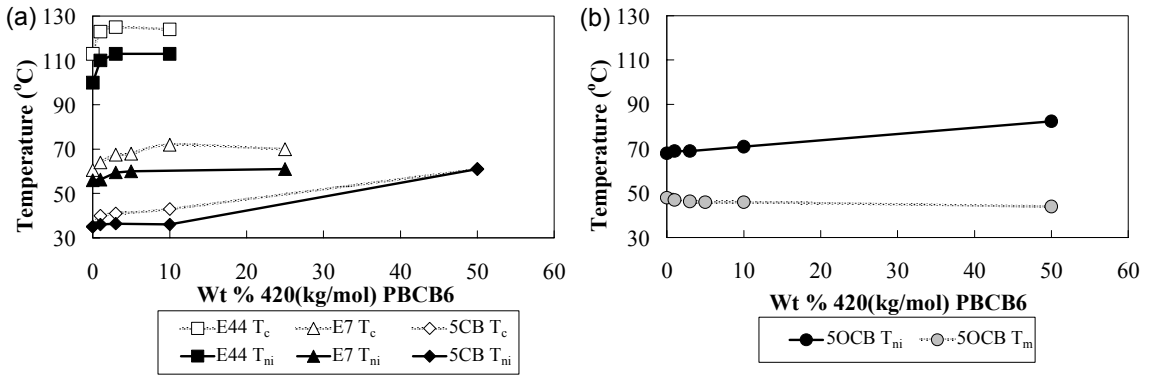

Figure 2.3. Phase diagram for solutions of 420 kg/mol PBCB6 dissolved in cyanobiphenyl-based small molecule liquid crystals. Phases were determined by DSC and POM. Similar results were found for solutions of the other polymers in this series, PBCBx. (a) T_{ni} indicates the transition from one nematic phase to a biphasic nematic/isotropic phase. And T_c indicates a transition from biphasic to an isotropic phase. (b) T_{ni} is the transition from a nematic to isotropic phase with a small biphasic region only visible while heating. T_m is the melting point of the crystalline phase.

The eutectic mixtures E7 and E44 are composed of mixtures of cyanobiphenyl-based LCs, primarily 5CB and 5OCB. These mixtures have a biphasic region, and the addition of PBCB6 (having a higher T_{ni}) increased the temperatures T_{ni} and T_c, Fig 2.3a. The presence of a biphasic region is a common occurrence in solutions of polymers dissolved in small molecule nematic LCs [40, 41, 42]. Significantly, miscibility was observed over a wider temperature range in the nematic phase than the nematic temperature window of the host LC itself. In general, the addition of polymer increased the temperature range of the nematic phase (decreasing T_g, Fig. 2.2a, or T_m, Fig. 2.3b, and increasing T_{ni}, Fig 2.3a).

2.2.4 Effect of Polymer on the Refractive Index of a Nematic Solution

The refractive indices of solutions of 420 kg/mol PBCB6 in 5CB were measured using an Abbe refractometer [43] equipped with a bandpass filter for 633 nm light. Alignment of the liquid crystal was obtained by washing the surfaces of the prisms with a solution of 1% lecithin in chloroform to promote homeotropic (perpendicular) alignment.

Since the liquid crystal was birefringent, light entering this phase was split into two beams with different polarization states. Therefore, the ordinary and extraordinary refractive indices , n_o and n_e, could be determined. Instead of a single transition from a light to a dark state, two transitions from bright to dim and from dim to dark were seen [44]. When the solution went through T_{ni}, a biphasic region was encountered in which the refractive index of the larger isotropic phase was easily discerned. Since the polymer-rich LC phase was present in significantly smaller quantities and was poorly aligned, it was difficult to measure its refractive indices. The uncertainty in measurements below T_{ni} was smaller than the symbol size in Fig. 2.4, but in the biphasic region the uncertainties were much larger, as indicated.

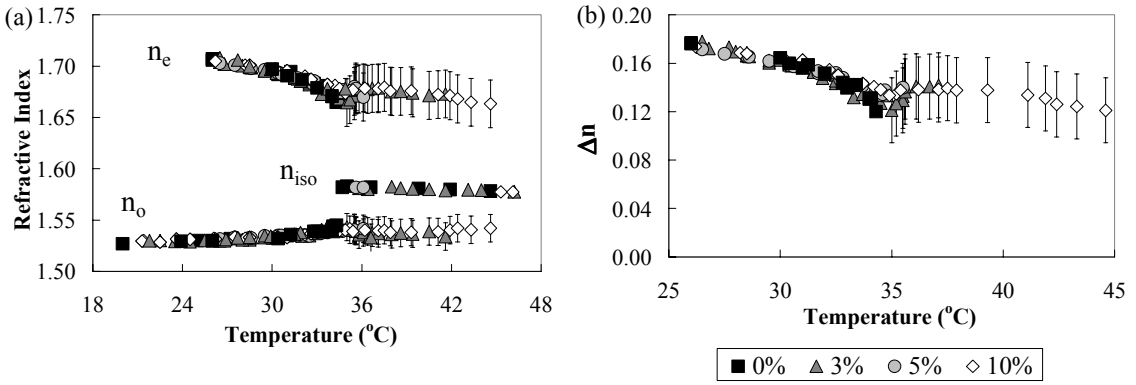

Figure 2.4. Effect of dissolved polymer 420 kg/mol PBCB6 on (a) refractive indices and (b) birefringence of solutions in 5CB. At temperatures above 35 °C, the solution was biphasic with the largest fraction in the isotropic phase. For temperatures below ~32 °C, within experimental uncertainties, the birefringence of the solutions was the same as bulk 5CB.

Solutions of up to 10 wt % polymer were compared to bulk 5CB. The change in Δn, n_o, and n_e due to the addition of polymer, was less than the experimental uncertainty for temperatures below ~32 °C, Fig. 2.4. In Figure 2.4b near T_{ni}, a larger Δn is seen for the solutions of 10 and 5 wt %. This behavior was expected since the polymer had a significantly higher T_{ni} than 5CB and served to stabilize the nematic phase [45, 46].

Coles and Bancroft [47] using a cyanobiphenyl-based SGLCP dissolved in E7 demonstrated that changes in Δn correlated with a reduction in the order parameter and K_{11}. In our system the negligible changes in Δn upon addition of polymer indicated that the order parameter was not significantly affected except near T_{ni}.

2.3 Conclusion

Using a cyanobiphenyl-based mesogenic unit in these SGLCPs confers excellent solubility in nematic cyanobiphenyl-based small molecule LCs even with high molecular weight polymers. This allowed us to explore concentration and molecular weight regimes that were previously unexplored. Because of this similarity in structure, the addition of polymer to 5CB did not change Δn for temperatures below 32 ^{o}C. This indicated that even up to 10 wt % polymer, the order parameter of the solvent was not significantly altered which allows parameters, such as the frank elastic constants, for bulk 5CB to be used as an estimate for the solutions.

Studying solutions of model polymers in LCs allows us to evaluate the effects of polymers on a nematic host as a function of molecular weight and spacer length. Since this series of SGLCPs extends to chain lengths an order of magnitude larger than that previously investigated in LC solutions, it has revealed new phenomena that were previously inaccessible; such as flow alignment of a calamitic LC near the velocity gradient direction [11, 12]. This also provides a way to evaluate the effect of a dissolved polymer on the Leslie-Ericksen viscous parameters as predicted by the Brochard theory [13], and to compare the rheologically predicted anisotropy with the anisotropy measured in small-angle neutron scattering experiments [11].

Bibliography

[1] H. E. A. Huitema, G. H. Gelinck, J. B. P. H. Van Der Putten, K. E. Kuijk, C. M. Hart, E. Cantatore, P.T. Herwig, A. J. J. M. van Breemen, and D. M. de Leeuw, *Nature*, **414**, 599 (2001).
[2] R. L. Sutherland, V. P. Tondiglia, L. V. Natarajan, T. J. Bunning, and W. W. Adams, *Appl. Phys. Lett*. **64,** 1074 (1994).
[3] R. A. M. Hikmet, H. M. J. Boots, and M. Michielsen, *J. Appl. Phys*. **79,** 8098 (1996).
[4] K. Kang, L. C. Chien, and S. Sprunt, *Liq. Cryst*. **29**, 9 (2002).
[5] H. Mori, Y Itoh, Y Nishiura, T. Nakamura, and Y. Shinagawa, *Jpn. J. Appl. Phys*. **36,** 143 (1997).
[6] D. L. Thomsen, P. Keller, J. Naciri, R. Pink, H. Jeon, D. Shenoy, and B. R. Ratna, *Macromolecules* **34**, 5868 (2001).
[7] W. Lehmann, H. Skupin, C. Tolksdorf, E. Gebhard, R. Zentel, P. Kruger, M. Losche, and F. Kremer, *Nature* **410**, 447 (2001).
[8] D. Gu, S. R. Smith, A. M. Jamieson, M. Lee, and V. Percec, *J. Phys. II France* **3,** 937 (1993).
[9] H. Mattoussi and R. Ober, *Macromolecules* **23,** 1809 (1990).
[10] P. Keller, B. Carvalho, J. P. Cotton, M. Lambert, F. Moussa, and G. Pepy, *J. Phys. Lett.* **46,** L-1065 (1985).
[11] M. D. Kempe and J. A. Kornfield, *Phys. Rev. Let*. **90**, 115501 (2003).
[12] M. D. Kempe, M. L. Auad, J. A. Kornfield, W. J. Zhou, and S. T. Wu, *Journal of Rheology* Manuscript in Preparation (2003).
[13] F. Brochard, *J. Polym. Sci., Polym. Phys*. **17,** 1867 (1979).
[14] A. M. Jamieson, Y. C. Chiang, and S. R. Smith, *Macromol. Symp.* **118**, 289 (1997).
[15] Y. C. Chiang, A. M. Jamieson, S. Campbell, Y. Lin, N. O'Sidocky, L. C. Chien, M. Kawasumi, and V. Percec, *Rheol. Acta* **36,** 505 (1997).
[16] F. M. Leslie, *Arch. Rat. Mech. Anal*. **28,** 265 (1968).
[17] J. L. Ericksen, *Arch. Rat. Mech. Anal*. **24,** 231 (1960).
[18] J. Roovers and P. M. Toporowski, *Rubber Chem. Technol.* **63,** 734 (1990).
[19] A. F. Halasa, D. F. Lohr, and J. E. Hall, *J. Polym. Sci., Polym. Chem. Ed*. **19,** 1537 (1981).
[20] S. Bywater, D. H. MacKerron, D. J. Worsfold, and F. Schue, *J. Polym. Chem. Ed*. **23,.** 1997 (1985).
[21] A. F. Halasa, D. N. Schultz, D. P. Tate, and V. D. Mochel, *Adv. Organomet. Chem*. **18,** 55 (1980).
[22] T. C. Chung, M. Raate, E. Berlunche, and D. N. Schulz, *Macromolecules* **21,** 1903 (1988).
[23] J. Adams and W. Gronski, *Makromol. Chem., Rapid Commun.* **10,** 553 (1989).
[24] G. Mao, J. Wang, S. R. Clingman, C. K. Ober, J. T. Chen, and E. L. Thomas, *Macromolecules*, **30,** 2556 (1997).
[25] G. Mao, J. Want, and C. K. Ober, *Chem. Mater*. **10,** 1538 (1998).
[26] J. Sanger and W. Gronski, *Macromol. Chem. Phys*. **199**, 555 (1998).
[27] G. R. Mitchell, M. Coulter, F. J. Davis, and W. Gou, *J. Phys. II France* **2,** 1121 (1992).
[28] A. A. Craig and C. T. Imrie, *J. Mater. Chem*. **4**, 1705 (1994).
[29] A. A. Craig and C. T. Imrie, *Macromolecules* **28**, 3617 (1995).
[30] E7 and E44 are cyanobiphenyl-based eutectic mixtures available through Merck composed primarily of the liquid crystals 5CB and 5OCB.
[31] M. D. Kempe, J. A. Kornfield, C. K. Ober, and S. D. Smith, *Macromolecules* **00,** 000 (2003) Manuscript in perparation.
[32] M. D. Kempe, J. A. Kornfield, and J. Lal, *Macromolecules*, **00,** 000 (2003) Manuscript in preparation.
[33] E. B. Barmatov, T. Yongjie, G. F. Kolbina, I. N. Shtennikova, N. Akhmedov, M. V. Kozlovskii, and V. P. Shibaev, *Polymer Science,* **43**, 5 (2001).
[34] V. P. Shibaev, S. G. Konstromin, and N. A. Plate, *Eur. Polym. J*. **18**, 651 (1982).
[35] J. C. Dubois, G. Decobert, P. LeBarny, S. Esselin, C. Friedrich, and C. Noel, *Mol. Cryst. Liq. Cryst*. **137**, 349 (1986).
[36] B. R. Nair, M. A. R. Osbourne, and P. T. Hammond, *Macromolecules* **31**, 8749 (1998).
[37] Y. Kawakami, K. Toida, and Y. Ito, *Macromolecules* **26**, 1177 (1993).

[38] V. Percec and M. Lee, *Macromolecules* **24**, 2780 (1991).
[39] J. D. Laffitte, M. F. Achard, F. Hardouin, H. T. Nguyen, and G. Sigaud, *Liq. Cryst*. **17**, 487 (1994).
[40] A. I. Hopwood and H. J. Coles, *Mol. Cryst. Liq. Cryst*., **130**, 281 (1985).
[41] M. C. Chang, H. W. Chiu, X. Y. Wang, T. Kyu, N. Leroux, S. Campbell, and L. C. Chien, *Liquid Crystals*, **25**, 733 (1998).
[42] H. Finkelmann, H. J. Kock, and G. Rehage, *Mol. Cryst. Liq. Cryst.* **89** 23 (1982).
[43] P. A. Santoro, J. R. D. Pereira, and A. J. Palangana, *Phys. Rev. E*, **65**, 057602 (2002).
[44] I. Haller, H. A. Huggins, and M. J. Freiser, *Mol. Cryst. Liq. Cryst*. **16**, 53 (1972).
[45] D. Demus, C. H. Fietkau, R. Schubert, and H. Kehlen, *Mol. Cryst. Liq. Cryst*., **25**, 215 (1974).
[46] D. S. Hulme, E. P. Raynes, and K. J. Harrison, *J. Chem. Soc. Chem. Comm*. **3**, 98 (1974).
[47] H. J. Coles and M. S. Bancroft, *Mol. Cryst. Liq. Cryst*. **237**, 97 (1993).

Chapter 3 Physical Properties of Perdeuterated 4'-Pentyl-4-cyanobiphenyl

This chapter is composed of the text and figures of a paper that was co-authored by Michael D. Kempe and Julia A. Kornfield at the California Institute of Technology and Shin-Tson Wu and Qiong-Hua Wang at the University of Central Florida [1]. The synthesis of the deuterated 5CB was performed in California, the bulk of the material characterization was performed in Florida, and the data analysis was performed jointly.

3.1 Relevance of Deuteration to Electro-Optics

Liquid crystal (LC) optical phased arrays (OPA) have been developed for laser beam steering, electronic lenses and network switching [2,3]. The performance of an OPA is determined by the LC material employed, such as birefringence, viscosity and elastic constant. To steer a high power laser, the absorption of the LC cell, including LC medium, substrates and electrodes, plays a crucial role. The absorbed laser light is converted to thermal energy which heats up the LC material. If the resultant temperature exceeds the LC's clearing point, the light modulation capability vanishes.

In the visible spectral region, most LC materials are transparent. However, in the mid (3-5 μm) and long (8-12 μm) infrared (IR) regions, some strong molecular vibration bands exist [4] For instances, the CH, CH_2 and CH_3 bands overlap closely in the 3.4-3.6

μm range, and the CN absorption band occurs at 4.45 μm. The overtones (second and third harmonics, etc.) of these vibration bands occur at near IR (1-2 μm) region where λ=1.55 μm is a common wavelength for telecom light switch. To clean up the 3-5 μm window, post-deuteration in the side chain of some LCs has been attempted [5]. The deuterium (D) atom has a larger atomic mass so that the CD stretching occurs at a longer wavelength than that of the CH band.

In this chapter, we report the physical properties of a perdeuterated 4'-pentyl-4-cyanobiphenyl (D5CB) liquid crystal. The mesogenic properties of D5CB remain very similar to 5CB. However, its IR absorption is substantially reduced. This opens up a new possibility for high power laser beam steering in the near and mid IR regions.

3.2 Effect of Perdeuteration on Electro-Optic Properties

The 5CB was obtained from Merck and used as is, and the synthesis of D5CB is described in section A4. The phase transition temperatures of D5CB and 5CB were measured using a high sensitivity differential scanning calorimeter (DSC, Model TA-Q100). Results are listed in Table 3.1. The melting and clearing point of D5CB is about 1-2 ^{o}C lower than that of 5CB. The dielectric and elastic constants were measured using an APT-III instrument devised by Displaytech Table 3.1. D5CB has a slightly smaller dielectric anisotropy along with its lower clearing temperature. From mean field theory, [6] the LC dielectric anisotropy ($\Delta\varepsilon$) is linearly proportional to order parameter (S) which is related to clearing point (T_c) as $S=(1-T/T_c)\beta$. For most LCs, β~0.25 and is insensitive to

molecular structures [7]. Thus, D5CB is expected to exhibit a slightly smaller $\Delta\varepsilon$ than 5CB.

	Nematic Phase (^{o}C)	$\varepsilon_{\parallel}$	$\varepsilon_{\perp}$	$\Delta\varepsilon$	K_{11} (pN)	K_{33} (pN)	K_{11}/K_{33}
D5CB	21.4 to 32.1	18.1	6.6	11.5	7.34	8.6	1.17
5CB	22.5 to 34.2	19.1	6.3	12.8	9.96	11.8	1.19

Table 3.1. The measured phase transition temperatures, dielectric constants, and elastic constants of 5CB and D5CB. T=22 ^{o}C.

The refractive indices of D5CB and 5CB were measured at T=22 ^{o}C for λ=546, 589 and 633 nm using a multi-wavelength Abbe refractometer (Atago, Model DR-M4). Results are listed in Table 3.2. Similar to $\Delta\varepsilon$, the LC birefringence ($\Delta n=n_e-n_o$) is also linearly proportional to S [8]. Thus, D5CB has a slightly smaller Δn than 5CB at all the wavelengths we studied.

Wavelength	5CB n_e	5CB n_o	5CB Δn	D5CB n_e	D5CB n_o	D5CB Δn
546 nm	1.7336	1.5387	0.1949	1.7241	1.5386	0.1855
589 nm	1.7233	1.5337	0.1896	1.7140	1.5340	0.1800
633 nm	1.7140	1.5297	0.1843	1.7048	1.5303	0.1745

Table 3.2. The measured refractive indices of 5CB and D5CB. T=22 ^{o}C.

The major advantage of D5CB over 5CB is its cleaner and lower IR absorption. Two IR spectrophotometers, Perkin-Elmer Spectrum-One and Cary-500, were used for these studies. For the mid- and long-IR absorption measurements, two sodium chloride

substrates were used. The LC cell gap was controlled at d~8 μm and the measurements were made at T=22 ^{o}C, in the nematic state. For the interest of identifying the red shift originating from deuteration, we only compared their relative transmission. Experimental results of 5CB and D5CB are shown in Figs. 3.1 and 3.2, respectively.

In Fig. 3.1, two major absorption bands (CH and CN) occur in the 3-5 μm (3300 to 2000 cm^{-1}) region and several absorption bands in the 8-12 μm (1250 to 833 cm^{-1}) region. The CH, CH_2 and CH_3 stretching vibration bands overlap closely in the 2800-3100 cm^{-1} range with a strong absorption intensity. As compared to Fig. 3.2, the $CH/CH_2/CH_3$ absorption of the 95% perdeuterated D5CB is reduced substantially. The remaining absorption centered at ν=2901cm^{-1} is due to residual alkyl CH bonds, Fig. A4.2, and the absorption due to the aromatic CH bonds (3000 to 3100 cm^{-1}) is almost completely eliminated. The alkyl CD absorption band shifts to ν=2099 cm^{-1} which is very close to the strongly absorbing CN band centered at 2225 cm^{-1}. To further remove the strong CN band, other polar groups such as F or CF_3 can be considered [9]. However, absorption from the aromatic CD stretching overlaps the CN stretching which would still reduce transmission at this frequency.

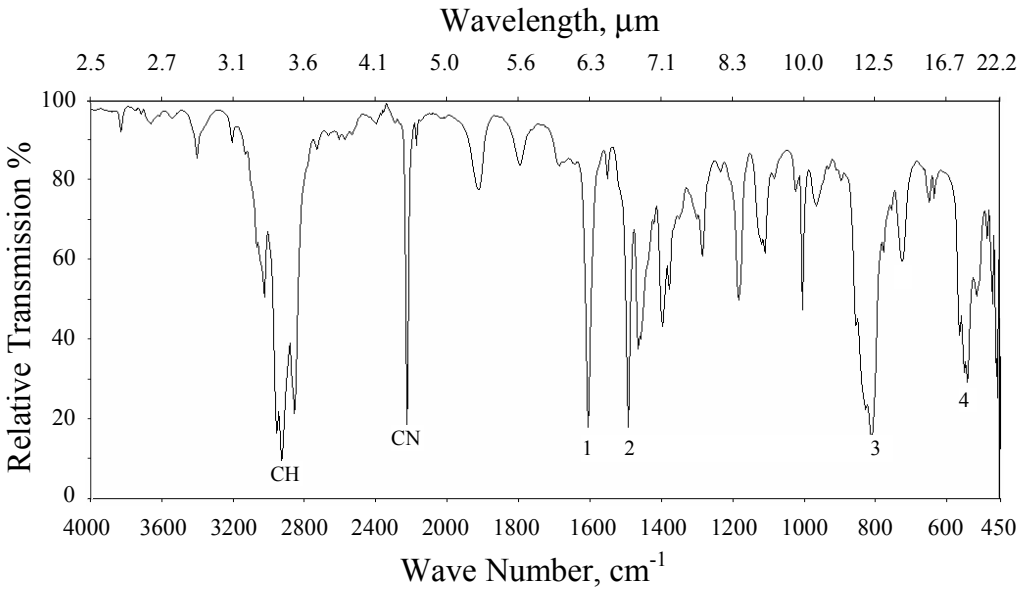

Figure 3.1. Measured IR transmittance of 5CB. Cell gap~8 μm. T=22 °C. The four designated vibration frequencies are 1604, 1492, 812 and 540 cm^{-1}, respectively.

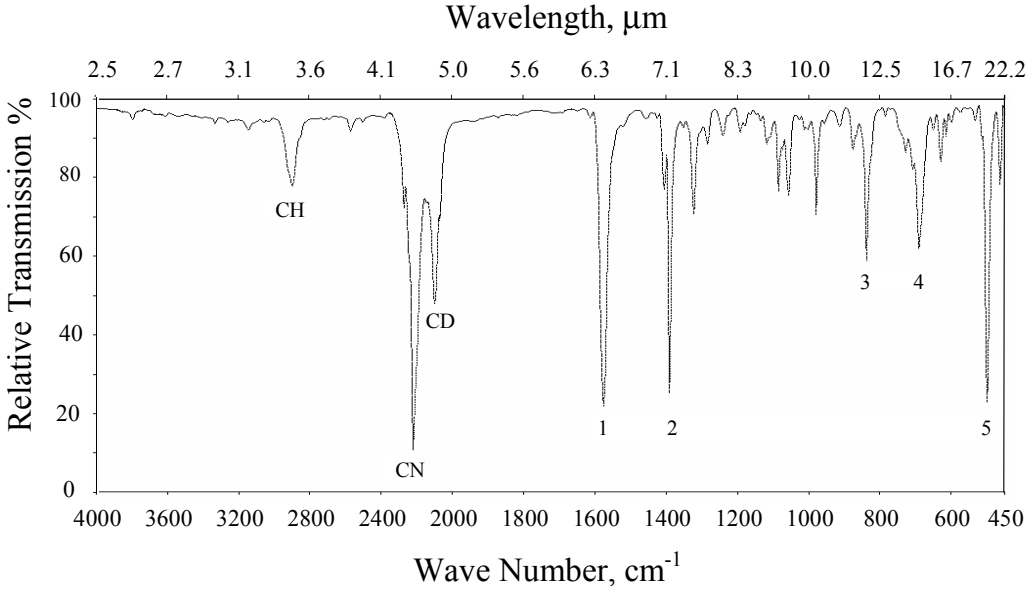

Figure 3.2. Measured IR transmittance of D5CB. Cell gap~8 μm. T=22 °C. The five designated vibration frequencies are 1575, 1391, 837, 691 and 500 cm^{-1}, respectively.

Figure 3.1 shows some absorption in the 1800 to 2000 cm^{-1} range which are the overtones resulting from the aromatic CH bonds. In contrast, these bands are absent in D5CB. Due to the absorption frequency shift, D5CB exhibits a much cleaner and smaller

absorption than 5CB in the 800 to 1300 cm^{-1} region. At λ=10.6 μm (ν=943cm^{-1}, a key CO_2 laser wavelength), D5CB has a much lower absorption than 5CB.

Liquid crystals have been used as light switch and variable optical attenuators for fiber-optic communication at λ=1.55 μm [10]. A lower absorption would enable an LC device to tolerate a higher power laser beam. We have compared the absorption spectrum of D5CB with 5CB in the 1-3.2 μm range. Since the absorption is relatively small in this spectral region, a 1 mm thick quartz cell was used for such experiments. For such a thick cell, it is impossible to align the LC employed. To avoid light scattering, the cell was heated to T~50 ^{o}C so that the LC is in the isotropic state. The measured results are plotted in Fig. 3.3. The dark and gray lines represent the measured optical density of D5CB and 5CB, respectively.

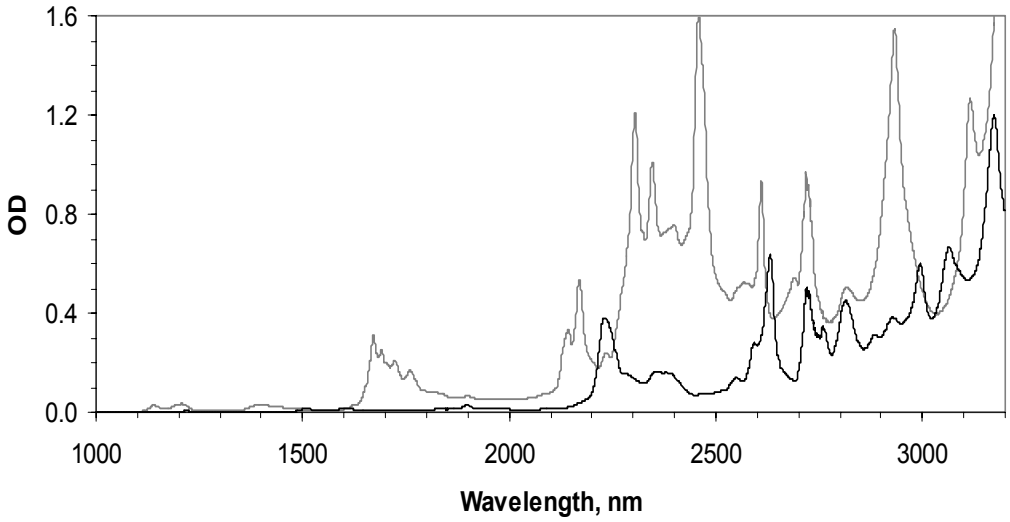

Figure 3.3. Measured optical density (OD) of D5CB (dark lines) and 5CB (gray lines) in the near IR region. Cell gap=1 mm. T~50 ^{o}C.

From Fig. 3.3, D5CB exhibits a much lower absorption in the near IR region. Several overtone absorption bands observed in 5CB are either eliminated or significantly reduced. For example, the λ=1.7 μm band which is the second harmonic wavelength of the strong

3.4 μm CH bands is absent in D5CB. Since most of the CH bonds in 5CB are replaced by CD, the 1.7 μm band no longer exists in D5CB.

3.3 Conclusions

In conclusion, the perdeuterated 5CB preserves the major mesogenic properties of 5CB while exhibiting much lower absorption in the near and mid IR regions. This new LC compound would extend the useable range of high power laser beam steering to mid IR and enhance the power handling capability of LC devices for telecommunication at λ=1.55 μm.

A perdeuterated 4'-pentyl-4-cyanobiphenyl (D5CB) was synthesized and its physical properties evaluated and compared to those of 5CB. D5CB preserves similar physical properties, such as phase transition temperatures, dielectric constants and refractive indices, to 5CB. An outstanding feature of D5CB is that it exhibits a much cleaner and reduced infrared absorption. Perdeuteration not only extends the useable range of liquid crystals to mid infrared but also significantly reduces the absorption in the near infrared, which is essential for telecom applications.

Bibliography

[1] S. T. Wu, Q. H. Wang, M. D. Kempe and J. A. Kornfield, *J. Appl. Phys*. **92**, 7147 (2002).
[2] P. F. McManamon, T. A. Dorschner, D. L. Corkum, L. Friedman, D. S. Hobbs, M. Holz, S. Liberman, H. Q. Nguyen, D. P. Resler, R. C. Sharp, and E. A. Watson, *Proc. of the IEEE* **84**, 268 (1996).
[3] P. F. McManamon, E. A. Watson, T. A. Dorschner and L. J. Barnes: *Opt. Eng*. **32,** 2657 (1993).
[4] S. T. Wu, *J. Appl. Phys*. **84**, 4462 (1998).
[5] L. Su and J. L. West, Proc. Laser Beam Steering Symposium, pp. 205-210 (June, 2000, Kent State University, Ohio).
[6] W. Maier and G. Meier, Z. Naturforsch. Teil A **16**, 262 (1961).

[7] S. T. Wu and D. K. Yang, *Reflective Liquid Crystal Displays*, Wiley, Chichester, (2001).
[8] S. T. Wu, *Phys. Rev. A* **30**, 1270 (1986).
[9] S. T. Wu, J. D. Margerum, H. B. Meng, C. S. Hsu and L. R. Dalton, *Appl. Phys. Lett*. **64**, 1204 (1994).
[10] K. Noguchi, *J. Lightwave Technology*, **16**, 1473 (1998).

Chapter 4 Polymer Chain Anisotropy in a Nematic Solvent

4.1 Introduction

When a polymer is dissolved in a nematic host, it adopts an anisotropic conformation which is coupled to the nematic order of the liquid crystal giving rise to rheologically complex behavior. The Brochard [1] theory describes how, in a dilute solution, the anisotropy of the polymer affects the six Leslie-Ericksen parameters used to describe the viscosity of a nematic material. Numerous rheological studies have been performed to test the qualitative validity of the Brochard theory [2, 3] or to obtain estimates for the chain anisotropy [4, 5, 6, 7]. In the work of Yao and Jamieson [7], electrorheological measurements of solutions of a side-group liquid crystalline polymer (SGLCP) in a nematic solvent were used to obtain estimates of the polymer chain anisotropy using the Brochard theory. They found that as the molecular weight is increased the anisotropy, $R_{\perp}/R_{//}$, increases. Despite interest in the anisotropy of SGLCPs in nematic solutions, very little research [8, 9, 10] has been performed to test the validity of the Brochard theory.

Two predominant types of chain conformations are found for SGLCPs: a prolate spheroid conformation with both the backbone and the mesogenic units aligned near the director, and an oblate, or disk-like, spheroid conformation with the backbone preferentially perpendicular to the director. Theoretical descriptions [11, 12, 13, 14] of the sense of the anisotropy and its magnitude predict a molecular weight dependence for low molecular weight and constant anisotropy at high molecular weight.

Although there are numerous theories and experiments designed to predict the dimensions of an SGLCP in a nematic solution, very little work has been done to measure the anisotropy of a liquid crystalline polymer in a small molecule nematic. In principle, the backbone anisotropy can be measured using small-angle neutron scattering [15] (SANS) or X-ray scattering [2, 16, 17]. In practice, the lack of data on polymers dissolved in nematic solvents reflects the difficulty of obtaining adequate scattering intensity to perform these experiments. Solution studies were performed with a relatively low concentration of about 5 wt % polymer, as opposed to a 50:50 deuterated/hydrogenated polymer mixture in melt studies. Furthermore, the effects of scattering from the bulky side chains are typically eliminated by only labeling the backbone (deuterium labeling in SANS or silicon atoms for SAXS). Unfortunately, this results in an order of magnitude lower effective concentration of scatterers [18, 19, 20].

To maximize the contrast in neutron scattering experiments it is possible to label either the entire polymer or solvent molecule with deuterium. The problem with these two approaches is that the effects of scattering on the mesogenic groups must be accounted for to determine the backbone conformation. Using an end-on SGLCP based on a poly(methylsiloxane) in which the terminal ends of the mesogenic units were labeled with deuterium, researchers [20, 21, 22, 23] observed a prolate conformation. With the same polymer labeled on the spacer near the backbone, an oblate conformation was observed [24]. When scattering results from deuteration of the mesogenic units, a larger radius is measured parallel to the director [20, 21, 22, 23, 24]. Unless the polymer is large, this leads to an erroneous determination of the polymer anisotropy. Casquilho and Volino [25] suggested that the results of labeling on different parts of the mesogenic unit

could be extrapolated to the case for labeling on the backbone only. Unfortunately, this method requires a series of differently labeled polymers making this method impractical. Therefore a method to account for scattering on partially or fully labeled SGLCPs is needed.

In this work, we use the solvent labeling approach to eliminate the need for labeling the polymer and demonstrate a way to account for the scattering from the mesogenic units. The SANS pattern of a series of low polydispersity polymers differing only in their molecular weight reveal an anisotropy that increases with molecular weight. Once the scattering due to the mesogenic units is accounted for, the backbone anisotropy is found to be independent of molecular weight. In addition, backbone anisotropy is found to be independent of spacer length in the side group over the range probed, x=4 to 8 in Fig. 1. By demonstrating a way to measure the polymer anisotropy in solution we provide direct measurements of chain anisotropy. This is required to test the relationships between chain anisotropy and the effect of polymers on the flow behavior of nematic LCs. [26] In turn, the results will reveal the relationships between polymer structure, conformation, viscoelastic response, and electro-optic response.

4.2 Materials

The details of the synthesis and characterization of the polymers used in this study are published elsewhere [27]. A series of SGLCPs differing in either the degree of polymerization (DP) or in the number of carbons in the spacer unit were produced by hydroboration/oxidation of 1,2-polybutadiene followed by attachment of a mesogenic side group using an acid chloride reaction, Fig. 4.1. By matching the structure of the

mesogen to the small molecule nematic LC, good solubility of these polymers was found in the liquid crystals 4'-pentyl-4-cyanobiphenyl (5CB), 4'-pentyloxy-4-cyanobiphenyl (5OCB), and in the eutectic mixtures E7 and E44 [28]. These polymers seem to be soluble in almost any nematic, cyanobiphenyl-based LC.

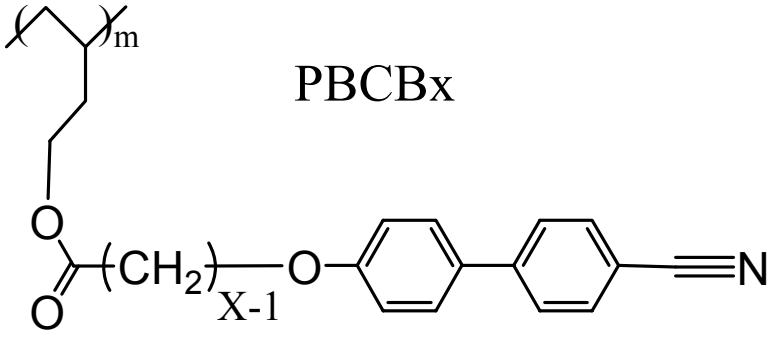

Figure 4.1. Structure for polymers used in this study. The 'X' in the polymer name indicates the size of the spacer where X+4 is the number of atoms between the mesogen and the polymer backbone.

The refractive indices of solutions of 420 kg/mol PBCB6 in 5CB were measured using an Abbe refractometer. For up to 10 wt % polymer at temperatures at least 3 ^{o}C away from the nematic-to-isotropic transition temperature ($T \leq 32$ ^{o}C), the ordinary and extraordinary refractive indices of the solution were equal to those of 5CB. This indicates that added polymer does no change the order parameter of the nematic host over this range of concentration.

4.3 Chain Conformation by Small-Angle Neutron Scattering.

The radii of gyration of a series of PBCBx polymers was determined by neutron scattering using hydrogenated polymers in a perdeuterated solvent 4'-pentyl-4-cyanobiphenyl-d_{19}, (D5CB). The D5CB was synthesized by exchanging the hydrogen in 4-pentylbiphenyl for deuterium using D_2O and a Pt catalyst, followed by attachment of a

nitrile group. The resulting material had 95% of its hydrogen exchanged for deuterium and had properties similar to its hydrogenated analog [29]. Solutions were prepared by mixing the polymer and D5CB in dichloromethane and removing the dichloromethane under vacuum. All solutions were made with 5 wt % polymer to keep them below the overlap concentration.

Neutron scattering experiments were conducted at the Intense Pulsed Neutron Source (IPNS) at Argonne National Laboratory using the Small-Angle Diffraction (SAD) instrument. The samples were loaded into a cell made up of two 1" diameter 1/8" thick quartz windows separated by a 0.5 mm spacer. Homogeneous (parallel) alignment of the sample was obtained by using both rubbed polyimide layers on the quartz windows and a 0.8 Tesla magnetic field oriented in the rubbing direction. A small gap was used so that excellent alignment could be obtained and so the sample would not flow out of the cell. A cell containing bulk D5CB was used as a blank, and the scattering patterns were acquired for between 5 and 10 hours at 25 ^{o}C.

The SANS patterns are anisotropic with elliptical iso-intensity contours with the major axis parallel to the director, Fig. 4.2. Since a higher scattering intensity is measured parallel to the director and quadratic characteristic sizes parallel and perpendicular to the director, $R_{//}$ and $R_{\perp}$, are inversely related to the scattering intensity, this shows that $R_{//}<R_{\perp}$ which corresponds to an oblate conformation. Typically [30], the values for the radii of gyration are found by analyzing a slice of the data both parallel and perpendicular to the director and fitting the low q data with a Guinier approximation to yield the quadratic characteristic size in a direction $\vec{x}$

$$\frac{I_o}{I(q)} = 1 + q^2 R_x^{\ 2} + \ldots, \quad (4.1)$$

The high molecular weight of our polymers resulted in fewer data points for the low q range ($q \cdot R_g < 1$); therefore, the scattering patterns were fit to the Debye equation

$$I(q) = I_o \left(\frac{2}{q^4 R_g^{\ 4}} \right) \left[q^2 R_g^{\ 2} - 1 + e^{\left(-q^2 R_g^{\ 2}\right)} \right], \quad (4.2)$$

so that the intermediate range ($1/R_g < q < 1/L$, where L is the mesogen length) could be used [13, 31, 32].

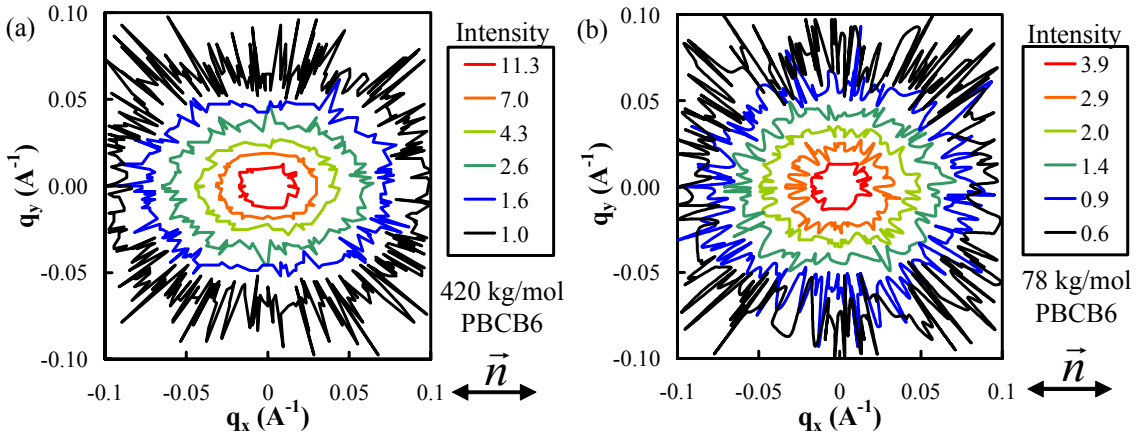

Figure 4.2. Contour intensity plot of the neutron scattering pattern for (a) 420 kg/mol PBCB6 and (b) 78 kg/mol PBCB6 dissolved in D5CB. In these plots, the director is oriented along the "x" direction.

We are concerned with determining the characteristic quadratic size, R_x, particularly where $\vec{x}$ is either parallel or perpendicular to the director. For an isotropic polymer the quadratic size is related to the radius of gyration by [33]

$$R_g = \sqrt{3} R_x, \quad (4.3)$$

Since the Debye equation is used to determine R_g for an isotropic polymer, the radius determined from a fit of Eq. 4.2 is divided by $\sqrt{3}$ to yield $R_\perp$ or $R_{//}$.

Since our polymers are in the dilute regime and the samples were thin, the scattering intensity is low. To overcome this problem we use the entire scattering pattern in our analysis to improve the statistics [34]. To do this the radius is determined as a function of azimuthal angle *(θ).* In an anisotropic medium a polymer is often in the shape of either an oblate or a prolate spheroid; therefore, the iso-intensity contours were modeled using an ellipse,

$$\left(\frac{1}{R_x(\theta)}\right)^2 = \left(\frac{\sin\theta}{R_{||}}\right)^2 + \left(\frac{\cos\theta}{R_{\perp}}\right)^2, \quad (4.4)$$

with θ defined as the angle between q and the director $(\vec{n})$ [35].

Since each monomeric unit has a large, fully hydrogenous side group, the Debye equation can only be applied as an approximation. The Debye model describes the scattering from a connected set of freely jointed scatterers of which the shape and size are not accounted for. Only for values of $q<<1/L$, where L is the characteristic length of a side group, can the mesogen be approximated as a single scatterer [36]. Since our polymers are large, the relative contributions of the side groups to the measured radii are still small. Therefore, to a first-order approximation, the side group simply increases the effective R_g as measured in the Debye equation [37].

Since the scattered intensity is a function of the product $q \cdot R_g$, the ratio of the quadratic characteristic sizes, $R_{\perp}/R_{//}$, was determined by plotting $I(q)$ versus $q_{//}$ and $I(q)$ versus $q_{\perp} \cdot R_{\perp}/R_{//}$ and adjusting the ratio $R_{\perp}/R_{//}$ until the profiles of the two plots matched with good overlap, Fig. 4.3. The uncertainty reported for this ratio was determined by finding the maximum and minimum values for which the data could be reasonably interpreted.

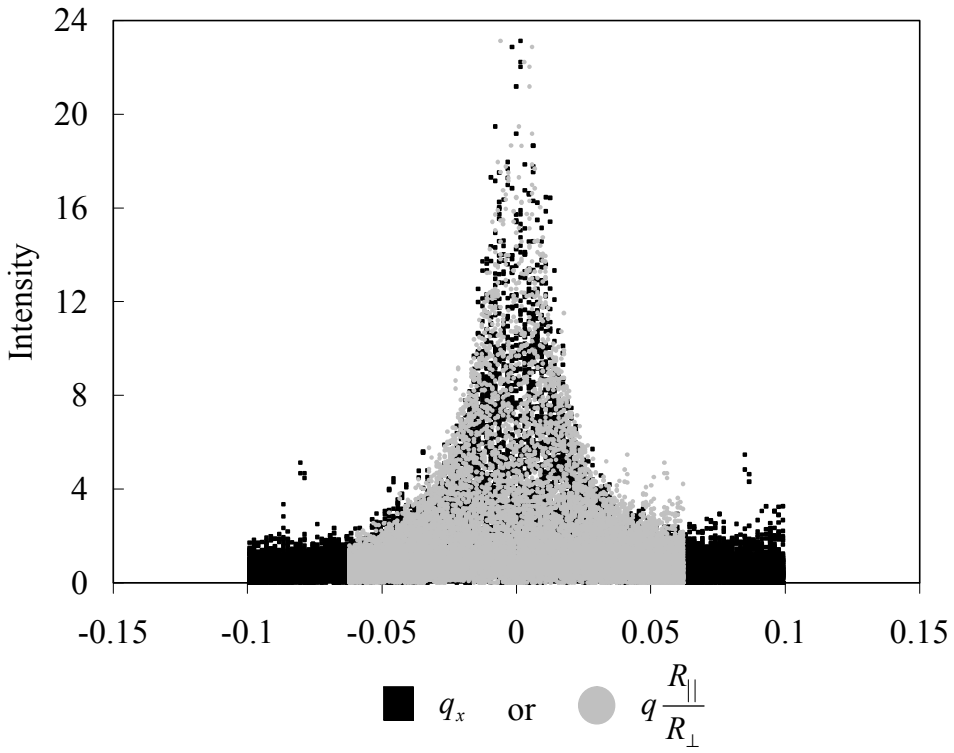

Figure 4.3. Neutron scattering plot used to determine anisotropy of 420 kg/mol PBCB6 in D5CB. This was done by overlapping the plots scaled in the parallel and perpendicular directions until good overlap was obtained.

Since there was a low signal-to-noise ratio in the measurement of the scattered intensity, data points that had similar values of $q \cdot R_x(\theta)$ were averaged prior to being fit to the Debye equation. With the ratio $R_{\perp}/R_{//}$ known, the Debye equation was fit to the data by adjusting I_o and $R_{//}$ on a plot of $I(q)/I_o$ versus $R_x(\theta)^2 \cdot q^2$ until a good fit to the data was found, Fig. 4.4. To confirm the validity of the radii obtained, plots of $I(q)/I_o$ versus q containing data points parallel or perpendicular to the director were plotted along with the intensity calculated with the Debye equation using $R_{//}$ or $R_{\perp}$, respectively, Fig. 4.5. The uncertainty in the measured values of the radii was obtained by finding the maximum and minimum values for which the data could be fit.

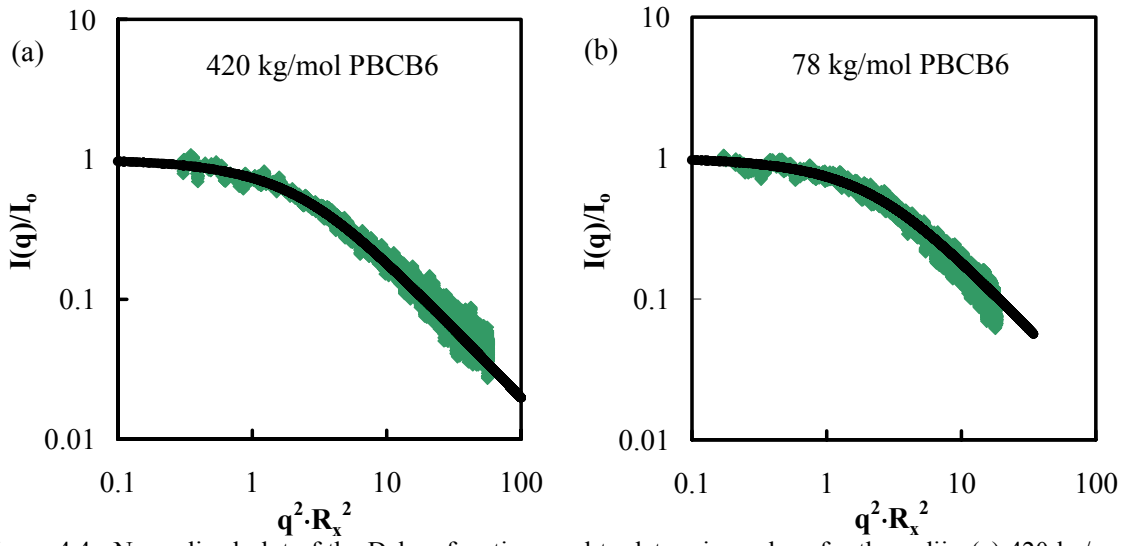

Figure 4.4. Normalized plot of the Debye function used to determine values for the radii. (a) 420 kg/mol PBCB6 and (b) 78 kg/mol PBCB6 dissolved in D5CB.

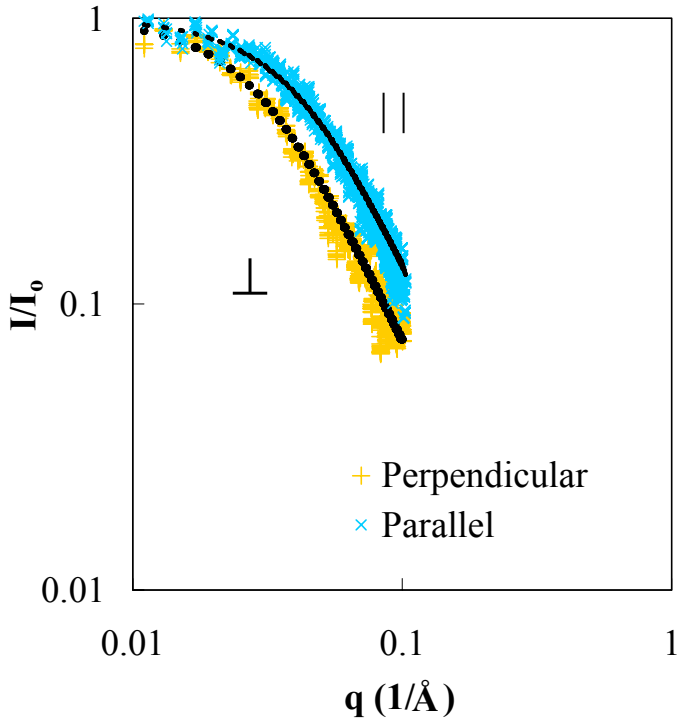

Figure 4.5. Plot of data points near the parallel and perpendicular directions used to confirm values for the radii. SANS for 5% 78 kg/mol PBCB6 in D5CB.

SANS results were obtained for a molar mass series of PBCB6 ranging from 78 kg/mol up to 420 kg/mol, Table 4.1. The spacer length is also varied from 4 to 8 carbons and the radii are reported for all but the samples PBCB8 and PBCB5 [27]. For these two

samples, unusually large values of R_x are linked to a high polydispersity resulting from cross-linking; therefore, these values are not reported.

Polymer Sample	M_n (kg/mol)	$R_\perp$ (Å)	$R_{//}$ (Å)	$R_\perp/R_{//}$	$R_{\perp b}$ (Å)	$R_{//b}$ (Å)	$R_{\perp b}/R_{//b}$
PBCB4	388	64±6	42±4	1.52±0.05	64±6	41±4	1.56±0.05
PBCB5[a]	404			1.52±0.15			1.57±0.15[b]
PBCB6	78	29±4	21±3	1.42±0.05	29±4	18±3	1.64±0.05
PBCB6	139	32±4	22±3	1.42±0.05	31±4	20±3	1.60±0.05
PBCB6	364	52±6	33±4	1.57±0.05	52±6	31±4	1.65±0.05
PBCB6	420	58±6	36±4	1.59±0.05	58±6	35±4	1.66±0.05
PBCB7	437	62±6	41±4	1.51±0.05	62±6	40±4	1.56±0.05
PBCB8[a]	453			1.5±0.1			1.54±0.1[b]

Table 4.1. Neutron scattering results. In this table, $R_\perp$ and $R_{//}$ represents the quadratic characteristic size of the polymer including the effects of the side groups. $R_{\perp b}$ and $R_{//b}$ represent the radii of the backbone only, calculated using Eqs. 4.18 and 4.19. Molar masses were computed assuming 100% attachment of mesogen to the 1,2-polybutadiene pre-polymer. [a] Some of the data for the samples PBCB5 and PBCB8 were omitted since these polymers had high PDIs of ~1.9 and ~2.2, respectively. [b] This anisotropy was estimated based on $R_\perp$=61 Å.

4.4 Chain Dimensions by Multi-Angle Laser Light Scattering.

The radius of gyration of the PBCB6 polymers and of the 1,2-polybutadiene pre-polymers was measured in tetrahydrofuran (THF) using multi-angle laser light scattering (MALLS). Gel permeation chromatography (GPC) was carried out on two PLgel 5 μm mixed-C columns (Polymer Labs) connected in series with a DAWN EOS (MALLS) detector and an Optilab DSP differential refractometer (both from Wyatt Technology).

No calibration standards were used and *dn/dc* values were obtained for each injection assuming 100% mass elution from the columns.

In the isotropic THF solution the quadratic characteristic size of the SGLCP is greater than that of the prepolymer, and both are greater than either of the dimensions of the SGLCP in the nematic LC D5CB, indicating better solubility of the polymer in THF, Table 4.2. Comparison of the SGLCPs versus the corresponding 1,2-polybutadienes indicates that the addition of the side group increases the radii significantly. This increase is caused by decreased backbone flexibility and by the added bulk of the side group. It will be shown, that at the large molecular weights of our polymers, the additional contributions to the radii from the side groups is very small; therefore, the increase in radii after attachment of the mesogen is primarily due to a decrease in the backbone flexibility.

Polymer Sample	[a]M_n (kg/mol)	$R_x = \frac{R_g}{\sqrt{3}}$ (Å)	PDI	[b]Pre-Polymer R_x (Å)
PBCB4	388	71±20	1.16	81±10
PBCB6	78		1.14	35±10
PBCB6	364	73±20	1.13	77±10
PBCB6	420	107±20	1.09	81±10
PBCB7	437	126±20	1.09	81±10

Table 4.2. MALLS results. [a] The molar masses listed in this table are those calculated based on 100% attachment of the mesogen to the backbone [27]. [b] Because of the large uncertainty in the measured radii of the 1,2-polybutadiene pre-polymer the numbers listed are based on a fit to $R_x \propto \sqrt{M_w}$ from a set of eight polymer samples.

4.5 Discussion

4.5.1 Origin of Molecular Weight-Dependent Anisotropy

The observed anisotropy of PBCB6 increases with chain length, Fig. 4.2. A molecular weight dependence of the backbone anisotropy is not expected for the polymers in this molecular weight series which are all long enough so that their conformation can be described by a Gaussian distribution in a direction either parallel or perpendicular to the director. For very small molecular weights, i.e., oligomers, the backbone behaves more like a rod than a freely jointed chain. For a large Gaussian polymer coil, the ratio of chain fluctuations parallel and perpendicular to the director should be independent of molecular weight and the anisotropy of the polymer should remain constant [11, 12, 13]. A Gaussian chain conformation is present as evidenced by a slope of -1 in the high q range on a plot of $I(q)/I_o$ versus $q^2 \cdot R_g^2$ [31], Fig. 4.4.

O'Allest et al. [38] found a nematic main chain liquid crystal polymer, for which a constant backbone anisotropy was achieved for molar masses above ~15 kg/mol. Similarly, Shibaev et al. [39] found the backbone anisotropy of a smectic polyacrylate SGLCP to increase with molar mass until approximately 100 kg/mol was achieved. They attributed the constant anisotropy to the ability of the long backbone to obtain a statistical number of layer crossings. Being free from smectic layering, our system would be expected to achieve a constant backbone anisotropy at a much smaller molar mass than 100 kg/mol.

The explanation for the change in anisotropy in our SANS experiment is that the measured anisotropy combines contributions from the polymer backbone and the mesogenic units. In a nematic solution, the presence of ordered side groups contributes

to the scattering pattern differently parallel and perpendicular to the director. In the case of an LC polymer composed of just a few monomers, Fig. 6a, the prolate shape of the mesogenic groups can dominate [20, 21, 22]. As the molecular weight is increases, the backbone adopts an oblate conformation, which can counter balance the mesogenic units that are preferentially parallel to the director, causing an overall spherical conformation, Fig. 6b. Finally, at high molecular weights the overall polymer anisotropy is dominated by the backbone conformation, Fig. 6c.

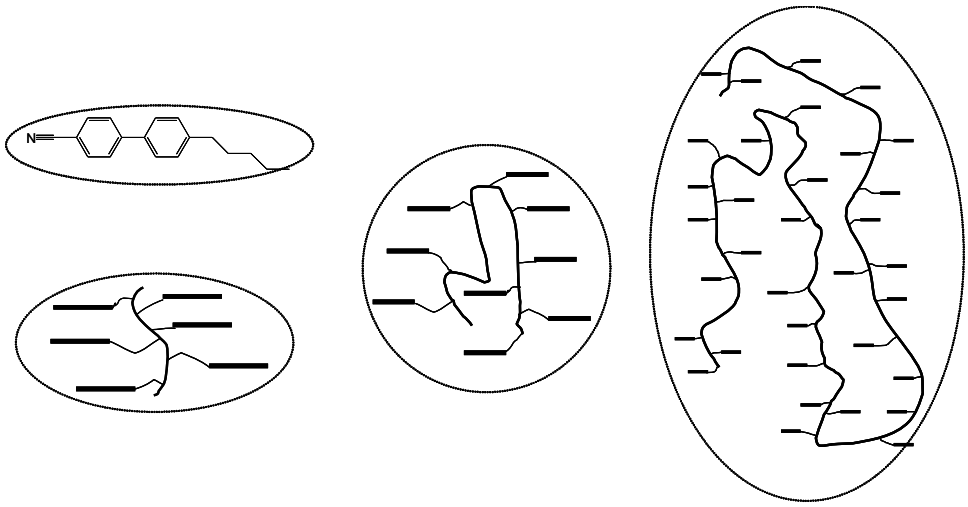

Figure 4.6. Schematic explanation of how the anisotropy of an oblate polymer can increase with increasing molecular weight.

Similar effects of pendant side groups have also been reported by Rawiso et al. [36] for polystyrene that was isotopically selectively labeled on either the backbone or on the phenyl ring. To explain the anomalous SANS patterns that resulted, they approximated the polystyrene molecule as a curved cylinder and accounted for the scattering of the side groups as a distribution of scattering length density around the axis of the cylinder. We follow a procedure similar to that used by Rawiso et al. [36] to model the scattering from

the mesogenic groups. Here we treat the polymer as a three-component particle (consisting of a backbone, a mesogenic unit, and spacer) and calculate the scattering length densities (δ) of the components as

$$\delta = \frac{\rho N_A \sum_k b_k}{M}, \quad (4.5)$$

where N_A is Avagadro's number, M is the component molar mass, ρ is the component density and b_k is the scattering length density of the k^{th} atom. The contribution of the different components to the total scattering is related to the contrast ($K=\delta_{D5CB}-\delta$) in their scattering length densities according to

$$I_{total}(q) = K_B^2 I_B(q) + K_M^2 I_M(q) + K_S^2 I_S(q) + 2K_B K_M I_{BM}(q) + 2K_B K_S I_{BS}(q) + 2K_S K_M I_{SM}(q), \quad (4.6)$$

The subscripts B, M and S refer to the backbone, mesogen and spacer, respectively; and BM, BS, and SM refer to cross terms. The calculated values of K and δ are listed in Table 4.3 along with the estimates of the component densities used for the calculations. Relative to D5CB, the scattering contrast in the spacer and the backbone, K_S=5.51 and K_B=5.57, are somewhat greater than the mesogenic unit, K_M=3.76. Furthermore, the component $I(q)$ values are related to the component sizes, which makes the contributions from the backbone less significant and the spacer and mesogenic unit contributions very significant.

Component	M (g/mol)	ρ (g/cm^3)	δ 10^{10} (cm^{-2})	$K=(\delta_{D5CB}-\delta)$ 10^{10} (cm^{-2})
PBCB6	363.5	0.95	1.36	4.63
Mesogen Including Oxygen	194.2	1	2.22	3.76
PBCB6 Spacer no Mesogen	142.2	0.9	0.472	5.51
Backbone	27.0	0.9	0.415	5.57
95% D5CB	267.5	1.08	5.98	0

Table 4.3. Calculation of PBCB6 component scattering length densities

4.5.2 Mathematical Compensation for Side-Group Scattering

In a solution, the radius of gyration of a polymer is typically defined as [40],

$$R_g{}^2 \equiv \frac{1}{N+1}\left\langle \sum_{j=0}^{N} \left(\vec{r}_j - \vec{r}_G\right)^2 \right\rangle, \quad (4.7)$$

with

$$\vec{r}_G \equiv \frac{1}{N+1}\left\langle \sum_{j=0}^{N} \vec{r}_j \right\rangle. \quad (4.8)$$

Here $\vec{r}_G$ represents the position vector of the center of gravity of the chain, $\vec{r}_j$ represents the position vector of the j^{th} segment of the polymer backbone, and the brackets indicate a statistical average over all polymer conformations. In a liquid crystalline system, the chain conformation is anisotropic with an axis of symmetry along the director, $\vec{n}$. For studies of SGLCPs in which labeling for neutron scattering contrast is localized on the

chain backbone, Eq. 4.7 can be rewritten to describe an anisotropic configuration using the quadratic characteristic size of the backbone *(R_{xb}),*

$$R_{xb}{}^2 \equiv \frac{1}{N+1}\left\langle \sum_{j=0}^{N}\left(\vec{r}_j \cdot \vec{x} - \vec{r}_G \cdot \vec{x}\right)^2 \right\rangle, \quad (4.9)$$

where $\vec{x}$ is a unit vector in an arbitrary direction. Here we take the further step of accounting for scattering from pendant groups on an SGLCP. We consider each monomeric unit as a set of *M* scatterers, instead of a single scatterer on the backbone, Fig. 4.7. This is accomplished by changing the summation in Eq. 4.9 to include scattering from each of *M* scatterers in the pendant group:

$$R_x{}^2 \equiv \frac{1}{N+1}\left\langle \sum_{j=0}^{N}\frac{1}{M}\sum_{k=0}^{M}\left(\vec{r}_{jk} \cdot \vec{x} - \vec{r}_G \cdot \vec{x}\right)^2 \right\rangle. \quad (4.10)$$

Here, $\vec{r}_{jk}$, is the position vector of the k^{th} scatterer on the j^{th} side group, and R_x is the quadratic characteristic size in the $\vec{x}$ direction including the effects of the bulky side group as observed by neutron scattering. If the j^{th} side group is described as having an orientation unit vector $\vec{u}_j$ with an effective length L_j, and if one assumes the scatterers are spaced evenly and contribute equally to the total intensity, then,

$$\vec{r}_{jk} = \vec{r}_j + \frac{kL_j\vec{u}_j}{M}, \quad (4.11)$$

and

$$R_x{}^2 \equiv \frac{1}{N+1}\left\langle \sum_{j=0}^{N}\frac{1}{M}\sum_{k=0}^{M}\left(\vec{r}_j \cdot \vec{x} + \frac{kL_j\vec{u}_j}{M} \cdot \vec{x} - \vec{r}_G \cdot \vec{x}\right)^2 \right\rangle. \quad (4.12)$$

In the limit as M becomes large, the side group can be modeled as a uniform distribution of scattering length density instead of as discrete scatterers, the summation can be approximated as an integral

$$R_x^{\,2} \equiv \frac{1}{N+1}\left\langle \sum_{j=0}^{N} \frac{1}{L_j} \int_0^{L_j} \left(\vec{r}_j \cdot \vec{x} + y\vec{u}_j \cdot \vec{x} - \vec{r}_G \cdot \vec{x}\right)^2 dy \right\rangle, \quad (4.13)$$

where $y=kL_j/M$. This assumption is valid since, as shown earlier, the scattering contrast of the different components are similar. Within this mathematical framework, the greater scattering density contrast of the spacer relative to the mesogen will cause the effective length L_j to be slightly smaller in SANS experiments. This factor is small enough so that the uncertainty in measurement should be greater than the uncertainty due to this approximation.

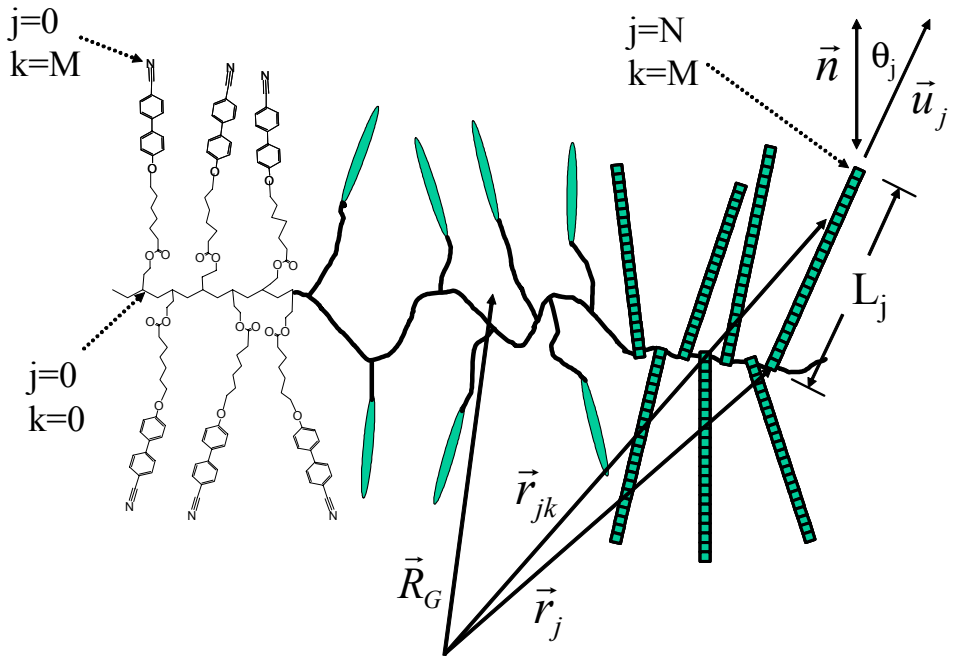

Figure 4.7. Schematic of PBCB6 showing the definitions of the variables used in the calculations. From left to right the schematic shows different levels of detail of an SGLCP: chemical structure, schematic structure, and the mathematical structure used for this study.

Integrating Eq. 4.13 and noting that

$$\frac{1}{N+1}\left\langle \sum_{j=0}^{N} L_j \vec{u}_j \cdot \vec{x}\left(\vec{r}_j - \vec{r}_G\right)\cdot \vec{x} \right\rangle = 0 , \quad (4.14)$$

yields

$$R_x{}^2 \equiv \frac{1}{N+1}\left\langle \sum_{j=0}^{N}\left[\left(\vec{r}_j \cdot \vec{x} - \vec{r}_G \cdot \vec{x}\right)^2 + \frac{\left(L_j \vec{u}_j \cdot \vec{x}\right)^2}{3} \right] \right\rangle , \quad (4.15)$$

The first term in this equation equals the characteristic size of the polymer backbone, Eq. 4.9. Here we use the subscript "b" to emphasize the fact that this term represents the radius one would measure if only the backbone was labeled,

$$R_x{}^2 = R_{xb}{}^2 + \left\langle \frac{\left(L_j \vec{u}_j \cdot \vec{x}\right)^2}{3} \right\rangle . \quad (4.16)$$

The second term in Eq. 4.16 represents the average, over the length of the polymer chains, of the squared extension of the side group in the $\vec{x}$ direction. In uniaxial liquid crystals the order parameter, *S*, is defined by

$$S = \frac{1}{2}\left\langle 3\cos^2\theta_j - 1 \right\rangle , \quad (4.17)$$

Here θ_j is the angle of an individual mesogen relative to the director and, in our case, a mesogenic side group of the SGLCP. If one assumes that the order parameter takes variations in the effective mesogen length and orientation into account, then

$$\left\langle \left(L_j \vec{u}_j \cdot \vec{x}\right)^2 \right\rangle = L^2 \left\langle \cos^2\theta \right\rangle , \quad (4.18)$$

when $\vec{x}$ is parallel to the director, and

$$\left\langle \left(L_j \vec{u}_j \cdot \vec{x}\right)^2 \right\rangle = \frac{1}{2} L^2 \left\langle \sin^2\theta \right\rangle , \quad (4.19)$$

when $\vec{x}$ is perpendicular to the director. The factor of ½ is present in Eq. 4.19 since there are two orthogonal axes perpendicular to the director and the squares of the projections of the director on the three axes must add up to 1. In terms of the order parameter and the ensemble averaged length of the side group, *L*, Eq. 4.16 yields

$$R_{||}^{\ 2} = R_{||b}^{\ 2} + \frac{L^2(2S+1)}{9}, \quad (4.20)$$

and

$$R_{\perp}^{\ 2} = R_{\perp b}^{\ 2} + \frac{L^2(1-S)}{9}, \quad (4.21).$$

In the nematic liquid crystal 5CB, an order parameter of ~0.57 is found at temperatures of ~25 ^{o}C [41]. Our refractive index measurements [Section 2.2.4] indicate that the order parameter was not significantly changed by the addition of polymer, therefore S=0.57 can be assumed for our solutions. Eqs. 4.20 and 4.21 indicate that the change in the measured radius due to the mesogenic groups is greater in the parallel direction than in the perpendicular direction. Also, since the effects of the mesogen add to the square of the radius of the backbone, this change will be greater for smaller radii or for lower molecular weights. Therefore, when the mesogenic units are accounted for in an oblate polymer, a greater difference between the anisotropy of the backbone ($R_{\perp b}/R_{//b}$) as compared to the whole molecule ($R_{\perp}/R_{//}$) is seen for lower molecular weight polymers than for higher molecular weights.

Using the software package MacSpartan, approximate values of 20, 22, and 23Å were obtained for the length of the mesogenic unit in the polymers PBCB4, PBCB6, and PBCB7, respectively. Using these, along with *S*=0.57, values for the backbone radii of

the polymers were obtained using Eqs. 4.20 and 4.21, Table 4.1. Once this effect is taken into account, so that one is considering the conformation of the backbone without the mesogenic units, the polymer anisotropy is $R_{\perp b}/R_{//b}\approx 1.6\pm 0.5$ for all the polymers.

In our thermal studies of these polymers [Section 2.2.2], we found that in the melt state there was only a weak odd-even effect with spacer length for the enthalpy of the isotropic to nematic transition. We typically observed slow trends toward stronger nematic order and higher transition temperatures as the spacer length was increased. Therefore, the solution properties of this polymer series would not be expected to have significant odd-even effects either. The polymers PBCB4, PBCB5, PBCB7, and PBCB8 are made from the same 63 kg/mol 1,2-polybutadiene prepolymer as the 420 kg/mol PBCB6 polymer. Since all these polymers have the same degree of polymerization and are expected to have only weak trends in the measured radii as the length of the spacer is increased, it is not surprising that they all have a similar anisotropy of $R_{\perp b}/R_{//b}\approx 1.6\pm 0.5$. The deviations of the measured backbone anisotropies from the average value are primarily due to experimental uncertainty, with some variability caused by intermolecular cross-links and an accompanying increase in polydispersity.

The absence of trends with spacer length is analogous to the results of Gu et al. [42], when studying the effects of spacer length on the director relaxation rate for a series of SGLCPs dissolved in 5CB. They found that for either very small or very large spacer lengths, the effect on the relaxation rate was the greatest, but for intermediate lengths there was no dependence on spacer lengths. This is similar to our system in that we are also at an intermediate spacer length where the mesogens are sufficiently decoupled from

the backbone to have only negligible differences in their effect on the backbone anisotropy.

4.5.3 Comparison with Literature on Liquid Crystalline Polymer Melts

We have applied this method of accounting for the effects of scattering from side-groups in SGLCPs to the melt studies of other researchers and will demonstrate how it explains inconsistencies in their measured anisotropy. Using a poly(methylsiloxane) where different parts of the side group were selectively deuterated, Fig. 4.8, Hardouin et al. [21], Moussa et al. [22], Pepy et al. [23], and Noirez et al. [24] found some dependence of the polymer anisotropy on molecular weight and on the location of the deuterium label. For the sample with DP=35, in both the nematic and smectic phases the polymer conformation was prolate with equal anisotropies of $R_{\perp}/R_{//} \approx 0.75$. This is unexpected for two reasons. First, in smectic SGLCPs the polymer backbone is primarily located in the space between the layers with infrequent crossings resulting in the backbone taking on an oblate conformation [39]. Second, in end-on SGLCPs the anisotropy of the nematic phase is usually lower than in the smectic phase.

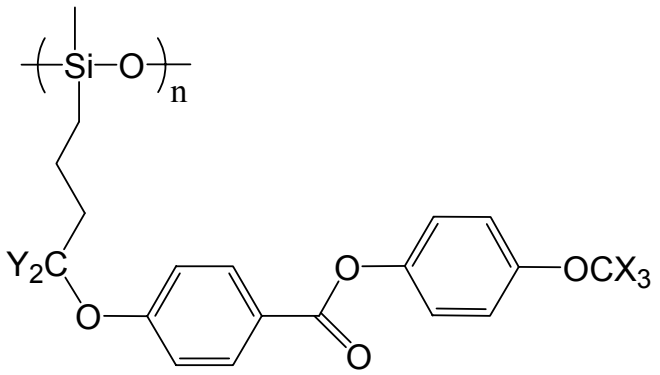

Figure 4.8. Polymer used by Hardouin et al. [21], Moussa et al. [22], and Pepy et al. [23] with (*X*=D, *Y*=H); and by Noirez et al. [24] with (*X*=H, *Y*=D).

When Hardouin et al. [21] and Pepy et al. [23] used a polymer with DP=80, the effects of the side group were less important and more typical results were obtained. They measured an anisotropy of $R_{\perp}/R_{//} \approx 1.61$ and $R_{\perp}/R_{//} \approx 0.95$ in the smectic and nematic phases, respectively. This anisotropy for the smectic phase is small, but still reasonable, and a transition from an oblate to a prolate conformation is possible but unusual [43].

The same reasoning applied to the PBCBx system can be applied to this siloxane-based system by modifying Eq. 4.10 to approximate the scattering from the polymer as a single scatterer located at a position $\vec{u}\vec{x}l_j$ from the backbone of each chain segment.

$$R_x^{\,2} \equiv \frac{1}{N+1}\left\langle \sum_{j=0}^{N} \left(\vec{r}_j \cdot \vec{x} + l_j \vec{u}_j \cdot \vec{x} - \vec{r}_G \cdot \vec{x}\right)^2 \right\rangle, \quad (4.22)$$

In an analogous approach, a similar result to Eq. 4.16 is found,

$$R_x^{\,2} = R_{xb}^{\,2} + \left\langle \left(l_j \vec{u}_j \cdot \vec{x}\right)^2 \right\rangle, \quad (4.23)$$

At this point, we have produced nearly the same equation to account for the labeling as Noirez et al. [24]. They, however, did not take into account the order parameter. This allowed them to demonstrate qualitative agreement between the measured anisotropy and their model. To obtain quantitative agreement between the model and the data, we take into account the order parameter, Eq. 4.17, as before.

$$R_{||}^{\,2} = R_{||b}^{\,2} + \frac{l^2(2S+1)}{3}, \quad (4.24)$$

and

$$R_{\perp}^{\ 2} = R_{\perp b}^{\ 2} + \frac{l^2(1-S)}{3}. \quad (4.25)$$

Hardouin et al. [21], Moussa et al. [22], and Pepy et al. [23] used the Guinier approximation, Eq. 4.1, to calculate the quadratic characteristic size. This equation is derived for any arbitrary set of scatterers, in the range where $q \cdot R_x < 1$, and can be applied to Eqs. 4.24 and 4.25 without any further assumptions.

An estimated value for the smectic order parameter, S_S=0.85, was obtained by comparison with a polymethacrylate [44] SGLCP with a similar structure at approximately 12 ^{o}C below its smectic to nematic transition temperature (T_{sn}). The nematic order parameter S_n=0.6 was estimated as the average value found by Demange et al. [45] using a polymethacrylate SGLCP. Labeling distances of l=17 and l=4, from Casquilho and Volino [25] corresponding to labeling on the terminal methoxy group and the spacer group, respectively, were used.

After the application of these values using Eqs. 4.24 and 4.25, more reasonable values for the anisotropy of the backbone were obtained, Table 4.4. In the smectic phase the anisotropy $R_{\perp b}/R_{//b}$=1.37 and 2.06 for a DP=35 and 80, respectively. These two values are not equal as one might expect, but this could be due to one of two reasons. First of all, the uncertainty in the measurements of the radii is ±3Å which, especially for the small polymer, could result in a large uncertainty. Secondly, the polymer may be too small to approach a steady-state high molecular weight value for the anisotropy. This second explanation fits well with the observations of Shibaev et al. [39] using polymethacrylates with a similar mesogenic group, that in the smectic phase the

anisotropy increased with molar mass and that the steady-state anisotropy was not reached until molar masses greater than 100 kg/mol were approached.

DP	[a]Temp. (°C)	Phase	$R_{\perp}$ (Å)	$R_{//}$ (Å)	$R_{\perp}/R_{//}$	$R_{\perp b}$ (Å)	$R_{//b}$ (Å)	$R_{\perp b}/R_{//b}$
35[b]	60	S	14.6±3	19.2±3	0.76	14.1	10.3	1.37
35[b]	88	N	14.4±3	19.6±3	0.74	13.0	13.0	1.00
80[b]	56	S	41.2±3	25.7±3	1.61	41.1	19.9	2.06
80[c]	85	N			1.12±0.1[d]			1.13±0.1[e]
80[b]	95	N	27.0±3	28.5±3	0.95	26.3	24.5	1.07

Table 4.4. Hardouin et al. [21], Pepy et al. [23], and Noirez et al. [24] data adjusted for side-group deuteration. [a] Data points for the polymer with a *DP* of 80 at temperatures of 70 and 82 °C were omitted because they both did not fit the trends for a transition between a nematic and a smectic phase and they had large inconsistencies with the measurements by Noirez et al. [24] at 85 °C. [b] Hardouin et al. and Pepy et al. data. [c] Noirez et al. data. [d] In Noirez et al. [24] the numerical value of the anisotropy was not given in the text, it was estimated by noting that the scattered intensity is a function of $I(q \cdot R_x)$. Therefore, by estimating the ratio of the slopes in Fig. 12 of Noirez et al., an estimation of the anisotropy was obtained similar to Casquilho and Volino [25]. [e] This estimate was obtained by assuming a value for $R_{\perp}$=27 Å.

In the nematic phase, the anisotropy is $R_{\perp b}/R_{//b}$=1.00 and 1.07 for *DP*=35 and 80, respectively, when the polymer is labeled on the terminal methoxy group. When the labeling is on the spacer group, a more reliable anisotropy is measured, $R_{\perp b}/R_{//b}$=1.13, where the effects of the labeling position only change the anisotropy by +0.01. The discrepancy between the anisotropy for terminal versus spacer labeling is most likely due to the ±3Å variability in the measurements of the radii. This method for accounting for the scattering due to the mesogenic units explains the inconsistencies due to the choice of labeling in this polymer.

4.6 Conclusions

This study demonstrates a way in which the radii of an SGLCP in a nematic solvent can be measured at low concentration while maintaining adequate scattering intensity. In melt studies, a 50:50 mixture of polymer with deuterium labeling on the backbone is typically used. For solution studies, concentrations of approximately 5% polymer were used to avoid interchain scattering. If a deuterated solvent is used, the amount of labeling per chain is increased by a factor of 8 to 10. The effects of these two conditions serve to cancel each other out to give scattering that is comparable with typical 50:50 mixtures. This method could also be used on a 50:50 mixture of perdeuterated and hydrogenated polymer resulting in greatly increased signal strength.

A polymer analogous synthetic approach enabled us to create a model series of large SGLCPs with narrow molecular weight distributions, matched backbone lengths and varied side groups. For the spacer lengths from 4 to 8 carbons an oblate conformation was found using SANS with a perdeuterated solvent, D5CB. Using a molecular weight series from DP≅220 to 1150 we show that the overall anisotropy increases with increasing molecular weight for oblate SGLCPs that are long enough to have a Gaussian-random coil conformation. Theories [11, 12] have predicted that for low molecular weights the backbone is modeled as a stiff rod but that as the molecular weight increases the polymer adopts a Gaussian conformation which should result in a backbone anisotropy that is independent of molecular weight. These theories only consider the conformation of the backbone; whereas SANS due to an unlabeled SGLCP in a deuterated solvent, measures scattering arising from the entire molecule. By taking into

account the contribution of the side groups to the scattering, Eqs. 4.20 and 4.21, the increase in the measured anisotropy can be explained and the radii, $R_{\perp b}$ and $R_{//b}$ can be determined.

The experimental method addresses the need for measurements of the radii of gyration of SGLCPs in nematic solvents to test predicted relationships between chain anisotropy and effects of SGLCP on the Leslie-Ericksen viscosity parameters. Due to the difficulty of measuring the polymer anisotropy in a nematic solution, very little work has been done in this area; but by using perdeuterated solvents with SGLCPs comparison of the Brochard theory with experiments is more easily accomplished.

Bibliography

[1] F. J. Brochard, *J. Polym. Sci., Polym. Phys*. **17**, 1867 (1979).
[2] H. Mattoussi, M. Veyssie, C. Casagrande, and M. A. Guedeau, *Mol. Cryst. Liq. Cryst*. **144**, 211 (1987).
[3] A. M. Jamieson, D. F. Gu, F. L. Chen, and S. Smith, *Prog. Polym. Sci*., **21**, 981 (1996).
[4] P. Y. Liu, N. Yao, and A. M. Jamieson, *Macromolecules* **32**, 6587 (1999).
[5] Y. C. Chiang, A. M. Jamieson, Y. Zhao, A. M. Kasko, and C. Pugh, *Polymer* **43**, 4887 (2002).
[6] Y. C. Chiang, A. M. Jamieson, S. Campbell, T. H. Tong, N. D. Sidocky, L. C. Chien, M. Kawasumi, and V. Percec, *Polymer* **41**, 4127 (2000).
[7] N. Yao and A. M. Jamieson, *Macromolecules* **30**, 5822 (1997).
[8] M. D. Kempe and J. A. Kornfield, *Phys. Rev. Let*. **90**, 115501 (2003).
[9] H. Mattoussi, *Mol. Cryst. Liq. Cryst*. **178**, 65 (1990).
[10] H. Mattoussi, R. Ober, M. Veyssie, and H. Finkelmann, *Europhys. Lett*. **2**, 233 (1986).
[11] X. J. Wang, M. Warner, *J. Phys. A, Math. Gen.* **20**, 713 (1987).
[12] P. L. Maffetone and G. Marrucci, *J. Rheol*. **36,** 1547 (1992).
[13] D. R. M. Williams and A. Halpern, *Macromolecules*, **26**, 2025 (1993).
[14] G. A. Carri and M. Muthukumar, *J. Chem. Phys.*, **109**, 11117 (1998).
[15] F. F. D'Allest, P. Maissa, A. T. Bosch, and P. Sixou, *Phys. Rev. Lett*. **61**, 2562 (1988).
[16] H. Mattoussi and R. Ober, *Macromolecules* **23**, 1809 (1990).
[17] A. S. Cherodian, N. J. Hughes, R. M. Richardson, M. S. K. Lee, and G. W. Gray, *Liq. Cryst*. **14**, 1667 (1993).
[18] L. Noriez and G. Pepy, *Phy. Scr*. **T25**, 102 (1988).
[19] R. G. Kirste and H. G. Ohm, *Makromol. Chem., Rapid Commun*. **6**, 179 (1985).
[20] G. Pepy, J. P. Cotton, F. Hardouin, P. Keller, M. Lambert, F. Moussa, L. Noirez, A. Lapp, and C. Strazielle, *Makrolmol. Chem., Macromol. Symp.* **15**, 251 (1988).
[21] F. Hardouin, L. Noirez, P. Keller, M. Lambert, F. Moussa, and G. Pepy, *Mol. Cryst. Liq. Cryst.,* **155**, 389 (1988).
[22] F. Moussa, J. P. Cotton, F. Hardouin, P. Keller, M. Lambert, G. Pepy, M. Mauzac, and H. Richard, *J. Physique* **48**, 1079 (1987).

[23] G. Pepy, L. Noirez, P. Keller, M. Lambert, F. Moussa, J. P. Cotton, C. Strazielle, A. Lapp, F. Hardouin, M. Mauzac, and H. Richard, *Makromol. Chem*. 191 1383 (1990).
[24] L. Noirez, P. Keller, and J. P. Cotton, *Liq. Cryst*. **18**, 129 (1995).
[25] J. P. Casquilho and F. Volino, *Mol. Cryst. Liq. Cryst*., **180B**, 357 (1990).
[26] M. D. Kempe, M. L. Auad, J. A. Kornfield, S. T. Wu, and W. J. Zhou, Manuscript in preparation.
[27] M. D. Kempe, J. A. Kornfield, C. K. Ober, S. D. Smith, *Macromolecules*, **00**, 000 (2003) Manuscript in Preparation.
[28] E7 and E44 are cyanobiphenyl-based eutectic mixtures composed primarily of the liquid crystals 5CB and 5OCB.
[29] S. T. Wu, Q. H. Wang, M. D. Kempe, and J. A. Kornfield, *J. Appl. Phys*. **92**, 7146 (2002).
[30] J. P. Cotton and F. Hardouin, *Prog. Polym. Sci*. **22**, 795 (1997).
[31] G. A. Carri and M. Muthukumar, *J. Chem. Phys.*, **109**, 11117 (1998).
[32] J. S. Higgins and H. C. Benoit, *Polymers and Neutron Scattering*; Oxford University Press, Oxford, (1996).
[33] P. Keller, B. Carvalho, J. P. Cotton, M. Lambert, F. Moussa, and G. Pepy, *J. Physique Lett*. **46,** L-1065 (1985).
[34] L. Noirez, C. Boeffel, and A. D. Aladine, *Phys Rev. Lett*. **80**, 1453 (1998).
[35] A. B. Kunchenko and D. A. Svetogorsky, *Liq. Cryst.* **2**, 617 (1987).
[36] M. Rawiso, R. Duplessix, and C. Picot, *Macromolecules* **20**, 630 (1987).
[37] R. M. Richardson, G. W. Gray, and A. R. Tajbakhsh, *Liq. Cryst*., **14**, 871 (1993).
[38] J. F. O'Allest, P. Sixou, A. Blumstein, R. B. Blumstein, J. Teixeira, and L. Noirez, *Mol. Cryst. Liq. Cryst*., **155**, 581 (1988).
[39] V. P. Shibaev, E. B. Barmatov, T. Yongjiee, R. Richardson, *Polymer Science*, **42**, 1680 (2000).
[40] J. D. Cloizeaux and G. Janink, *Polymers in Solution*; Claredon Press, Oxford, (1990).
[41] W. Guo, B. M. Fung, *J. Chem. Phys*. **95**, 3917 (1991).
[42] D. F. Gu, S. R. Smith, A. M. Jamieson, M. Lee, and V. Percec, *J. Phys. II France* **3**, 937 (1993).
[43] L. Noirez, P. Keller, P. Davidson, F. Hardouin, and J. P. Cotton, *J. Phys. France* **49**, 1993 (1988).
[44] J. C. Wittmann, S. Meyer, P. Damman, M. Dosiere,and H-W. Schmidt, *Polymer* **39**, 3545 (1998).
[45] V. F. Demange, F. Boue, A. Brulet, P. Keller, and J. P. Cotton, *Macromolecules* **31**, 801 (1998).

Chapter 5 Unprecedented Shear Alignment Behavior of Nematic Solutions Induced by Ultra-Long Side-Group Liquid Crystalline Polymers

This chapter is composed of the text and figures of a paper that was co-authored by Michael D. Kempe and Julia A. Kornfield at the California Institute of Technology [1]. The text and figures presented here were reprinted with permission from M. D Kempe and J. A. Kornfield, *Physical Review Letters* **90**, 115501, (2003).

5.1 Why Is the Tumbling Parameter Important?

The effects of polymeric materials on the orientation and dynamics of liquid crystals (LC) are used to enhance the performance and fabrication of electro-optic devices by conferring desired alignment, mechanical stability, or viscosity. Polymers are used in conjunction with LCs as alignment layers, polymer-dispersed LCs [2, 3], polymer-stabilized LCs [4, 5], polymer LC gels [6, 7], and polymers dissolved in LC hosts [8, 9]. Therefore, the coupling of orientation and dynamics between polymers and liquid crystals is of great interest. Here we focus on polymers that are dissolved in an LC host and probe the coupling between them by examining the orientational response during shear.

In nematic LCs the orientational distribution of the molecules is uniaxial with a preferred orientation called the "director." The flow behavior of nematic LCs are rich due to the transient response of the director. For example, if initially aligned along the gradient direction, inception of shear causes the director of all known calamitic (i.e., rod-

shaped as opposed to disc-shaped, "discotic" LCs) nematic liquid crystals to rotate in the same direction as the vorticity, analogous to rod-like particles in suspension. However, the constraints of thermodynamics and the symmetry of the fluid admit the possibility that the nematodynamic torque could rotate the director in the opposite direction. Here we provide the first report of such behavior.

Two classes of behavior, flow-aligning and tumbling, of the nematic director occur under the influence of shear. Under deformations fast enough that viscous effects dominate over elastic effects, Ericksen's transversely isotropic fluid (TIF) model [10, 11] can describe the evolution of the director

$$\frac{D\vec{n}}{Dt} = \vec{n} \cdot \underline{\underline{\omega}} + \lambda\left(\vec{n} \cdot \underline{\underline{d}} - \vec{n}\vec{n}\vec{n} : \underline{\underline{d}}\right). \quad (5.1)$$

Here, $\underline{\underline{d}}$ is the symmetric part of the velocity gradient tensor and $\underline{\underline{\omega}}$ is the vorticity tensor. The tumbling parameter, λ, of a given LC determines its response to an imposed strain. For values of $|\lambda|>1$ the LC is flow-aligning and will rotate under shear to a steady-state angle determined by λ. When $|\lambda|<1$ the LC is a tumbling nematic and the director continuously rotates in response to a shear strain.

Calamitic LCs typically have a tumbling parameter slightly greater than 1 [12] and adopt a steady-state angle close to the velocity direction. Occasionally, a calamitic LC will have a tumbling parameter between 0 and 1, usually associated with a nematic LC at a temperature near a smectic transition [13, 14, 15]. However, nematic discotic LCs are predicted to have tumbling parameters less than -1 [16, 17], in accord with experiment [18, 19]. Under a steady shear stress, the discotic director will align nearly parallel to the velocity gradient direction enabling the plate-like molecules to slide over each other.

Dissolving a polymer with an anisotropic conformation in a small-molecule LC host can affect the tumbling parameter. The rheological theory of Brochard [20] predicts changes in the viscosity coefficients as functions of the polymer anisotropy, concentration and relaxation time. In particular, this model predicts that oblate polymers ($R_{//} < R_{\perp}$) will reduce λ while prolate polymers will increase λ. These general predictions have been borne out: oblate SGLCPs have been shown to convert a flow-aligning host (λ>1) to a tumbling type, and main-chain liquid crystalline polymers can convert a tumbling host (0.1<λ<1) to flow-aligning (λ>1) [21].

Furthermore, Brochard predicts that if enough oblate polymer is added to a calamitic LC, the tumbling parameter can be made to fall below –1, resulting in alignment near the velocity gradient direction [22]. Despite more than two decades of research, this prediction has not been validated prior to this work. Values of λ only as low as ~0.7 [23] have been reached for a flow-aligning host [24, 25, 26]. Only in the high concentration limit of a polymer melt has λ<0 been observed [27, 28, 29]. Strikingly, prior investigations have been limited to relatively short polymers (degree of polymerization DP ≤100) [30]. By examining much longer chains (DP~1200) with comparable anisotropy to previous systems ($R_{\perp}/R_{//}$≈1.5) [31] much more dramatic effects are observed. In particular, we show that at modest concentration (>7.5 wt %) a conventional flow-aligning host (λ>1) can be converted to one that is flow-aligning with λ<-1.

5.2 Experimental Determination of λ for Large Liquid Crystalline Polymers

The polymer used in our study was synthesized with a 1,2-polybutadiene backbone by attaching a cyanobiphenyl-based mesogen to each pendant vinyl group, Fig. 5.1 [32, 33]. The details of the synthesis and characterization of this polymer will be published elsewhere [34]. Starting with an anionically produced 1,2-polybutadiene backbone of M_w=65,000 g/mol, a final polymer of M_w=440,000 g/mol was obtained with a low polydispersity ($M_w/M_n \cong 1.15$). This polymer was dissolved in the nematic solvent 4'-pentyl-4-cyanobiphenyl (5CB) at concentrations of 0.5% to 10% by weight. To do this, the polymer and LC were dissolved in dichloromethane and placed under vacuum at room temperature for two days to remove the dichloromethane leaving behind the polymer solutions in 5CB.

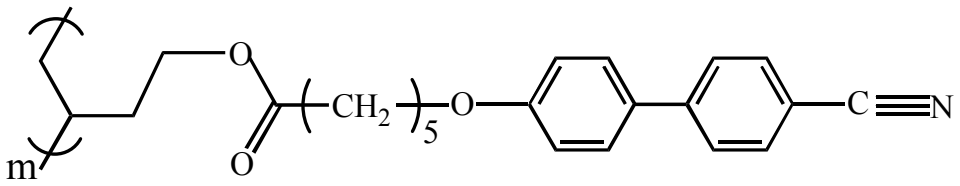

Figure 5.1. Side-group liquid crystalline polymer PBCB6.

Experimental determination of λ is based on a 2-D version of Ericksen's TIF model describing director motion that remains in the plane defined by the velocity and the velocity gradient directions [35]. This approximation is valid when the Ericksen number, $Er = h^2\dot{\gamma}(\alpha_3 - \alpha_2)/K_1$, which is the ratio of the viscous to elastic torques, is much greater than one. When Er>>1, rheological transients in nematic LCs are predicted to scale with

strain. To confirm the regime in which *Er*>>1, experiments with 5CB were performed at different strain rates and/or sample thicknesses. Typically [36], addition of polymer increases viscosity while leaving elasticity relatively unchanged, thereby increasing *Er*; therefore, shear rates that correspond to *Er* >>1 for 5CB all lie in the high *Er* regime for all our polymer solutions as well.

For director rotation the 2-D TIF model yields

$$\frac{\partial\theta}{\partial\gamma} = \frac{\left(\alpha_3 \sin^2\theta - \alpha_2 \cos^2\theta\right)}{\alpha_3 - \alpha_2}, \quad (5.2)$$

with the transient stress described in terms of an apparent viscosity given by

$$\eta_{app} \equiv \frac{\tau_{xy}}{\dot{\gamma}} = \left[\alpha_1 + \frac{(\alpha_2 + \alpha_3)^2}{\alpha_3 - \alpha_2}\right]\sin^2\theta\cos^2\theta + \frac{1}{2}(\alpha_3 + \alpha_4 + \alpha_6) - \frac{{\alpha_3}^2}{\alpha_3 - \alpha_2}. \quad (5.3)$$

Here, θ is the angle of the director measured relative to the velocity gradient, γ is the strain, and the α's are the Leslie-Ericksen viscous coefficients. Using Eq. 5.2 for small strains, measurement of $\theta(\gamma)$ can be used to determine the tumbling parameter

$$\lambda = \frac{\alpha_2 + \alpha_3}{\alpha_2 - \alpha_3} = 2\frac{\theta(\gamma)}{\gamma} - 1. \quad (5.4)$$

If the LC is of the flow-aligning type, then the magnitude of the steady-state angle, θ_{ss}, of the director under shear can also be used:

$$\lambda = -\frac{1}{\cos(2\theta_{ss})}. \quad (5.5)$$

For a tumbling nematic, integration of Eq. 5.2 yields

$$\tan(\theta) = \left(\frac{1+\lambda}{1-\lambda}\right)^{1/2} \tan\left(\frac{\gamma}{2}\sqrt{1-\lambda^2}\right). \quad (5.6)$$

From this, the period of the stress oscillations corresponding to a director rotation of 180^o, γ_p, can be used to determine the tumbling parameter using

$$\lambda = \pm\sqrt{1-\frac{4\pi^2}{\gamma_p^{\,2}}}\,. \quad (5.7)$$

Here, one must look at the transient stress response to determine the sign of λ. By inspection of Eq. 5.3 one can see that stress maxima occur when the director is at an angle of $\pm 45^o$ and that minima occur at 0^o or 90^o. Furthermore, Eq. 5.2 indicates that the relative rate of change of θ with strain is determined by α_2 or α_3 when the director is at 0^o or 90^o, respectively. Therefore, if $|\alpha_2|>|\alpha_3|$ the director will rotate faster at 0^o than it will at 90^o indicating a positive tumbling parameter or vice versa.

For the case where $|\lambda|>1$, flow-aligning, integration of Eq. 5.2 yields

$$\tan(\theta) = \pm\left(\frac{1+\lambda}{\lambda-1}\right)^{1/2}\tanh\left(\frac{\gamma}{2}\sqrt{\lambda^2-1}\right). \quad (5.8)$$

Using this expression for $\theta(\gamma)$, one can fit Eq. 5.3 to the rheological response and obtain a value for λ. Furthermore, inspection of this equation shows that the two different cases of flow-aligning nematic LCs are readily distinguished in their transient rheological response during inception of steady shear from an initially homeotropic monodomain $(\theta=0^o)$. For $\lambda>1$, the steady-state angle is in the range $45^o<\theta_{ss}<90^o$ and a stress overshoot occurs as θ rotates through $+45^o$. However, for $\lambda<-1$, θ_{ss} lies between -45^o and 0^o, so the stress monotonically increases as the director rotates from 0^o to θ_{ss}.

Here we use measurements of both $\theta(\gamma)$ and $\tau_{xy}(\gamma)$ to obtain two independent determinations of λ. In both conoscopy [25, 26, 35, 37] and rheology experiments, the

sample was placed between lecithin treated surfaces to promote perpendicular orientation of the director relative to the surfaces. For conoscopy, samples were placed between two parallel glass plates separated by 0.25 to 0.50 mm and viewed between crossed polarizers using a highly convergent beam of light. The observed interference figure is used to determine the angle of the director relative to the velocity gradient direction, θ [38]. The value of λ is determined from $\theta(\gamma)$ at small θ using Eq. 5.4, Fig. 5.2. For samples that are flow-aligning, the steady-state angle provides an alternate determination of λ, Eq. 5.5. In practice, the center of the interference figure only remains in the field of view at steady-state for samples with λ<-1; in this case the values of λ determined by Eqs. 5.4 and 5.5 gave consistent results that only differ by 0.04.

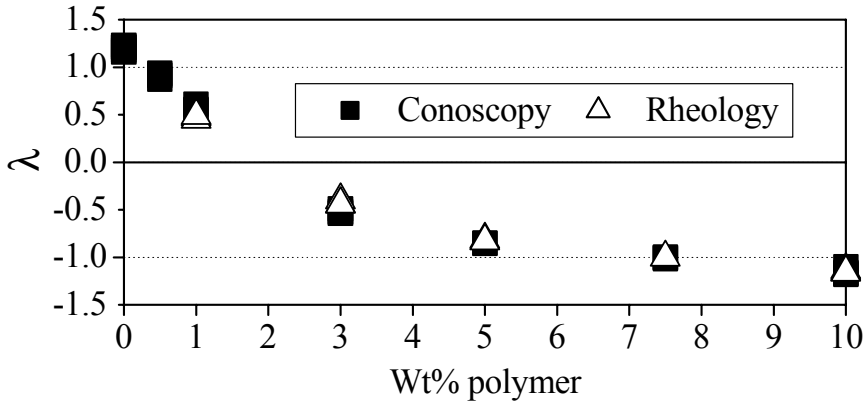

Figure 5.2. Rheological and conoscopic measurements of the tumbling parameter for PBCB6 dissolved in 5CB at 25 ^{o}C.

For the rheological determination of λ, a Rheometrics Fluids Rheometer was used with a 50 mm diameter cone and plate having a cone angle of 0.02 rad. The apparent viscosity was recorded as a function of strain during inception of steady shear. For the tumbling case the strain period, γ_p, was used in Eq. 5.7 to determine $|\lambda|$. The sign of λ

was determined by inspection of $\tau_{xy}(\gamma)$. Since our experiments were conducted with the director initially in the perpendicular position (θ=0°), the presence of a single stress maximum followed by two stress maxima closer together, e.g., Fig. 5.3(b), results from faster director movement at 0° than 90°. This indicates that $|\alpha_2|>|\alpha_3|$ and that the tumbling parameter is positive. Conversely, observing the first two peaks closer together indicates a negative tumbling parameter, e.g., Fig. 5.3c.

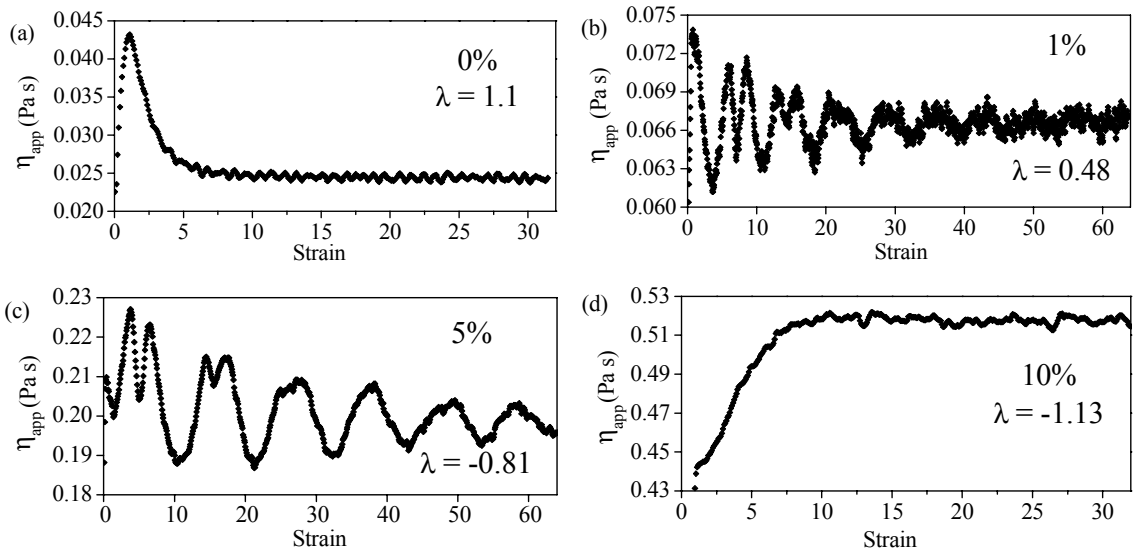

Figure 5.3. Transient response of (a) bulk 5CB and solutions containing (b) 1% (c) 5% and (d) 10% PBCB6. Strain rate was 16 s^{-1} at 25 °C.

At all concentrations of polymer, measurements of the tumbling parameter using both conoscopy and rheology gave consistent results. At 7.5 wt % polymer, even under shear strains as high as 20, the conoscopic image barely moves ($\lambda\approx$-1). This is in sharp contrast to bulk 5CB, for which the center of the conoscopic figure moves out of view after only 0.14 strain units. While performing conoscopic measurements with 7.5 wt % polymer at temperatures from 20 to 33 °C it was noted that the direction of deflection of the conoscopic image changed sign at 24 °C indicating that $\alpha_2 \cong 0$ and $\lambda \cong$ -1. This value

for λ produces a nematic solution that, in contrast to typical calamitic LCs, will align nearly parallel to the velocity gradient direction rather than the flow direction. To our knowledge, this is the first report of $\lambda \cong -1$ for a calamitic nematic system.

At 10 wt % polymer, the solution is distinctly flow-aligning with $\lambda<-1$, Fig. 5.3d. Conoscopic observation of $\theta(\gamma)$ gives $\lambda=-1.19$ based on the small strain response, Eq. 5.4. Under large strains a steady-state alignment angle of $\theta_{ss} = -15^{o}$ gives $\lambda=-1.15$, Eq. 5.5. The stress response also indicates that the director never goes through an angle of $\pm 45^{o}$ which would produce a stress overshoot as is seen for flow alignment with $\lambda>1$ (e.g., bulk 5CB, Fig 4.3a [24]). Instead a steady stress is monotonically approached with $\tau_{xy}(\gamma)$ corresponding to $\lambda=-1.13$.

To estimate the polymer relaxation time, the dynamic rheological response of the LC solutions was also characterized. For all polymer concentrations examined, only the terminal region was accessible. For the 10% solution at 25 ^{o}C, it was possible to estimate the cross-over frequency, *G'=G",* by extrapolating using a slope of two and one for *G'* and *G"*, respectively. The intercept of these two lines was at a frequency of $\omega=1770$ rad/s. This frequency corresponds to a strain rate of 280 s^{-1} which is more than an order of magnitude greater than the strain rates of 4 to 32 s^{-1} that were used in the transient rheology experiments. This indicates that the new phenomena seen in these experiments are not due to significant stretching of the polymer.

5.3 Why a Nematic Polymer Solution Aligns Near the Velocity Gradient Direction

The appearance of a flow-aligning condition near the velocity gradient direction can be explained as resulting from the competition between two opposing torques on the director, Fig 4.4. A shearing force applied to an oblate polymer would tend to orient its long axis along the extensional axis of shear (+45°). Since in the oblate polymer the mesogen is perpendicular to the backbone, the pendant mesogens will exert a torque on the director rotating it toward an angle of –45°; from an initial orientation $\theta = 0^{o}$, this rotates $\vec{n}$ against the vorticity. This contrasts the LC host, 5CB, which under shear starting from $\theta = 0^{o}$ experiences a torque on the director rotating it with the vorticity toward the velocity direction. The competition between these two torques leads to flow alignment near the velocity gradient direction with λ<-1.

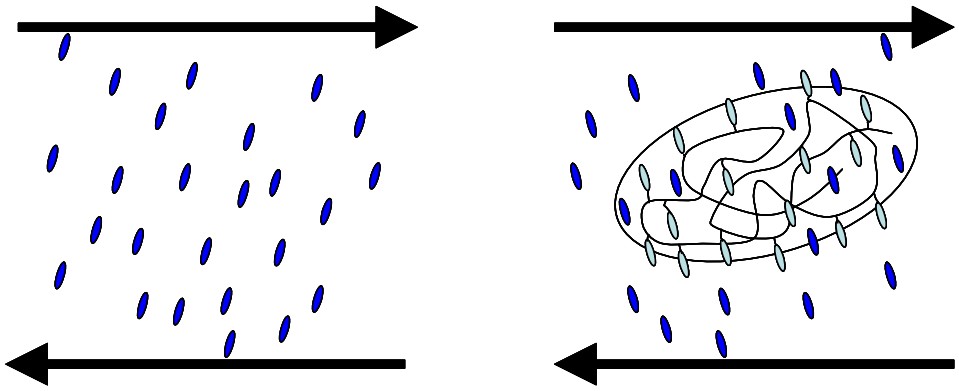

Figure 5.4 Schematic diagram showing how the presence of an oblate polymer can create a negative tumbling parameter and cause the director to rotate counter to the vorticity.

For the tumbling parameter to be less than –1 and for the director to rotate counter to the vorticity when $\theta = 0^{o}$, α_2 must be positive. This is in qualitative agreement with Brochard theory. To date, the only other measurements of negative tumbling parameters

has been in discotic [18, 19] systems and with melt SGLCPs [27]. By using polymers with a molecular weight that is typically at least an order of magnitude larger than other researchers [30], we were able to get much greater changes in viscoelastic properties using less polymer. Not only does this study open up new regimes of the tumbling parameter for study, but it also verifies some aspects of Brochard theory. She predicted that the addition of an oblate polymer to a flow-aligning LC can cause the tumbling parameter to be reduced below -1 to produce flow alignment near $\nabla\vec{v}$ instead of $\vec{v}$ as is seen in typical calamitic LCs.

Bibliography

[1] M. D. Kempe and J. A. Kornfield, *Phys. Rev. Lett*. **90**, 115501 (2003).
[2] R. L. Sutherland, V. P. Tondiglia, L. V. Natarajan, T. J. Bunning, and W. W. Adams, *Appl. Phys. Lett*. **64**, 1074 (1994).
[3] H. S. Kitzerow, *Liq. Cryst*., **16**, 1 (1994).
[4] H. Furue, H. Yokoyama, and S. Kobayashi, *Jpn. J. Appl. Phys*. **40**, 5790 (2001).
[5] K. Kang, L. C. Chien, and S. Sprunt, *Liq. Cryst*. **29**, 9 (2002).
[6]C. C. Chang, L. C. Chien, and R. B. Meyer, *Phys. Rev. E* **56**, 595 (1997).
[7] R. A. Hickmet, J. M. Boots, and M. Michielsen, *J. Appl. Phys*. **79**,15 (1996).
[8] H. J. Coles and M. S. Bancroft, *Mol. Cryst. Liq. Cryst*., **237**, 97 (1993).
[9] M. C. Chang, H. W. Chiu, X. Y. Wang, T. Kyu, N. Leroux, S. Campbell, and L. C. Chien, *Liq. Cryst*., **25**, 733 (1998).
[10] J. L. Ericksen, *Arch. Rat. Mech. Anal*., **24**, 231 (1960).
[11] F. M. Leslie. *Arch. Rat. Mech. Anal*., **28**, 265 (1968).
[12] D. F. Gu and A. M. Jamieson, *J. Rheol*. **38**(3), 555 (1994).
[13] P. Pieranski and E. Guyon, *Phys. Rev. Lett*. **32**, 924 (1974).
[14] C. Gahwiller, *Phys. Rev. Lett.* **28**, 1554 (1972).
[15] P. E. Cladis and S. Torza, *Phys. Rev. Lett.* **35**, 1283 (1975).
[16] T. Carlsson, *Mol. Cryst. Liq. Cryst*. **89**, 57 (1982);
[17] G. E. Volovik, *JETP Lett*. **31**, 273 (1980).
[18] J. T. Mang, S. Kumar, and B. Hammouda, *Mol. Cryst. Liq. Cryst*. **303**, 244 (1997).
[19] A. B. D. Brown and A. R. Rennie, *Chem. Eng. Sci.* **56**, 2999, (2001).
[20] F. Brochard, *J. Polym. Sci. Polym. Phys. Ed*. **17**, 1367 (1979).
[21] D. F. Gu and A. M. Jamieson, *Macromolecules* **27**, 337 (1994).
[22] D. F. Gu, A. M. Jamieson, and S. Q. Wang, *J. Rheol*. **37,** 985 (1993).
[23] N. Yao, and A. M. Jamieson, *Macromolecules* **31**, 5399 (1998).
[24] Even though tumbling nematic LCs can have tumbling parameters as low as λ~0.2, only λ~0.4 has been reported for a solution of a polymer dissolved in a tumbling nematic.
[25] D. J. Ternet, R. G. Larson, and L. G. Leal*, Rheol. Acta* **38**, 183 (1999).
[26] N. Yao and A. M. Jamieson, *Macromolecules* **31**, 5399 (1998).

[27] I. Quijada-Garrido, H. Siebert, P. Becker, C. Friedrich, and C. Schmidt, *Rheol. Acta*. **38**, 495 (1999);
[28] I. Quijada-Garrido, H. Siebert, C. Friedrich, and C. Schmidt, *Macromolecules* **33**, 3844 (2000);
[29] H. Siebert, P. Becker, I Quijada-Garrido, D. A. Grabowski, and C. Schmidt, *Solid State Nucl. Magn. Reson.* **22**, 311 (2002).
[30] A. M. Jamieson, D. Gu, F. L. Chen, and S. Smith, *Prog. Polym. Sci*. 21, 981 (1996).
[31] Preliminary results of SANS data on solutions of SGLCP in deuterated 5CB indicate a polymer anisotropy of about $R_{\perp}/R_{//}$=1.6 and that the overlap concentration is around 24%. This anisotropy is similar to SANS studies on SGLCPs in the melt. Brochard theory predicts that greater polymer anisotropy will have a greater affect on the tumbling parameter.
[32] J. Sanger, W. Gronski, S. Maas, B. Stuhn, and B. Heck, *Macromolecules* **30**, 6783 (1997).
[33] T. C. Chung, M. Raate, E. Berluche, and D. N. Schulz, *Macromolecules* **21**, 1903 (1988).
[34] M. D. Kempe. J.A. Kornfield. C. K. Ober, and S. D. Smith, Macromolecules 00, 000 (2003). Manuscript in Preparation.
[35] P. T. Mather, D. S. Pearson, and W. R. Burghardt, *J. Rheol*. **39**, 627 (1995).
[36] P. Y. Liu, N. Yao, and A. M. Jamieson, *Macromolecules* 32, 6587 (1999).
[37] W. Zhou, J. A. Kornfield, and W. R. Burghardt, *Macromolecules*, **34**, 3654 (2001).
[38] F. D. Bloss, *An introduction to the Methods of Optical Crystallography*; Holt, Rheinhart & Winston (1961).

Chapter 6 Anomalous Viscous Responses

For this chapter, the efforts of Maria Lujan Auad must be acknowledged. She conducted the rheological and conoscopic measurements on 78 and 360 kg/mol samples of PBCB6.

6.1 Introduction

6.1.1 Motivation

Liquid crystals (LCs) can enormously amplify orientation-dependent interactions with polymers. Interactions between small molecule LCs and polymers at interfaces propagate over microns in the case of a small molecule LC between rubbed alignment layers and in the LC droplets in the case of polymer-dispersed and polymer-stabilized LCs (PDLCs and PSLCs). LCs can amplify the binding of a few molecules at the interface between the LC and an aligning substrate [1]. Therefore, it should be possible for a very dilute polymer solvated in a small molecule LC to command the orientation of the LC as a whole. Here we use shear alignment behavior to show that long side-group liquid crystalline polymers (SGLCPs) are indeed capable of commanding the orientation of an LC host.

In this work, the addition of very long SGLCPs (degree of Polymerization DP>1000) is shown to have a much greater effect upon the shear alignment behavior than has been reported previously. We have previously shown (Chapter 5) that low concentrations (≈7.5 wt %) of a cyanobiphenyl-based SGLCP, 420 kg/mol PBCB6, can induce unprecedented flow-alignment with the director nearly along the velocity gradient in

shear (tumbling parameter λ<-1) in contrast to the usual flow-aligning behavior of calamitic nematic LCs (λ>1, director nearly along the flow direction) [2]. The reduction of λ by addition of an SGLCP with transverse alignment tendency [3] (oblate chain conformation with backbone on average perpendicular to the director) can be qualitatively explained by Brochard [4]. However, using an LC solvent that has λ>1 in bulk, Gu et al. [5] using a 12 kg/mol SGLCP predicted this to occur at a much higher concentration of 30 wt % polymer. Using neutron scattering measurements of chain anisotropy we have shown that the exceptionally strong effects of 420 kg/mol PBCB6 is not due to an unusually anisotropic conformation ($R_{\perp}/R_{//}\approx$1.63, similar to previously studied oblate-type melt SGLCPs [6]). In the present research we examine a series of SGLCPs differing only in chain length, showing that their effect on λ increases strongly with chain length.

We demonstrate the need for improvements to current theories predicting the effect of a dissolved polymer on a small molecule nematic LC. In accord with prior literature [7, 8, 9, 10, 11] we observed a very nonlinear dependence of the Leslie Ericksen viscosity coefficients upon addition of polymer at concentrations well below the overlap concentration. Although this nonlinear concentration dependence has been know for almost two decades, a good physical explanation has not been offered (models predict linear dependence in dilute solutions). Since the nematic order of the solutions is macroscopic, it provides a means by which the molecules could produce strong nonlinearities without physically toughing each other.

Secondly, the sense and the magnitude of the changes in the Leslie Ericksen viscous parameters with addition of polymers are not currently explained by theory. The

Brochard theory predicts that the changes in α_2 and α_3 upon addition of polymer would have the same sign. In work by Liu et al. [12] and Yao and Jamieson [13, 14], the changes in α_2 and α_3 were found to have opposite signs, but by using a modified Brochard theory they were able to get good fit to their data. In our measurements, we found that the relative signs of the changes in α_2 and α_3 had a molecular weight dependence that is not captured by Jamieson's modification of the Brochard theory indicating that further advances in theory are necessary.

6.1.2 Characterization of the Polymers

The details of the methods used to synthesize this series of polymers, Fig. 6.1, are given in Appendix A2, and a detailed characterization is given in Chapter 2. These high molecular weight polymers were found to have a low polydispersity, PDI≤1.16, and excellent solubility in the liquid crystal 4'-pentyl-4-cyanobiphenyl (5CB).

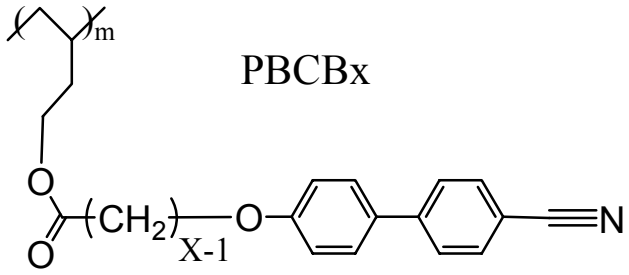

Figure 6.1. Structure of the side-group liquid crystalline polymer used in these experiments. PBCBx denotes a 1,2-polybutadiene backbone, with a cyanobiphenyl mesogen. The "X" in the polymer name indicates the size of the spacer where X+4 is the number of atoms between the mesogen and the polymer backbone. In these experiments X=4 to 8.

Measurement of the refractive indices showed that for solutions up to 10% polymer in 5CB, the change in both refractive indices was small until about 32 ^{o}C, near the nematic to isotropic transition temperature (T_{ni}). Since (Chapter 2) the addition of polymer did

not significantly affect birefringence (Δn), and the splay elastic constant (K_{11}) is typically related to Δn^2 [15], values for K_{11} from bulk 5CB can be used in calculations for these experiments.

Small-angle neutron scattering experiments were also performed on solutions of these polymers in perdeuterated 5CB (Chapter 4). It was found that for the different molecular weights and spacer lengths used in these experiments, the ratio of the polymer backbone quadratic characteristic lengths perpendicular and parallel to the director was $R_{\perp}/R_{//}$=1.63±0.05.

6.2 Role of Chain Length in the Unprecedented Tumbling Parameter

Previously in Chapter 5 [3], the tumbling parameter for a sample of 420 kg/mol PBCB6 dissolved in 5CB was measured and excellent agreement was found between the rheological and conoscopic methods (Appendix 7.2 and Appendix 5, respectively). In the present chapter, λ is presented for two series of polymers in which either the molecular weight or the spacer length was systematically varied. Similarly to the results presented in Chapter 5, good agreement was found between the two methods, Fig. 6.2.

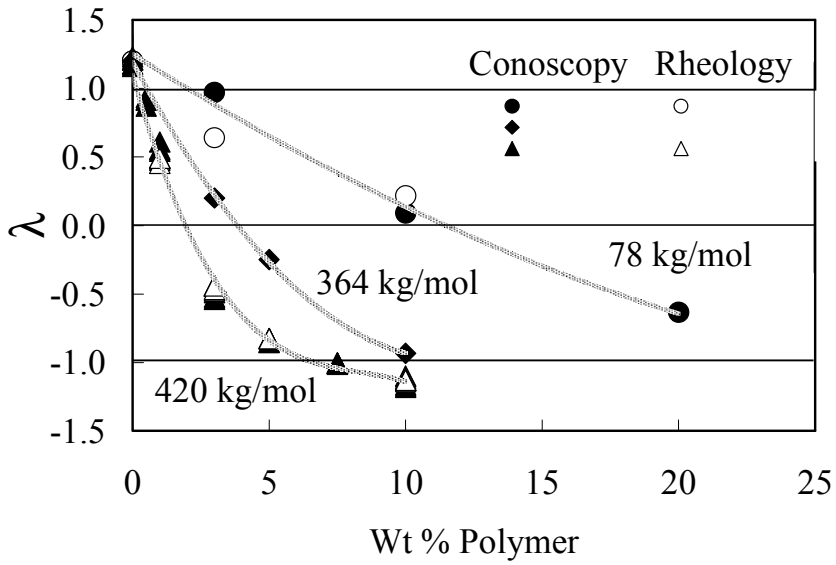

Figure 6.2. Comparison of the tumbling parameter at 25 °C for PBCB6 with different molar masses using the rheological method (open symbols) and the conoscopic method (filled symbols) (Appendix 7.2 and Appendix 5, respectively). The Curves are to guide the eye.

To test the hypothesis that the unprecedented appearance of λ<-1 was due to the high molar mass of our polymers as compared to other researchers, the molar mass of PBCB6 was varied and λ was measured as a function of concentration for each molar mass. Figure 6.3 shows the viscous response of 3% solutions of PBCB6 in 5CB. The sample with the larger molar mass, Fig. 6.3b, showed a much lower tumbling parameter. This experiment also showed that increasing the molar mass by a factor of 5.4 only increased the average viscosity by approximately 40%, but produced a large change in the tumbling parameter. By varying the size of our PBCB6 polymer a strong dependence of λ on the molar mass was observed, Fig. 6.2.

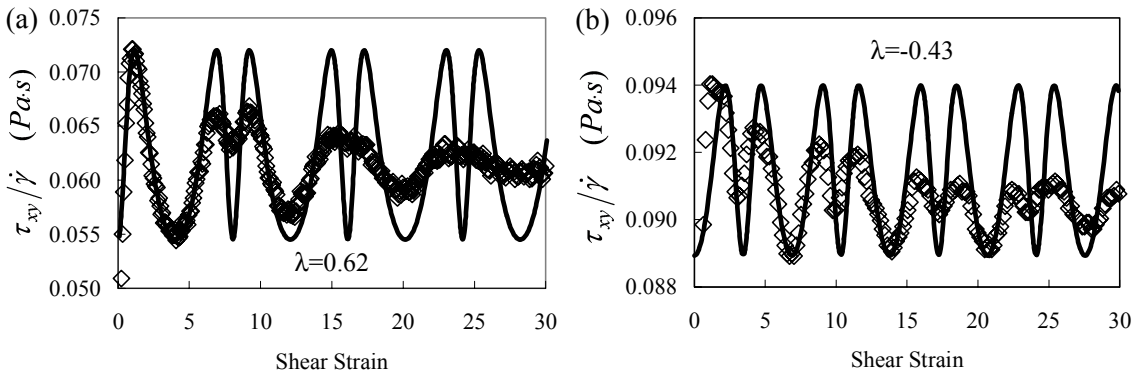

Figure 6.3. Representative rheological response, diamond symbols, of solutions showing theoretical fit, black line, to data. (a) 3% 78 kg/mol PBCB6 at 30 ^{o}C $\dot{\gamma}$=16 1/s (b) 3% 420 kg/mol PBCB6 at 30 ^{o}C $\dot{\gamma}$=32 1/s.

Limited by polymer solubility or by the range of molecular weights available, other researchers have used polymers with degree of polymerization <200 (M_w<80 kg/mol, [2]). Using a 12 kg/mol polymer, Gu et al. [5] found that with 4.5 wt % polymer in 5CB, their tumbling parameter had only been reduced to 0.90, whereas our 420 kg/mol PBCBx polymers reduced the tumbling parameter to –0.8 at 5% polymer. Gu estimated that approximately 30 wt % polymer would be necessary for λ<-1. The data for 78 kg/mol PBCB6 is more comparable to the work by Gu et al. and, as can be seen by Fig. 6.2, should produce λ<-1 at approximately 30 wt %. This proves that the unprecedented effects of the 420 kg/mol PBCB6 are indeed due to its unusual length. As chain length is reduced to the range typically investigated, results in accord with prior literature are obtained.

The tumbling parameter λ was found to be independent of spacer length for polymers with the same degree of polymerization (DP), Fig. 6.4. According to the Brochard [4] theory, the effect of a polymer on λ depends primarily on its molar mass and conformational anisotropy. Since it was previously found that changing the spacer length

did not significantly affect the polymer anisotropy or overall radii, Table 4.1, the absence of an effect of spacer length on λ is consistent with Brochard theory and experimental findings of Gu et al. [16] that the effect of a polymer on the twist viscosity is independent of spacer length at intermediate spacer lengths.

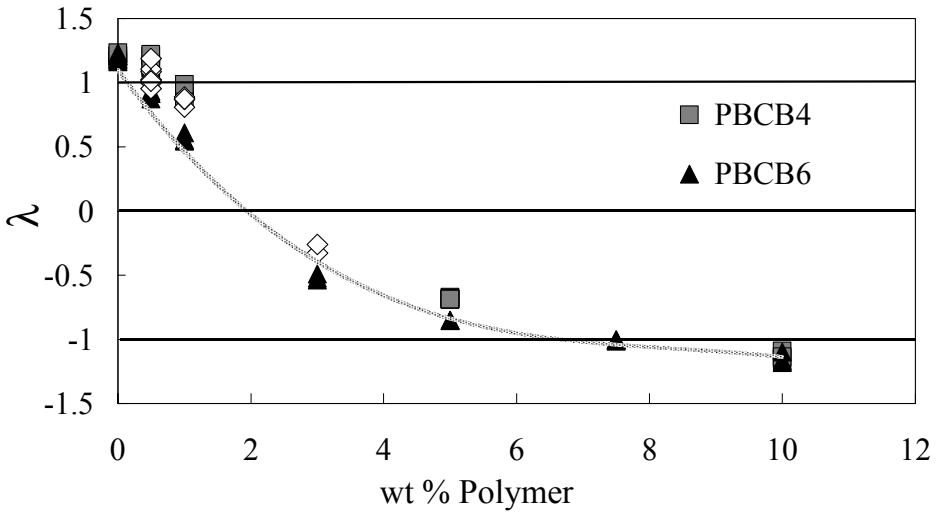

Figure 6.4. Conoscopically determined tumbling parameter for polymers with DP=1150 but different spacer lengths. The curve is to guide the eye only.

6.3 Unexplained Nonlinear Concentration Dependencies

6.3.1 Reorientational Response Time

Reorientational response time measurements, proportional to γ_1/K_{11}, were made (Appendix 7.1) for solutions in 5CB where either the degree of polymerization (DP) or the spacer length was systematically varied. For the samples with DP=1150, γ_1/K_{11} is independent of the spacer length, Fig. 6.5. This result is analogous to the results of Gu et al. [16] measuring director relaxation rates using light scattering techniques. They found that the effect of a dissolved polymer on the director reorientation rate was greatest for very small (4 atoms long) and the smallest for intermediate lengths (7 to 9 atoms). They

interpreted this observation to indicate that at sufficiently long spacer lengths (with polymers of similar molecular weights) the mesogens are decoupled from the backbone making changes in spacer length insignificant. Similarly, the PBCBx series of polymers had no noticeable dependence of the director reorientation rate with spacer length, Fig. 6.5. As noted above, this result was also expected because previous neutron scattering studies (Chapter 4) indicate that the polymers with the same DP have the same anisotropy and molecular dimensions. For samples with different DPs and the same spacer, γ_1/K_{11} is significantly different as would be expected since their hydrodynamic volumes are different.

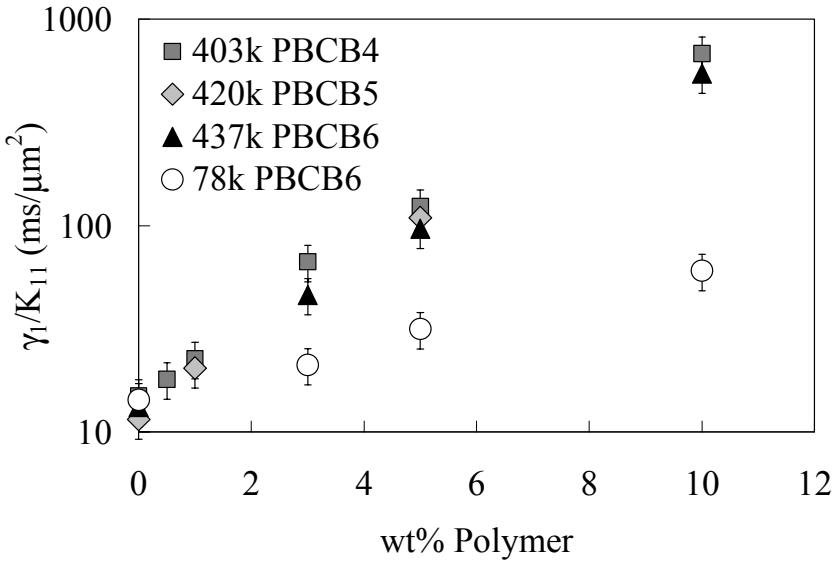

Figure 6.5. Reorientational response time, γ_1/K_{11}, for polymers with a different spacer and DP=1150 or 210 at 25 °C.

The reorientational response time measurements are seen to increase with a highly nonlinear, approximately exponential, dependence on polymer concentration, Fig. 6.5. This is an unexpected result that does not fit the Brochard theory, which predicted a

linear dependence of $\delta\gamma_1$ with concentration for dilute polymer solutions. To verify that we are in the dilute regime, the overlap concentration [17, 18] was calculated using

$$c^* = \frac{3M_n}{4\pi R_g^{\,3} N_A \rho}. \qquad (6.1)$$

Here M_n is the number averaged molar mass determined by multi-angle laser light scattering (MALLS) in Table 3.1, N_A is Avagadro's number, ρ=1.01 g/cm^3 is the solution density, and the radius of gyration (R_g) was calculated as

$$R_g = \sqrt{R_{||}^{\,2} + 2R_{\perp}^{\,2}}. \qquad (6.2)$$

The radii $R_{//}$ and $R_{\perp}$ were determined for the polymers using small-angle neutron scattering (SANS), Table 4.1. Values that included scattering from the mesogenic groups were used. This resulted in c^*≅24 wt % and c^*≅31% for the two PBCB6 polymers in Fig. 6.1, verifying that polymer overlap was not responsible for the nonlinear concentration dependence. While these overlap concentrations seem very high, in Chapter 2 it was shown that the addition of the mesogenic unit did not significantly affect the radii of gyration relative to an isotropic solution of the 1,2-butadiene prepolymers in tetrahydrofuran, and that the radii of gyration of the SGLCP were smaller in 5CB than in THF. The unusually large side groups and relatively small radii explain the high overlap concentrations.

Estimates of γ_1 were obtained using the measurements of γ_1/K_{11} along with measurements of K_{11} from of Skarp et al. [19]. Using values for K_{11} from bulk 5CB is justified because Δn was not affected by the addition of polymer Fig. 2.4. Furthermore, other researchers [7] have typically found a weak linear dependence of K_{11} on polymer concentration. Since the ratio γ_1/K_{11} has a nearly exponential dependence on

concentration, any uncertainties in K_{11} are negligible and do not explain the highly nonlinear behavior.

A similar highly nonlinear dependence of the twist viscosity has been seen by many other investigators [7, 8, 9, 10, 11]. Similarly, a transition from a linear dependence of γ_1 with polymer concentration at low concentrations to an exponential dependence as the polymer concentration is increased was reported by Pashkovskii et al. [20, 21] at ~3 wt % and Mattoussi et al. [22, 23] at ~7 wt %.

Some researchers who restricted their studies to low polymer concentration observed only the linear regime. Gu et al. [24] at <15 wt % with a methacrylate-based SGLCP in 5CB, Pashkovsky et al. [25] at <4 wt % using a main chain LCP in 5CB, Chen and Jamieson [26] at <1.5 wt % using a main chain LCP in 5OCB, and Pashkovsky and Litvina [27] at <3 wt % with a cyanobiphenyl SGLCP.

Mattoussi et al. [22, 23] described three regimes with different dependence of γ_1 on concentration; an initial linear regime, a small inflection region at 7.9 wt % polymer, and an exponential region, Fig. 2. from Mattoussi et al. [22]. They attributed the exponential region to interchain interactions claiming that the polymers had exceeded the overlap concentration. On a plot of the change in twist viscosity $(\Delta\gamma_1)$ versus wt % polymer, the inflection region was characterized by a change from a curve that was concave down to one that was concave up as polymer was added. For the initial linear curve to become concave down, the effect of the addition of polymer must decrease with concentration. The premise for a linear regime was that the polymers are non-interacting; furthermore, the transition to an interacting region should have a net result that is a sum of the two effects. Therefore, one would expect the slope to increase when transitioning between

these regions, resulting in a curve that is concave up at all polymer concentrations. The observation of an inflection point was counter-intuitive.

Mattoussi et al. attributed the presence of the inflection region to a change in anisotropy due to interchain interactions at the overlap concentration. The overlap concentration was determined using values for the radii of gyration obtained by Mattoussi et al. [28]. In Fig. 2 of that work, a plot of *1/I* versus q^2 is shown with the line used to calculate the radius of gyration with

$$\frac{I_o}{I(q)} = 1 + \frac{q^2 R_{g\perp}^2}{3}, \quad (6.3)$$

where $R_{g\perp}$ is a characteristic radius that is equal to the radius of gyration for an isotropic phase. The radius measured with the curve was $R_{g\perp}$=31 Å for the polymer labeled P_3^{95}. Here they used a range of data from $q^2 \cdot R_{g\perp}^2$=0.1 to 8 even though Eq. 6.3 is only valid for $q^2 \cdot R_{g\perp}^2$<1. They claimed that since the first part of the line was within the Guinier regime ($q^2 \cdot R_{g\perp}^2$<1), that the line going through the rest of the data was valid. If one assumes that a polymer is long enough to have the Gaussian conformation of a freely jointed chain, then the scattering intensity can be modeled in a given direction by the Debye equation [29],

$$I(q) = I_o \left(\frac{2}{q^4 R_{g\perp}^4} \right) \left[q^2 R_{g\perp}^2 - 1 + e^{\left(-q^2 R_{g\perp}^2\right)} \right]. \quad (6.4)$$

As can be seen in Fig. 6.6, if one plots Eq. 6.4 and allows for a little scatter in the data, a slope of approximately 0.442 is found by a least squares fit, Fig. 6.6. Then by using this slope in Eq. 6.3, as was done by Mattoussi, the radii will be overestimated by 15% leading to a 50% under estimation of the overlap concentration. The radius used in Fig. 2

of Mattoussi et al. [28] was the smallest of all their radii; therefore, it should have the most low q scattering, $q \cdot R_{g\perp} < 1$, and the smallest over estimation. Using this method, the largest overestimation possible for $R_{g\perp}$ is 22.5% which would result in an 83% underestimation of the overlap concentration. Examining the range of their scattering, the parallel characteristic radius of $R_{g//}$=53 Å should have an over estimation of ~20% resulting in a 74% overestimation of the overlap concentration. In their paper they stated that "$R_G \cong$55 Å appears to be larger than the estimated value for a flexible chain with 95 subunits,…" Therefore, the true overlap concentration should be closer to 20 instead of 13 wt % for P_3^{95} and 13 instead of 7.6 wt % for P_5^{95} and Mattoussi et al. did see the onset of strong nonlinearities well before the overlap concentration.

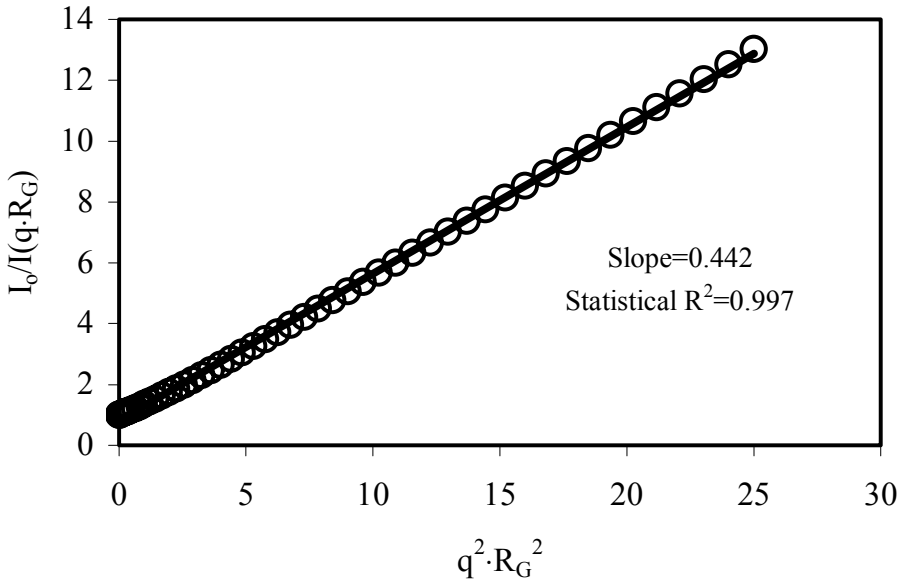

Figure 6.6. This figure demonstrates how exceeding the Guinier range will produce an erroneously large measurement of the radius of gyration. The data points were spaced with a constant interval of $q \cdot R_G$, similar to what one would see in experimental data, and the intensity is calculated using the Debye Equation, Eq. 6.4. Application of the Guinier equation, Eq. 6.3, overestimates the radii by 15% and underestimates the overlap concentration by 50%.

All of these studies reporting the concentration dependence of γ_1 used polymers with an order of magnitude smaller molar mass than that used in our study. Therefore, they should be well below the overlap concentrations for those systems. With the exception of the work by Gu et al. [24] at 15%, when a linear regime was found it was limited to very dilute concentrations, <7%. Since the studies reporting nonlinear behavior were well below their overlap concentration, direct inter-polymer contact could not explain these results.

6.3.2 Viscous Parameters α_1, α_2, α_3, and η_b.

The fits of the transient viscous responses, Fig. 6.3, of the solutions of polymer in 5CB along with the results of the reorientational response time experiments, Fig. 6.5, were used to determine the viscous parameters α_1, α_2, α_3, and η_b for solutions of 420 and 78 kg/mol PBCB6 at temperatures between 20 and 34 ^{o}C and concentrations up to 10% polymer, Fig. 6.7. The details of the experimental procedure are outlined in Appendix A7.2. It can be seen that for all the viscous parameters their absolute values decrease as T_{ni}=35 ^{o}C is approached. Since the Leslie-Ericksen viscous parameters are equal to zero in the isotropic state (except α_4 which is equivalent to a Newtonian viscosity), all of them are expected to decrease in magnitude as T_{ni} is approached and the order parameter decreases.

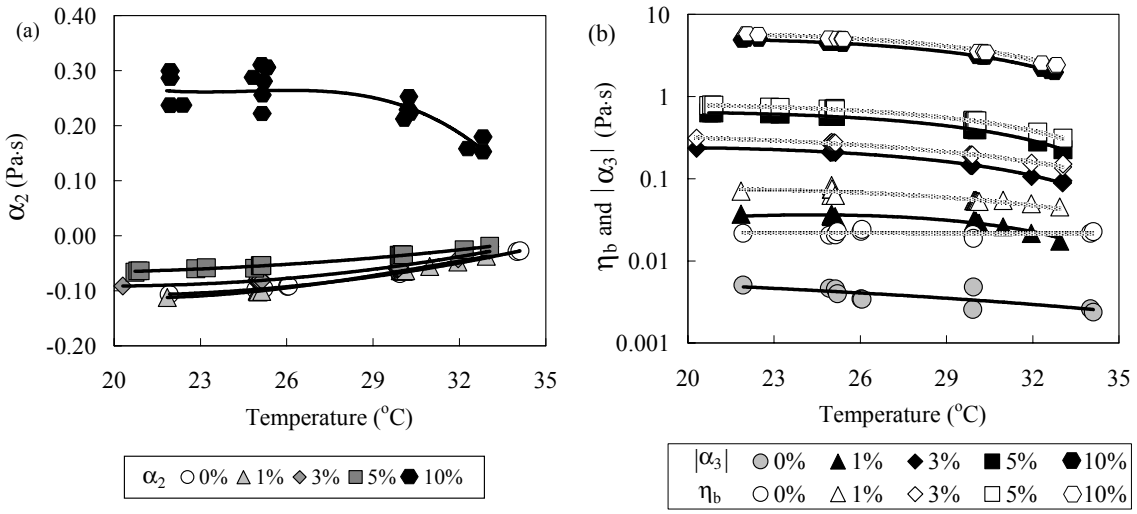

Figure 6.7. Temperature dependence of α_2, α_3, and η_b. The trend-lines are simply to guide the eye. (a) α_2. (b) $|\alpha_3|$ and η_b. The absolute values for α_3 were plotted since they had negative values for bulk 5CB.

The effect of polymer concentration on α_3 and η_b is strongly nonlinear and the magnitudes of these two viscosities are correlated, especially for 420 kg/mol PBCB6, Figs 6.7 and 6.8. It follows from the definitions of $\lambda \equiv (\alpha_2+\alpha_3)/(\alpha_2-\alpha_3)$ and $\gamma_1 \equiv \alpha_3-\alpha_2$ that as λ approaches –1, $\alpha_2 \approx 0$ and $\gamma_1 \approx \alpha_3$. The transient viscous response

$$\tau_{xy} = \dot{\gamma}\left\{\left[\alpha_1 + \frac{(\alpha_2+\alpha_3)^2}{\alpha_3-\alpha_2}\right]\sin^2\theta\cos^2\theta + \eta_b - \frac{\alpha_3^{\,2}}{\alpha_3-\alpha_2}\right\}, \quad 6.5$$

demonstrates that the difference between α_3 and η_b is approximately equal to the minimum in the stress versus strain as the tumbling parameter approaches a value of –1 where $|\alpha_3| >> |\alpha_2 \cong 0|$. Therefore, if the minimum in the stress versus strain curve is small, relative to γ_1, then much of the nonlinearity in α_3 and η_b is also correlated with the nonlinearity in γ_1.

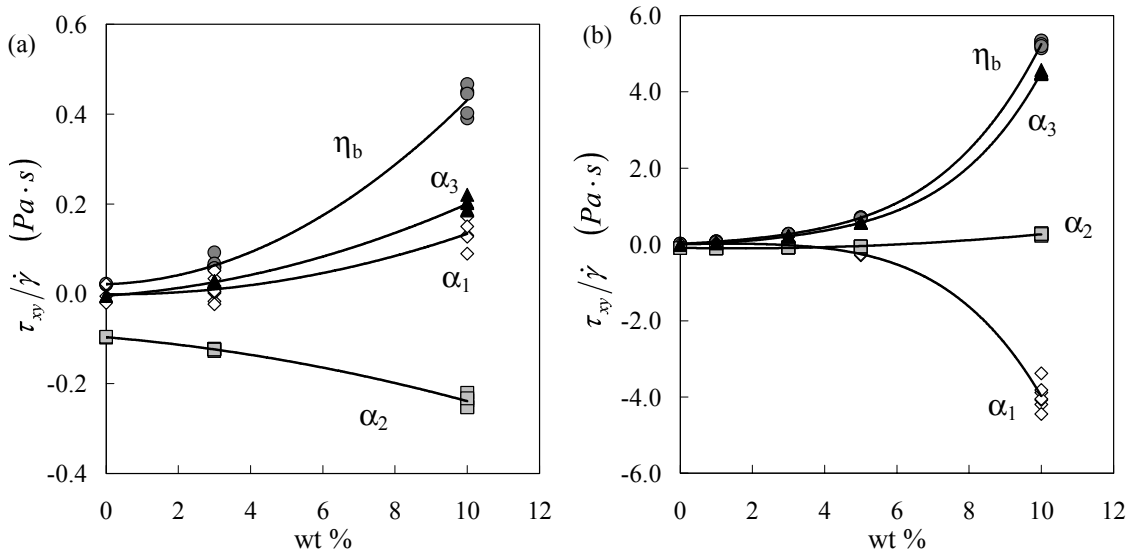

Figure 6.8. Concentration dependence of viscous parameters upon addition of (a) 78 kg/mol (b) 420 kg/mol PBCB6 in 5CB at 25 ^{o}C. The data were arbitrarily fit to second or fourth order polynomials to visualize the trends.

For large changes in γ_1 and $\lambda \approx 1$, much of the nonlinearities in the viscosities are correlated to the twist viscosity γ_1 Fig. 6.5. Though an order of magnitude smaller, nonlinearities are also seen in the magnitude of the transient viscous response, $\tau_{xy}/\dot{\gamma}$. Inspection of Fig. 6.9 for the 420 kg/mol SGLCP shows a linear region between 0.5 and 4 wt % polymer in the maximum and between approximately 2 to 5 wt % in the minimum of $\tau_{xy}/\dot{\gamma}$. The lower limits were estimated from a semi log plot, Fig. 6.9, and the upper limits were estimated from the same data plotted on linear plot. The nearly exponential nonlinear concentration dependence of the viscous parameters at concentrations below overlap is a robust result evident in reorientational response following application of an electric field, as well as transient director responses and stress upon inception of shear.

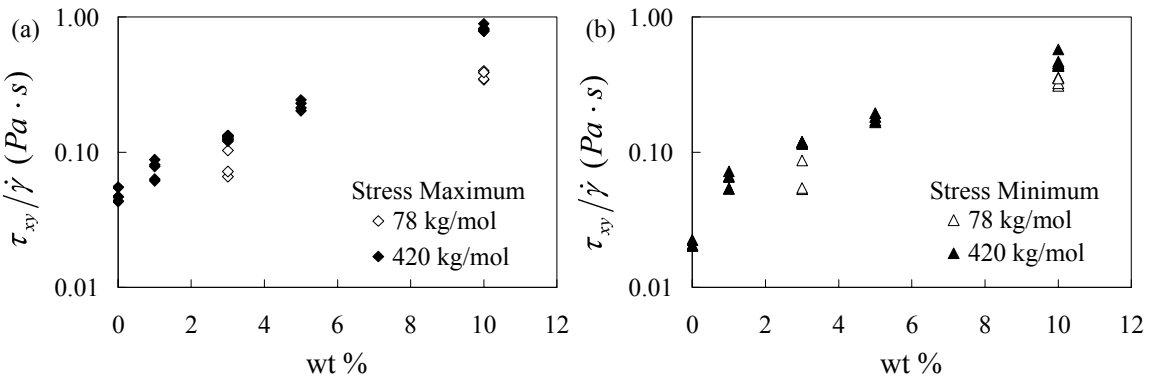

Figure 6.9. (a) Maximum and (b) minimum in viscous response, $\tau_{xy}/\dot{\gamma}$, for 78 kg/mol and 420 kg/mol PBCB6 in 5CB. It should be noted that for 10% solutions of 420 kg/mol PBCB6 the maximum was not actually measured but was calculated based on λ, the minimum, and the steady-state value.

As mentioned earlier, the 420 and 78 kg/mol PBCB6 polymers have an overlap concentration of c*≅31 and c*≅24 wt %, respectively. For polymer solutions well below c* the chains do not directly interact with each other and therefore they are expected to increase the viscosity by a specific amount for every polymer chain present, i.e., a linear concentration dependence. Instead, the presence of strong nonlinearities at concentrations well below c* indicates that the polymer chains can "see" each other. The main distinction between this and a conventional polymer solution is the presence of nematic order. This order is long-range and, as indicated by the presence of nonlinearities at low concentrations, must provide a means by which SGLCPs can interact with each other at a distance without direct physical contact.

The changes in the viscous parameters are compared with the Brochard theory [4], which predicts the changes in γ_1 and γ_2 upon addition of polymer to be

$$\delta\gamma_1 = \frac{\left(R_\perp{}^2 - R_{||}{}^2\right)^2}{R_\perp{}^2 R_{||}{}^2}\left(\frac{ckT}{N}\right)\tau_R, \quad (6.6)$$

and

$$\delta\gamma_2 = \frac{R_\perp{}^4 - R_{||}{}^4}{R_\perp{}^2 R_{||}{}^2}\left(\frac{ckT}{N}\right)\tau_R, \quad (6.7)$$

where k is Boltzmann's constant, T is absolute temperature, c is the monomer concentration, N is the degree of polymerization, and τ_R represents a characteristic polymer relaxation rate. Using the definitions of $\gamma_1 \equiv \alpha_3 - \alpha_2$ and $\gamma_2 \equiv \alpha_3 + \alpha_2$, algebraic manipulation of Eqs. 6.6 and 6.7 leads to

$$\delta\alpha_2 = \left(\frac{R_\perp{}^2 - R_{||}{}^2}{R_\perp{}^2}\right)\left(\frac{ckT}{N}\right)\tau_R, \quad (6.8)$$

and

$$\delta\alpha_3 = \left(\frac{R_\perp{}^2 - R_{||}{}^2}{R_{||}{}^2}\right)\left(\frac{ckT}{N}\right)\tau_R. \quad (6.9).$$

This indicates that the changes in α_2 and α_3 should have different magnitudes but the same sign. For 78 kg/mol PBCB6 in 5CB $\delta\alpha_2$ is negative and $\delta\alpha_3$ is positive, Fig. 6.8a, contradicting the Brochard theory. For 420 kg/mol PBCB6 in 5CB, $\delta\alpha_2$ and $\delta\alpha_3$ are both positive, but $\delta\alpha_3$ increases much more strongly than $\delta\alpha_2$, Fig. 6.8b. This contradicts Eqs. 6.8 and 6.9 which indicate that the prefactors for $\delta\alpha_2$ and $\delta\alpha_3$ by only a factor of ~3 for $R_\perp/R_{||} \approx 1.63$ (Chapter 4). Thus, we find contradictions with the Brochard theory in the nonlinear concentration dependence of the viscosities, the relative signs of the changes in α_2 and α_3 (for 78 kg/mol PBCB6 only) and in the magnitude of the changes in α_2 and α_3.

The trends for the changes in the viscous parameters of 78 kg/mol PBCB6 with polymer concentration, Fig. 6.8a, are similar to those observed by Yao and Jamieson [13, 14] and Liu et al. [12]. Working with a polysiloxane SGLCP they found that $\delta\alpha_2$ and $\delta\alpha_3$

had different signs, in contradiction to the Brochard theory. According to the Brochard theory, Eqs. 6.8 and 6.9, the sign of the changes in the viscous parameters α_2 and α_3 should be the same. For 420 kg/mol PBCB6 this is true for concentrations greater than 1 wt % but for 78 kg/mol PBCB6 the changes have opposite signs up to at least 10 wt %. Yao and Jamieson [13, 14] and Liu et al. [12] also found opposite signs and reconciled this difference by modifying the Brochard theory. They added a viscous dissipation term to the twist viscosity arising from the elastic torque between the director rotation and the LCP orientation yielding

$$\delta\alpha_2 = \left(\frac{1}{2} - \frac{R_{||}^{\ 2}}{R_{\perp}^{\ 2}}\right)\left(\frac{ckT}{N}\right)\tau_R, \quad (6.10)$$

and

$$\delta\alpha_3 = \left(\frac{R_{\perp}^{\ 2}}{R_{||}^{\ 2}} - \frac{1}{2}\right)\left(\frac{ckT}{N}\right)\tau_R, \quad (6.11)$$

which produced good fits to their data. These modifications do not allow for a molar mass dependence of the sign or a concentration dependence on the magnitude of the changes in α_2 and α_3 upon addition of polymer as was seen in PBCB6, Fig. 6.8.

Many studies [20, 21, 22, 23] show a linear dependence of γ_1 for the addition of small amounts of polymer which transitions into an exponential dependence. In contrast, this study along with Coles and Sefton [7], Coles and Bancroft [8], Humphreys et al. [9], Pashkovskii and Litvina [10], and Pashkovskii et al. [11], have measured an exponential-like dependence for all concentrations tested. Deviations like these are predicted to occur for polymers near the overlap concentration or even a little before due to interchain interactions. Since these polymers are below their overlap concentration one would

expect them to behave as non-interacting coils. The macroscopic nature of the nematic order must enable physically separated polymers to "see" each other therefore the linear regime for dilute polymer solutions is at best very small.

Yao and Jamieson [13] proposed that "an additional contribution to the torque can arise because of an elastic coupling between director rotation and the orientation of the LCP chain." Coles and Bancroft [8] similarly attributed an exponential variation in γ_1 with polymer concentration to "the resistance of the polymer chain to distortion, and the frictional forces which resist motion of the chain relative to the solvent." More research into additional contributions to the viscous parameters is necessary to obtain a better understanding of the effect of polymers on a nematic host.

6.4 Inconsistencies in Rheologically Estimated Polymer Anisotropy

For the past two decades, the Brochard theory has been used to obtain estimates for the polymer anisotropy from the results from the transient rheology experiments with

$$\frac{R_\perp}{R_{||}} = \left(\frac{\delta\eta_b}{\delta\eta_c}\right)^{1/4}, \quad (6.12)$$

given by Brochard [4]. However, this method has not previously been tested using direct measurements of $R_\perp$ and $R_{//}$; nor has the Brochard theory been tested for internal self consistency. Algebraic manipulation of Eqs. 6.6 and 6.7 (Section 1.2.2) yields an alternative relationship between ratio $R_\perp/R_{//}$, λ and γ_1,

$$\frac{R_\perp}{R_{||}} = \left[\frac{\delta\gamma_1 + \delta\gamma_2}{\delta\gamma_2 - \delta\gamma_1}\right]^{\frac{1}{2}} = \left[\frac{(1-\lambda)\gamma_1 - (1-\lambda_o)\gamma_{1o}}{(1+\lambda_o)\gamma_{1o} - (1+\lambda)\gamma_1}\right]^{\frac{1}{2}}, \quad (6.13)$$

where the subscript "o" refers to values for the pure nematic solvent. These equations are based on changes in viscosity relative to the pure nematic solvent; therefore, uncertainties in the inferred values of ratio $R_{\perp}/R_{//}$ are largest for low polymer concentration. For the 1 wt % solution of 420 kg/mol PBCB6, half of the data points, using both Eqs. 6.12 and 6.13, produced imaginary numbers. Similarly, Eq. 6.13 produced imaginary numbers for all concentrations of 78 kg/mol PBCB6. For all the other solutions real values were obtained, Fig. 6.10.

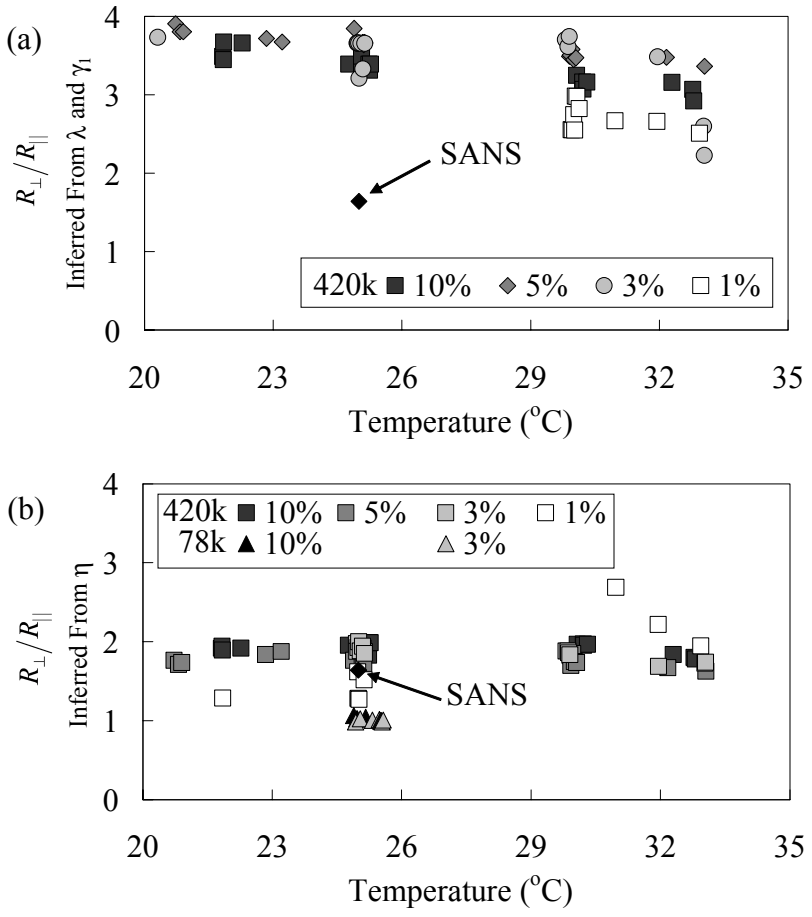

Figure. 6.10. Comparison of measured anisotropy (SANS) from Chapter 4 and two different methods of inferring anisotropy using the Brochard theory. (a) Using λ and γ_l in Eq. 6.13 yielded real values for 3 wt % or more 420 kg/mol PBCB6; only imaginary values were obtained for 78 kg/mol PBCB6. (b) Using $\delta\eta_b$ and $\delta\eta_c$ in Eq. 6.12 yielded real values for both 420 and 78 kg/mol PBCB6 in 5CB at concentrations of 3 wt % or more.

For all solutions that yielded real values of $R_\perp/R_{//}$ it is clear that there are substantial inconsistencies between the two methods, with $R_\perp/R_{//}\approx3.5$ using Eq. 6.13 and $R_\perp/R_{//}\approx1.8$ using Eq. 6.12 for the same 420 kg/mol PBCB6 polymer solutions. The molecular weight dependence of $R_\perp/R_{//}$ inferred from the Brochard theory can only be examined using Eq. 6.12. The backbone anisotropy is expected to be independent of chain length for DP>100 (Chapter 4) [30, 31, 32, 33]. Therefore it is quite surprising that the anisotropy inferred from Eq. 6.12 drops from $R_\perp/R_{//}\approx1.8$ for 420 kg/mol PBCB6 to a nearly spherical conformation ($R_\perp/R_{//}\approx1$) for 78 kg/mol PBCB6.

Direct measurements of $R_\perp$ and $R_{//}$ using SANS (Table 4.1) show that the backbone anisotropy for both polymers are the same with $R_\perp/R_{//}=1.64\pm0.05$. Even though Eqs. 6.12 and 6.13 both predict the correct sense of the anisotropy ($R_\perp>R_{//}$) they produced erroneous values of $R_\perp/R_{//}$. The closest values are for the 420 kg/mol sample using Eq. 6.12 where the average calculated value is $R_\perp/R_{//}=1.8$. Therefore, we conclude that the Brochard theory does not provide a means to infer the anisotropy of liquid crystalline polymers in nematic solvents. It appears to accurately indicate the sense of the anisotropy (oblate or prolate), so it is valid for qualitative characterization of chain conformation.

The known values of the chain anisotropy and relaxation time can be used to compute rheological properties using the Brochard theory. The anisotropy measured using SANS can be used along with a fit to the transient rheology data using Eq. 6.5 to compute γ_1 using Eq. 6.12 of the Brochard theory. For the 420 kg/mol polymer, this produces values that were typically approximately half the value measured using the reorientational response time experiments for 5 and 10 wt % polymer. For 78 kg/mol at 10 wt % and

420 kg/mol at 3% PBCB6, negative values for γ_1 are calculated. A negative value for γ_1 is an impossible condition according to the Leslie-Ericksen theory. Even when the calculated and predicted values are close, 1% 420 kg/mol and 3% 78 kg/mol, this is only seen because the deviations from bulk 5CB are very small and the Brochard calculated anisotropy, Eqs. 6.12 and 6.13 still gave values that were inconsistent with SANS data. This demonstrated that neither the uncertainty in measurement nor a systematic uncertainty in γ_1 could account for the inconsistencies in the Brochard theory.

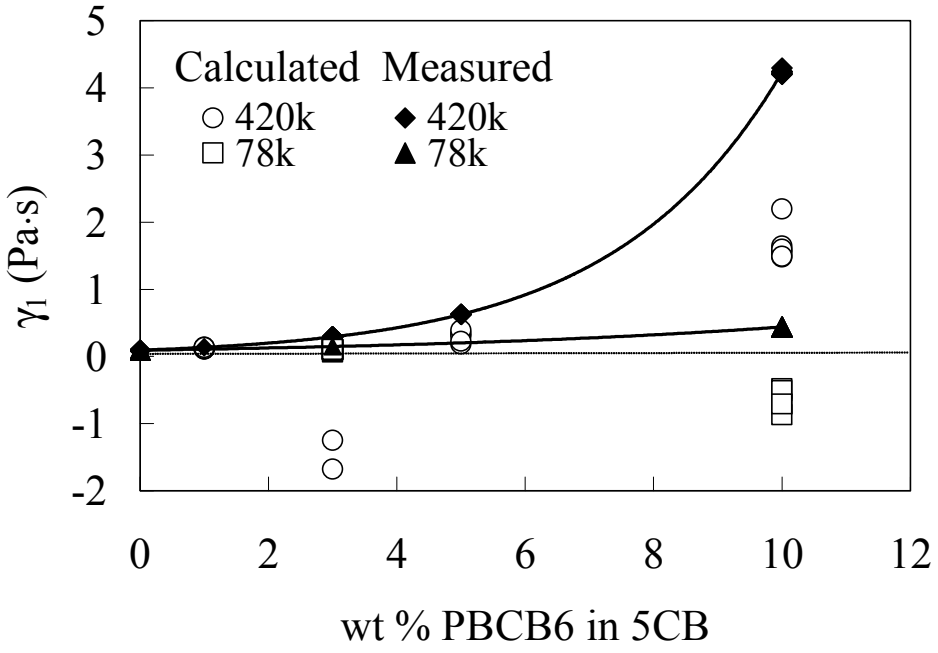

Figure 6.11. Comparison of measured values for γ_1 at 25 °C with the values necessary to produce $R_\perp/R_{//}$=1.64 using Eq. 6.12 from the Brochard theory and a fit to the transient rheological data using Eq. 6.5. The lines are arbitrary exponential fits to the data measured using the reorientational response time experiments.

6.5 Conclusion

The experimental results presented here have demonstrated the need for improvements to current theories predicting the effect of dissolved polymers on the Leslie-Ericksen viscosity coefficients. We have seen inconsistencies in the Brochard

theory between the anisotropy it predicts and that measured using SANS, and between the measured and predicted sign of the changes in some viscous parameters. Highly nonlinear variation of viscosity with polymer concentration is observed below c*. This behavior, also reported in previous studies [7, 8, 9, 10, 11] contrasts with isotropic polymer solutions and is not predicted by the Brochard theory.

A larger molecular weight polymer has a longer relaxation time that increases viscosity more using less polymer. This indicates that a larger molecular weight polymer is much more effective in controlling the orientation of the director than a low molecular weight polymer at the same concentration. Thus, the use of high molecular weight polymers enables control over alignment characteristics even under more dilute conditions.

Regarding the design of LC gels, this implies that a homogeneously solvated gel with low polymer concentration could be effective in controlling the alignment of the LC as a whole.

Bibliography

[1] V. K. Gupta, J. J. Skaife, T. B. Dubrovsky, and N. L. Abbott, Science 279, 2077 (1998).
[2] A. M. Jamieson, D. Gu, F. L. Chen, and S. Smith, *Prog. Polym. Sci*. **21**, 981 (1996).
[3] M. D. Kempe and J. A. Kornfield, *Phys. Rev. Lett*. **90,** 115501 (2003).
[4] F. Brochard, *J. Polym. Sci. Polym. Phys. Ed*. ***17*,** 1367 (1979).
[5] D. F. Gu, A. M. Jamieson, and S. Q. Wang, *J. Rheol*. **37**, 985 (1993).
[6] V. F. Demange, F. Boue, A. Brulet, P. Keller, and J. P. Cotton, *Macromolecules* **31**, 801 (1998).
[7] H. J. Coles and M. S. Sefton, *Mol. Cryst. Liq. Cryst. Lett*., **1**, 159 (1985).
[8] H. J. Coles and M. S. Bancroft, *Mol. Cryst. Liq. Cryst.*, **237**, 97 (1993).
[9] R. G. Humphreys, H. A. Tarry, and M. J. Bradshaw, *Liq. Cryst*. **3**, 1039 (1988).
[10] Y. E. Pashkovskii and T. G. Litvina, *Poly. Sci*. **33**, 655 (1991).
[11] E. E. Pashkovskii, T. G. Litvina, W. Stille, and G. Strobl, *Vysokomol. Soedin., Ser. A* Ser. *B*, **37**, 1272 (1995).
[12] P. Y. Liu, A. M. Jamieson, and N. Yao, *Macromolecules*, **33**, 1692 (2000).
[13] N. Yao and A. M. Jamieson, *Macromolecules*, **31**, 5399 (1998).
[14] N. Yao and A. M. Jamieson, *Rheol. Acta*, **39**, 338 (2000).
[15] I. C. Khoo and S. T. Wu, *Optics and Nonlinear Optics of Liquid Crystals*, World Scientific, New Jersey (1993).

[16] D. F. Gu, S. R. Smith, A. M. Jamieson, M. Lee, and V. Percec, *J. Phys. II France*, **3**, 937 (1993).
[17] I. Noda, N. Kato, T. Kitano, and M. Nagasawa, *Macromolecules*, **14**, 668 (1981)
[18] H. Mattoussi and R. Ober, *Macromolecules* **23**, 1809 (1990).
[19] K. Skarp, S. T. Lagerwall and B. Stebler, *Mol. Cryst. Liq. Cryst*., **60**, 215 (1980).
[20] Y. E. Pashkovskii, A. Y. Bilimin, A. Y. Saminskii, and S. Y. Frenkel, *Vysokomol. Soedin., Ser. A Ser. B,* **31**, 350 (1989).
[21] Y. E. Pashkovskii, T. G. Litvina, and A. Y. Bilibin, *Vysokomol. Soedin., Ser. A Ser. B*, **32**, 381 (1990).
[22] H. Mattoussi, M. Veyssie, C. Casagrande, and M. A. Guedeau, *Mol. Cryst Liq. Cryst.*, **144**, 211 (1987).
[23] H. Mattoussi, *Mol. Cryst. Liq. Cryst*., **178**, 65 (1990)
[24] D. F. Gu, A. M. Jamieson, C. Rosenblatt, D. Tomazos, M. Lee, and V. Percec, *Macromolecules*, **24**, 2385 (1991).
[25] E. E. Pashkovsky, T. G. Litvina, S. G. Kostromin, and V. P. Shibaev, *J. Phys. II France* **2,** 1577 (1992).
[26] F. L. Chen, and A. M. Jamieson, *Macromolecules*, **27**, 1943 (1994).
[27] E. E. Pashkovsky, and T. G. Litvina, *J. Phys. II France*, **2**, 521 (1992).
[28] H. Mattoussi, R. Ober, and M. Veyssie, *Europhys. Lett*. **2**, 233 (1986).
[29] J. S. Higgins and H. C. Benoit, *Polymers and Neutron Scattering*; Oxford University Press, Oxford, (1996).
[30] X. J. Wang, M. Warner, *J. Phys. A, Math. Gen.* **20**, 713 (1987).
[31] P. L. Maffetone and G. Marrucci, *J. Rheol*. **36,** 1547 (1992).
[32] D. R. M. Williams and A. Halpern, *Macromolecules*, **26**, 2025 (1993).
[33] G. A. Carri and M. Muthukumar, *J. Chem. Phys.*, **109**, 11117 (1998).

Chapter 7 Rheology of ABA Nematic Gels

The research presented in this chapter was conducted as collaboration between Michael Kempe, Rafael Verduzco, and Neal Scruggs. All the work with the polymer ABASiCB5 was performed by Michael Kempe, the work with ABASiCB4 was performed jointly with Neal Scruggs and Michael Kempe, and the work with ABASiBB was performed jointly with Rafael Verduzco and Michael Kempe.

7.1 Introduction

Liquid crystals (LCs) have order and dynamics intermediate between isotropic liquids and crystalline solids. Their anisotropic structure is manifested in their macroscopic properties, such as birefringence, dielectric anisotropy, diamagnetic anisotropy, and orientational elasticity [1]. It is the coupling of these unique properties with fluidity that make LCs useful for a large variety of electro-optic devices. LCs are often combined with polymers to confer mechanically stability. This is usually accomplished by photo or thermally initiating the polymerization of reactive monomers dissolved in an LC mixture to create polymer-dispersed LCs (PDLCs), polymer-stabilized LCs (PSLCs), or LC gels.

In a PDLC [2, *3*, 4, 5], Fig. 7.1a, droplets of phase-separated LCs are embedded in a polymer matrix. The LC phase can be aligned by application of an electric field. If the indices of refraction of the LC and the polymer matrix are matched, an optically transparent state is achieved. The main problem with these systems is a hazy appearance due to the difficulty of matching the refractive indices in all directions. Alternatively in PSLCs [6, 7, 8], Fig. 7.1b, a dilute phase-separated polymer "network" is formed in an LC host to control the director orientation. The lack of control over the polymerization

process can cause the PSLCs to have regions of significantly higher or lower polymer content, creating optical or viscoelastic nonuniformities.

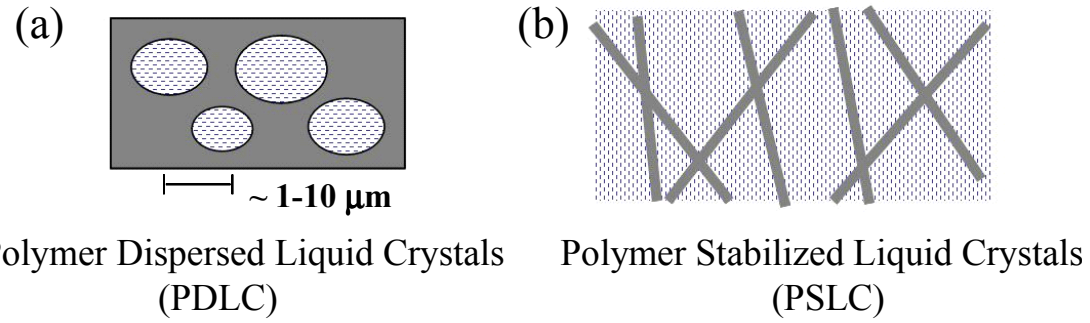

Figure 7.1. Schematic diagrams of (a) polymer-dispersed liquid crystals and (b) polymer-stabilized liquid crystals.

Single-phase LC gels [9, 10, 11] with improved optical properties can be made if better compatibility between the polymer network and the small molecule LC is maintained [9]. Such gels have only been achieved with polymer concentrations above 8 wt %, which have extremely slow reorientational responses [7, 12].

Scientifically, progress has been hampered by the difficulty of creating a well characterized and reproducible PDLC, PSLCs, or LC gel material. The random nature of photoinitiated cross-linking results in a broad distribution in the length of polymer between cross-links and also in the formation of dangling chains and free-floating polymers. Since the minimum concentration of polymer necessary to form a gel is determined by the length between cross-links, long, well-solvated polymers are necessary to form a dilute gel. With in situ polymerization it is not possible to produce extremely long distances between cross-links because of the high rate of termination reactions and the improbability that dilute chain ends will react to form a cross-link.

In this chapter, we present a method for creating a well-characterized nematic gel using an ABA block copolymer with long side-group liquid crystalline midblock and LC-phobic end blocks. The polymer was dissolved in a small molecule LC, and self-assembly occurred by microphase separation of the end-blocks, creating a physically cross-linked network. Because these gels self-assembled from monodisperse polymers, they had a well-defined chain length between cross-links. The high molecular weight of these polymers allowed gels to be formed with as little as 3 wt % polymer. The resulting single-phase gel was thermoreversible and optically uniform. Alignment was readily induced by electric fields with reorientation times of ~10 ms.

7.2 Polymers Used for the Nematic Gels

Two different methods were used to make high molecular weight SGLCPs. The first one used hydroboration/oxidation followed by attachment of an acid chloride functionalized mesogen. The second method used a hydrosilylation reaction to attach mesogenic units directly to the backbone. Since the second method had only one step that involved the polymer, it was much more reliable and was used for this ABA nematic gel study. A limited number of experiments (SANS, transient rheology, and director response time measurements) determined that both types of polymers had very similar effects on a nematic host.

The polymers used in this study, Fig. 7.2, are ABA block copolymers where the "A" blocks consist of polystyrene with number average molar masses of 57 and 67 kg/mol. The "B" blocks are side group liquid crystalline polymers (SGLCPs) with molar masses between 1,000 and 1,200 kg/mol, Table 7.1. The nematic liquid crystal 4'-pentyl-4-

cyanobiphenyl (5CB) was selected as the solvating medium for the gels since it is one of the most thoroughly characterized small molecule nematic LCs. Cyanobiphenyl-based polymers, ABASiCB4 and ABASiCB5, were chosen to promote solubility in 5CB [13]. Similarly, the butoxy-benzoate-benzaldehyde-based polymer ABASiBB was chosen because of its side group's proven ability to dissolve in cyanobiphenyl-based LCs [14].

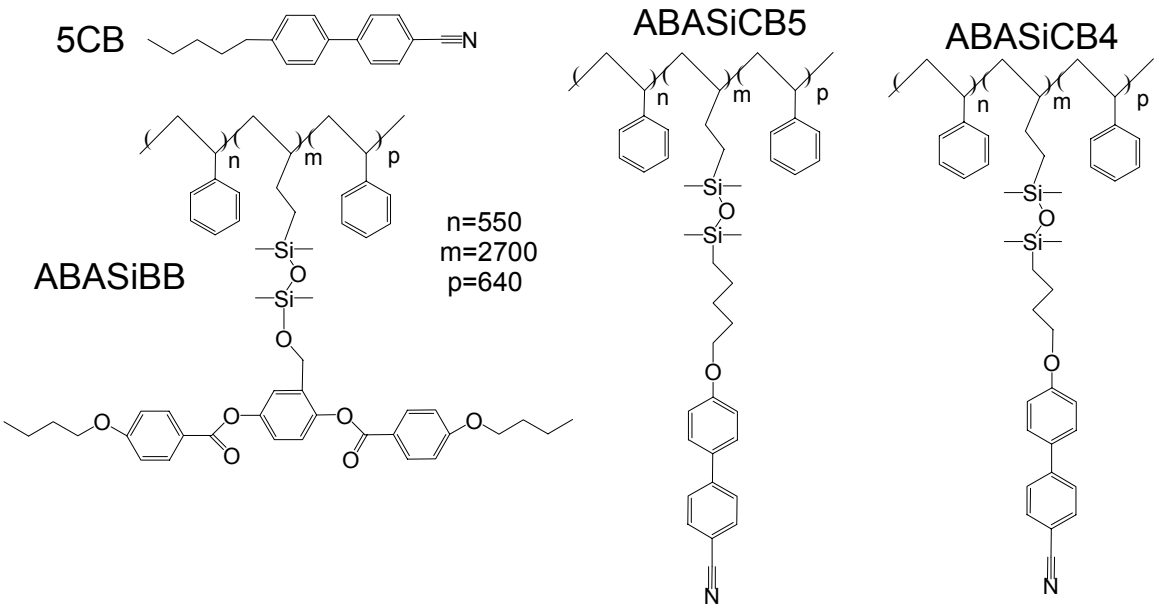

Figure 7.2. Molecular structure of the nematic solvent 5CB and the ABA liquid crystalline polymers. These polymers were also made in a homopolymer form and named PBSiBB, PBSiCB5, and PBSiCB4.

A "polymer analogous" approach to synthesis allowed a model series of high molecular weight polymers to be created with different mesogenic side groups but the same degree of polymerization. First, the polymer backbone was synthesized using anionic polymerization with sequential addition of styrene, butadiene, and styrene [15]. A single ABA triblock, with block lengths given by n, m and p in Fig. 7.2, was used as the prepolymer for ABASiBB, ABASiCB5 and ABASiCB4, Table 7.1. The various mesogenic units were attached to the pendant vinyl groups of the 1,2-polybutadiene by hydrosilylation [16, 17, 18]. SGLCP homopolymers PBSiCB4, PBSiCB5, and PBSiBB were also synthesized to characterize their conformation and thermal characteristics in

5CB. A single 1,2-polybutadiene having DP=1200 was used as the prepolymer for all three SGLCP homopolymers, Table 7.2. The details of these syntheses are given in Appendices A1 and A3.

[a]Polymer	[b]Total M_n (kg/mol)	PDI	LC Block M_n (kg/mol)	[c]LC Block % 1,2	[c]LC Block % 1,4	[c]LC Block % Mesogen	[d]T_i (^oC)
[e]ABA	270	1.26		88	12		
ABASiBB	1341	1.5	1217	17	12	71	74
ABASiCB5	1172	1.4	1048	4	12	84	64
ABASiCB4	1134	1.4	1010	4	12	84	40

Table 7.1. ABA block copolymer characterization. [a] The polymer names start with ABA because they were made from poly[styrene-block-(1,2-butadiene)-block-styrene] triblock copolymer. Polymers whose name ends with CB5 or CB4 have a cyanobiphenyl mesogen with a 4 or 5 methylene spacer connecting the siloxane group to the mesogen. Polymers ending with BB have the side-on mesogenic unit, Fig. 7.2. [b] The molar masses of the butadiene pre-polymers were measured using MALLS but the final polymer molar masses listed were calculated based on the fractional conversion of the vinyl groups. [c] The percents are based on the number of monomers in the LC block only. [d] T_i refers to the temperature at which the polymer becomes completely isotropic upon heating determined using a Zeiss polarized optical microscope (POM) equipped with a Mettler FP82 hot stage. [e] For the ABA triblock copolymers, the two styrene end-blocks had molar masses of 57 and 67 kg/mol and the initial 1,2-polybutadiene center block had a molar mass of M_n=146 kg/mol.

The polymers were made into nematic gels or homopolymer solutions by dissolving desired amounts of polymer and 5CB in dichloromethane, removing the solvent by blowing air over it until a nematic phase appeared, and then placing it in a vacuum oven at room temperature for 2 days. To be sure the polymer was homogeneously mixed throughout the 5CB solvent, the solution was heated to ~45 ^oC and stirred periodically during the drying process.

[a]Polymer	[b]Total M_n (kg/mol)	PDI	[c]% 1,2-units	[c]% 1,4-units	[c] % mesogen	[d]T_i (^{o}C)	[e]$R_{\perp b}$ (Å)	[e]$R_{\|\|b}$ (Å)	[e] $\frac{R_{\perp b}}{R_{\|\|b}}$
PB	63	1.04	~98	~2					
[f]PBSiBB	743	1.10	4	~2	94	120	26±2	163±30	0.16±0.02
PBSiCB5	497	1.12	5	~2	93	70	75±5	51±5	1.47±0.04
PBSiCB4	467	1.10	6	~2	92	60	63±4	38±3	1.65±0.05

Table 7.2. Homopolymer characterization. [a] The polymer names start with PB because they were made with 1,2-polybutadiene. Polymers whose name ends with CB5 or CB4 have a cyanobiphenyl mesogen with a 4 or 5 methylene spacer connecting the siloxane group to the mesogen. Polymers ending with BB have the side-on mesogenic unit, Fig. 7.2. [b] See note "b" in Table 7.1. [c] Mol percent of LC block. [d] See note "d" in Table 7.1 [e] The radii listed are for the quadratic characteristic distances and were calculated after subtracting the scattering due to the mesogenic units (Chapter 4). [f] Because of the bow tie shape of the SANS pattern the uncertainties in the radii and anisotropy are large.

7.3 Phase Behavior of Polymers, Solutions and Gels

In the bulk, homopolymers PBSiCB4 and PBSiBB were nematic and transitioned to an isotropic state at temperatures (T_i) of 60 and 120 ^{o}C, respectively, Table 7.2. The sample PBSiCB5 was smectic in the melt and did not transition directly to an isotropic state; rather, it has a biphasic temperature range (62.5 to 70 ^{o}C) where a smectic and isotropic phase coexist prior to becoming fully isotropic [19]. In the triblock copolymer form, all three polymers had a reduced isotropic transition temperature relative to their homopolymer analogs, Table 7.1. This was due to the reduced percentage of mesogenic units in the SGLCP midblock (71-84%) relative to the SGLCP homopolymers (92-94%) primarily as a result of the reduced 1,2-repeat units (88% compared to 98%) in the prepolymer.

In 5CB, the triblock copolymers ABASiCB4 and ABASiBB formed single-phase solutions or gels for all concentrations tested; however, ABASiCB5 formed two-phase mixtures for concentrations less than ~18 wt % polymer. The reduced compatibility of ABASiCB5 with 5CB is a typical result for mixing a smectic and a nematic material [20]. Despite this reduced compatibility the homopolymer form, PBSiCB5 dissolved in 5CB similarly to the other two homopolymers PBSiCB4 and PBSiBB.

Block copolymers were mixed with 5CB at concentrations up to 10 wt % polymer for ABASiCB4 and ABASiBB, and up to 50 wt % for ABASiCB5. The resulting gels were examined by POM to observe the effect of the polymer network on T_{ni}. All three systems showed a single sharp transition from a nematic to an isotropic state upon heating. For 20 wt % ABASiCB5 T_{ni}=38 ^{o}C, for 5 wt % ABASiCB4 T_{ni}=34.5, and for 10 wt % ABASiBB T_{ni}=35.6, as compared with 35 ^{o}C for bulk 5CB. This demonstrated that the presence of the polymer network did not significantly affect the local nematic order of 5CB itself.

The dissolution of a polymeric material in a small molecule solvent is entropically driven. In the isotropic state the polystyrene end-blocks were soluble in 5CB, Fig. 7.3a. In a solution with nematic order, the entropy of a dissolved polymer is reduced, resulting in lower polymer solubility. Since the polystyrene end-blocks have no intrinsic nematic order, they were more strongly influenced by this entropic effect. Therefore, when the mixtures were cooled from the isotropic state, Fig. 7.3a, into the nematic state, the polystyrene blocks aggregated, forming microphase-separated domains, Fig. 7.3b,c,d.

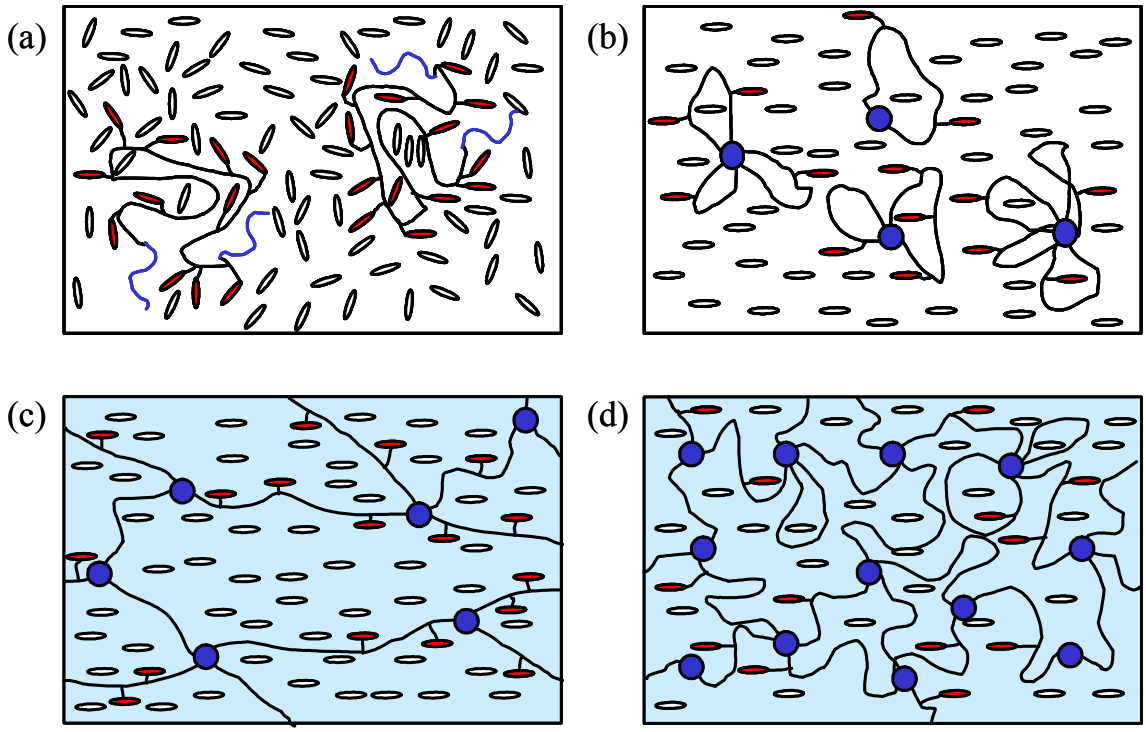

Figure 7.3. Schematic of the phase behavior of the nematic gels. Circles represent polystyrene aggregates while ovals represent mesogenic units. (a) Non-aggregated ABA block copolymer in the isotropic state. (b) Formation of a micellar solution in the nematic phase. (c) Nematic gel formed with a highly elongated polymer. (d) Nematic gel formed using a moderately elongated polymer.

In the nematic state all three gel types exhibited solid-like behavior [21]. If strongly deformed, the 5 wt % ABASiCB4 and ABASiBB gels held their new shape for a few days and the 20 wt % ABASiCB5 gel, indefinitely. When any of these gels were heated into the isotropic state they reversibly transitioned into a viscous fluid, see Section 7.6. This demonstrated that we had created a thermoreversible nematic gel.

The ABASiCB5 gel began to form a two-phase system when the concentration of polymer was reduced to approximately 18 wt %. Similar phase behavior is common in telechelic physical gels [22] and results from strong aggregation of the end-blocks.

The gels made from ABASiCB4 and ABASiBB did not have a two-phase region. In these systems, as the polymer concentration was reduced, the fraction of polymers forming a bridge between two end-block aggregates decreased, and, the fraction forming

loops (both end-blocks in the same aggregate) increased. It was the three-dimensional, space filling nature of the polymer network that gave the gels their solid-like characteristics. With decreasing polymer concentration, the spatial extent of the network was reduced and at a sufficiently low concentration, the material became a viscous liquid solution of polymer micelles, Fig. 7.3b. Increased backbone flexibility favors the formation of loops over bridges, Fig. 7.3c,d. Thus, the choice of the mesogenic unit can significantly affect phase characteristics since it controls the distance spanned by the mid-block, Table 7.2.

7.4 Effect of Microphase-separated End-Blocks on Refractive Indices

The refractive indices, n_e and n_o, of the gel composed of 20% ABASiCB5 in 5CB were measured to determine the effect of phase-separated end-blocks on these optical properties. The details of the measurement of the birefringence are given in Appendix A6. The microphase-separated end-blocks, did not affect the macroscopic optical uniformity of the material because their disruptions to the nematic field were significantly smaller than the wavelength of light. As the gel goes through an order to disorder transition at T_{ni} (no biphasic region), one observes a sharp change in the refractive indices and birefringence, Fig. 7.4.

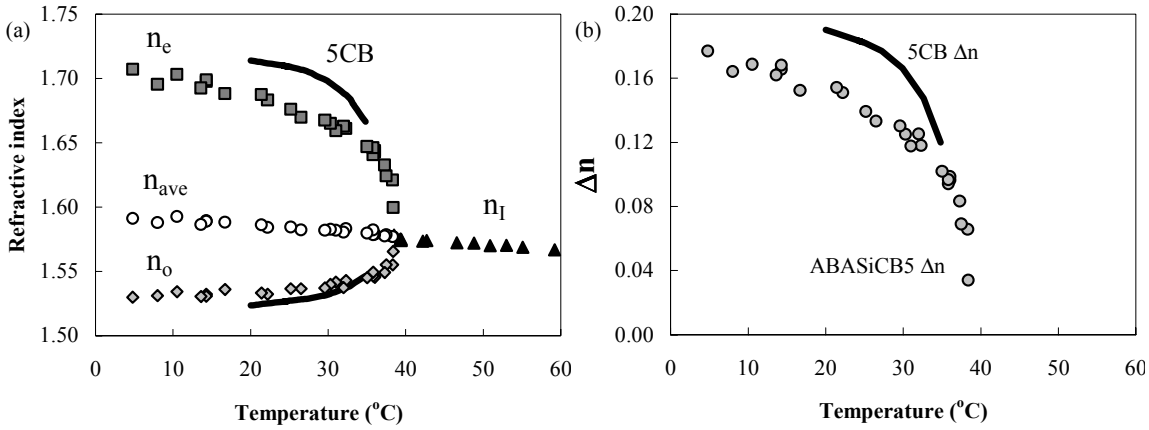

Figure 7.4. (a) Refractive indices and (b) birefringence of nematic gel with 20 wt % ABASiCB5 plotted next to bulk 5CB for λ=632.8 nm. Δn is the birefringence, n_e is the extraordinary refractive index, n_o is the ordinary refractive index, n_I is the refractive index in the isotropic state, and n_{ave} indicates the average refractive index calculated using Eq. 7.1.

Because of the uncertainty in the alignment of the gel, the accuracy of the measurement of the extraordinary refractive index n_e was in question. To check for consistency in the refractive indices in the isotropic and nematic phases, an average refractive index was calculated for the nematic phase using [23]

$$n_{ave} = \sqrt{\frac{n_e^{\,2} + 2n_o^{\,2}}{3}} . \quad (7.1)$$

Since the electronic properties of the molecules are not significantly changed by an isotropic to nematic phase transition, the average refractive index should not change either. Using Eq. 7.1 a straight line was found connecting the average refractive index in the nematic phase to the refractive index of the isotropic phase, Fig. 7.4a, indicating that the calculated values for the refractive indices and birefringence are valid.

The measured birefringence of this ABASiCB5 gel was compared with the birefringence of bulk 5CB, Fig. 7.4b. It was found that the birefringence decreased by approximately 20 to 35% with the addition of only 20 wt % polymer. If one assumes the birefringence of the nematic block of the polymer is comparable to 5CB and that the

refractive indices add up linearly, then one would only expect a 2 to 3% decrease in birefringence. The large decrease in birefringence can be attributed to localized director misorientations around the microphase-separated end-blocks along with some swelling of the end-blocks with 5CB, Fig. 7.5. At distances further away from the microphase-separated end-blocks, the LC adopts the macroscopic director orientation. Because these phase-separated end-blocks and the areas of director misorientations are smaller than the wavelength of light, no significant light scattering occurred and an optically uniform material was achieved.

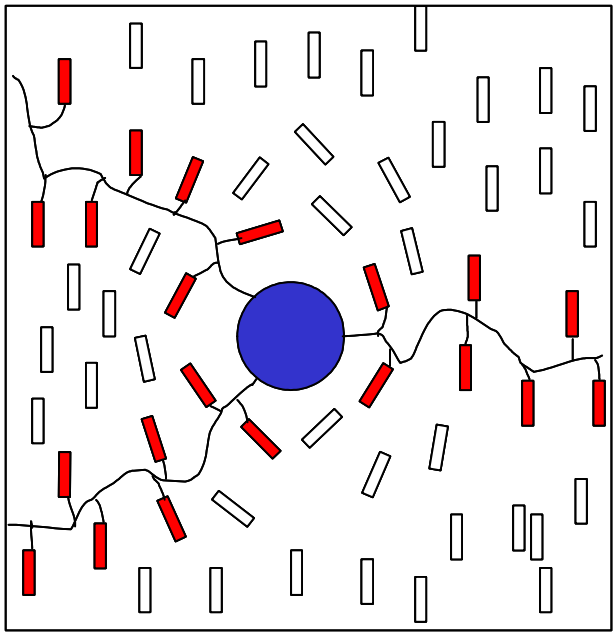

Figure 7.5. Schematic explaining the large change in Δn upon addition of 20 wt % ABASiCB5 to 5CB. Near the microphase-separated end-blocks there is significant director misorientation; but further away the macroscopic alignment is achieved.

7.5 Neutron Scattering from Homopolymer Solutions

In a physical gel composed of ABA block copolymers, the length spanned by the center block is an important factor for determining the minimum concentration of polymer necessary to form a gel. Therefore, neutron scattering studies were conducted

on solutions of the homopolymers dissolved in 5CB to determine how the structure of the side group affects the polymer anisotropy and molecular dimensions.

Perdeuterated 5CB (D5CB) was synthesized in which 95% of the hydrogen atoms were exchanged for deuterium (Appendix 4). Characterization of the D5CB, [24] (Chapter 3) demonstrated that it was very similar in T_{ni} and Δn to its hydrogenous analog 5CB, enabling results from either solvent to be directly compared. All three homopolymer samples were dissolved in D5CB at a concentration of 5 wt %. Scattering patterns were obtained using the Small-Angle Diffraction (SAD) instrument at the Intense Pulsed Neutron Source (IPNS) at Argonne National Laboratory using the same techniques as were used for the PBCBx series of polymers in Chapter 4. The samples were loaded into a cell made of two 25.4 mm diameter 3 mm thick quartz windows separated by a 0.5 mm spacer. Homogeneous (parallel) alignment of the sample was obtained by using rubbed polyimide layers on the quartz cell along with a 0.8 Tesla magnet. A cell containing bulk D5CB was used as a blank, and the scattering intensity was acquired for 10 hours at 25 ^{o}C.

The scattering patterns of PBSiCB4 and PBSiCB5 were very similar, Figs. 7.6a,b. Since the scattered intensity is inversely related to the characteristic length, directions with higher intensity at a given $|q|$ correspond to smaller dimensions [25]. In this way inspection of Figs. 7.6a,b indicated that PBSiCB4 and PBSiCB5 adopt a conformation that is extended perpendicular to the direction of mesogen orientation; thus, these polymers adopt similar anisotropic oblate, or disk-like, spheroidal conformations in solution. In contrast, PBSiBB extended parallel to the direction of mesogen orientation and produced a much more highly anisotropic scattering pattern, Fig. 7.6c. While the

scattering patterns of PBSiCB4 and PBSiCB5 had elliptical symmetry, the PBSiBB pattern had a bow tie shaped pattern. Preliminary data analysis indicated that deviations from elliptical symmetry were due to the polymer exceeding the overlap concentration along the long axis and/or to an elongated, rod-like conformation [26]. Further experiments at lower concentrations or using lower molecular weights are necessary to definitively determine the cause of the non-elliptical scattering pattern.

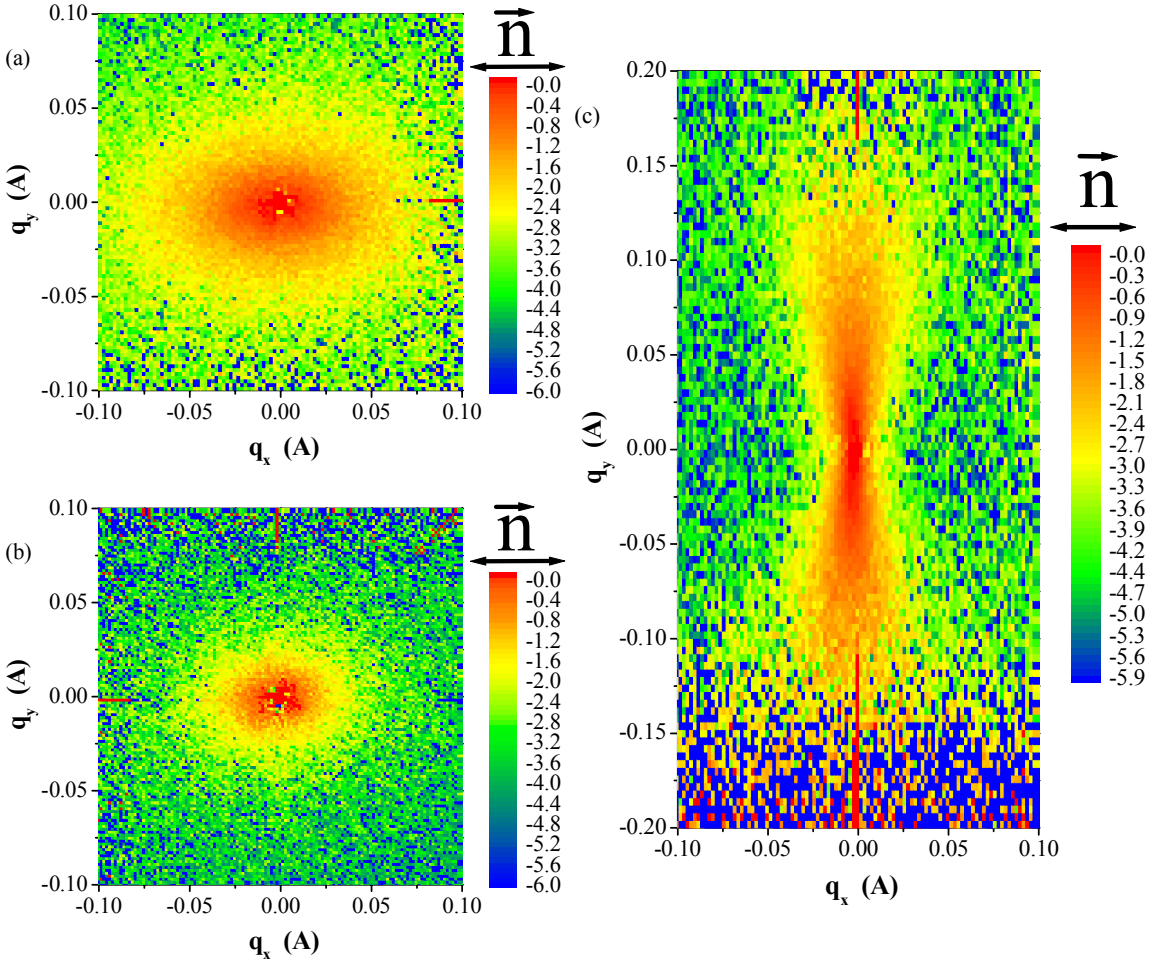

Figure 7.6 Neutron scattering patterns for homopolymers in D5CB. (a) 470 kg/mol PBSiCB4. (b) 500 kg/mol PBSiCB5. (c) 743 kg/mol PBSiBB. The scale is for values of $ln(I(q)/I_o)$.

In a hydrogenous sample dissolved in a perdeuterated solvent, scattering from the mesogenic units must be accounted for to determine the backbone characteristic quadratic

sizes parallel ($R_{//b}$) and perpendicular ($R_{\perp b}$) to the director. For the polymers PBSiCB4 and PBSiCB5 the procedure outlined in Chapter 4 was followed using

$$R_{||b}{}^2 = R_{||}{}^2 - \frac{L^2(2S+1)}{9}, \quad (7.2)$$

and

$$R_{\perp b}{}^2 = R_{\perp}{}^2 - \frac{2L^2(1-S)}{9}, \quad (7.3)$$

where S is the order parameter and L is the mesogen length. Using the software package MacSpartan, approximate values of L=22 and L=23Å were estimated for PBSiCB4 and PBSiCB5, respectively, and used to compute their radii, Table 7.2. PBSiCB4 was found to have a slightly smaller radii indicating greater flexibility of the backbone. This could be due either to reduced steric hindrance by the slightly smaller side group in PBSiCB4, or to smectic fluctuations in PBSiCB5.

Because of the anomalous bow tie-shaped scattering pattern of PBSiBB, there is a large uncertainty in the estimates of the polymer anisotropy and radii. The overall anisotropy of the scattering pattern can be estimated by plotting the scattered intensity versus q_y and $q_x \cdot R_{//}/R_{\perp}$ and adjusting the anisotropy $R_{//}/R_{\perp}$ until good overlap of the data sets is found, Figure 7.7. Figure 7.7 was generated using an anisotropy of $R_{\perp}/R_{//}$=0.138, but since the anomalous shape of the scattering pattern shows reduced intensity in the direction parallel to the director, it is most likely causing an over estimation of the anisotropy. Because of this, analysis of the pattern can only be used to accurately determine a maximum anisotropy. Therefore an anisotropy of $R_{\perp}/R_{//} \leq 0.16 \pm 0.02$ represents the highest anisotropy within the uncertainty of the experiment. Since the scattering parallel to the director is so low, a direct measurement of $R_{//}$ was not possible.

The scattering perpendicular to the director however was strong enough to infer $R_{\perp}$ using a small wedge-shaped section of data fit to the Debye equation,

$$I(q) = I_o\left(\frac{2}{q^4 R_g{}^4}\right)\left[q^2 R_g{}^2 - 1 + e^{\left(-q^2 R_g{}^2\right)}\right], \quad (7.4)$$

in which the radius of gyration is related to the quadratic characteristic size [27],

$$R_g = \sqrt{3} R_{\perp}. \quad (7.5)$$

From the estimated quadratic characteristic length $R_{\perp}$=26±2, a upper bound of $R_{//}$=163±30 Å was inferred from the polymer anisotropy. The greater dimensions of PBSiBB relative to PBSiCB4 enable a larger distance between cross-links to be at the same degree of polymerization.

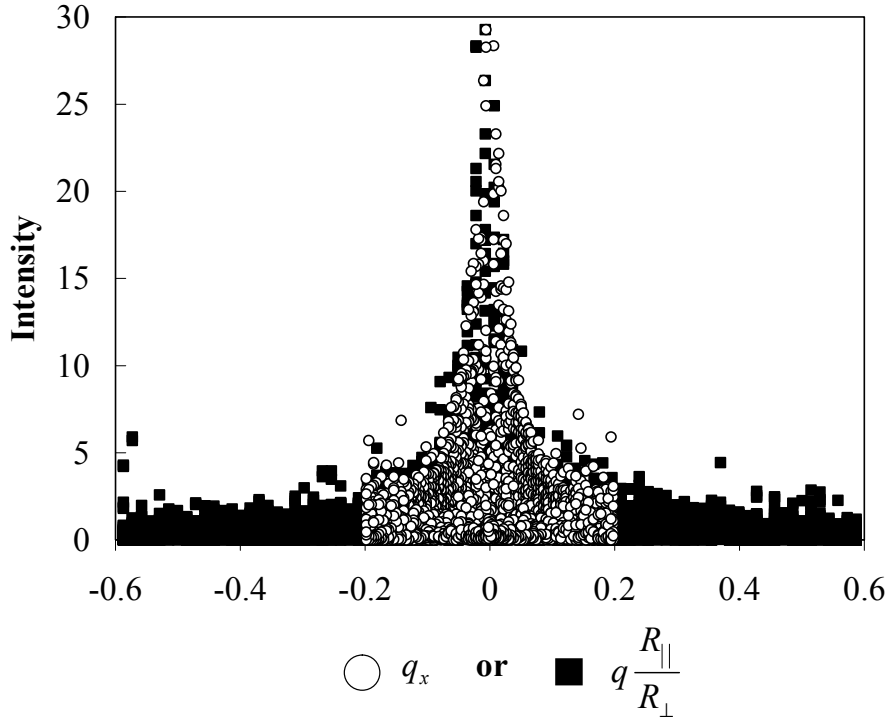

Figure 7.7. Plot of scattering pattern for PBSiBB demonstrating how the anisotropy was calculated by overlapping the plots scaled in the parallel and perpendicular directions. This plot was generated using $R_{\perp}/R_{//}$=0.138, but since the anomalous scattering pattern probably caused an over estimation of the anisotropy, a value of 0.16±0.02 was reported so that 0.138 represents the lower limit of the uncertainty.

In end-on SGLCPs similar to PBSiCB4 and PBSiCB5, both oblate and prolate conformations have been observed in bulk [28, 29]. In side-on SGLCPs like PBSiBB prolate conformations are, to the best of our knowledge, always found. This high anisotropy has been linked to what is called a "jacketed" conformation [30, 31]. Here a short group linking the mesogen to the backbone induces steric crowding of the mesogenic units, preventing the backbone from bending easily. When this decreased flexibility is coupled to nematic order, a large anisotropy is produced.

With respect to gels formed from an ABA block copolymer, a prolate conformation is more likely to produce a greater distance between cross-links. In an oblate conformation two of the three orthogonal axes correspond to the large axis, whereas a prolate conformation only has one axis corresponding to the larger axis. Therefore, comparing polymers with the same degree of polymerization, the inverse anisotropy, and the same backbone flexibility, a prolate conformation will produce a longer distance between cross-links. When one considers the reduced flexibility, due to steric interactions between adjacent side groups [30], combined with the greater anisotropy of PBSiBB relative to PBSiCB4 and PBSiCB5, this explains the observation ABASiBB can form gels at significantly lower molar concentration, Fig. 7.3c, than ABASiCB4 or ABASiCB5 can, Fig. 7.3d.

7.6 Dynamic Moduli Indicate the Formation of Gels

Dynamic rheological measurements were conducted to verify that the polymer end-blocks are physically linked to form a gel. These experiments were performed on a Rheometrics Fluids Spectrometer (RFS II) rheometer equipped with a shear cell made of

a 50 mm diameter titanium cone and plate having a 0.0202 radial cone angle. No surface treatment was applied and the gels were heated into the isotropic state prior to measurement to erase any thermal history. Because the behavior of these gels was distinctly different in the isotropic and nematic phases, time temperature superposition could not be accomplished using a single reference temperature (T_o). To facilitate comparison of $G^*(\omega)$ in the two different phases, reference temperatures were chosen from data sets closest to the nematic to isotropic transition temperature. For gels where time temperature superposition did not work for all frequencies, the higher frequency data points were used to determine the time temperature shift factors [21, 32].

For temperatures in the nematic phase, the ABASiCB5 gel behaves like a solid with both the storage *G'* and loss *G''* moduli nearly independent of frequency, Fig 7.8. As the gel is heated into the isotropic state, at 38 ^{o}C, the physically cross-linked end-blocks dissolve producing a slope of –2 for G' and a slope of -1 for G" indicating a fluid-like response. Inspection of Fig. 7.8 shows that time-temperature superposition did not produce exact overlap for the curves measured at 38 and 40 ^{o}C with those at 50 ^{o}C and above. The curves for 38 and 40 ^{o}C have a lower terminal relaxation frequency than the others. This observation is consistent with the idea that the formation of a nematic field induces a change in solubility of the end-blocks, and that at temperatures close to T_{ni}, nematic fluctuations in the isotropic state make the end-blocks slightly less soluble. This reduced solubility is not enough to cause microphase separation and gel formation, but causes transient end-block associations making the polymer relax more slowly.

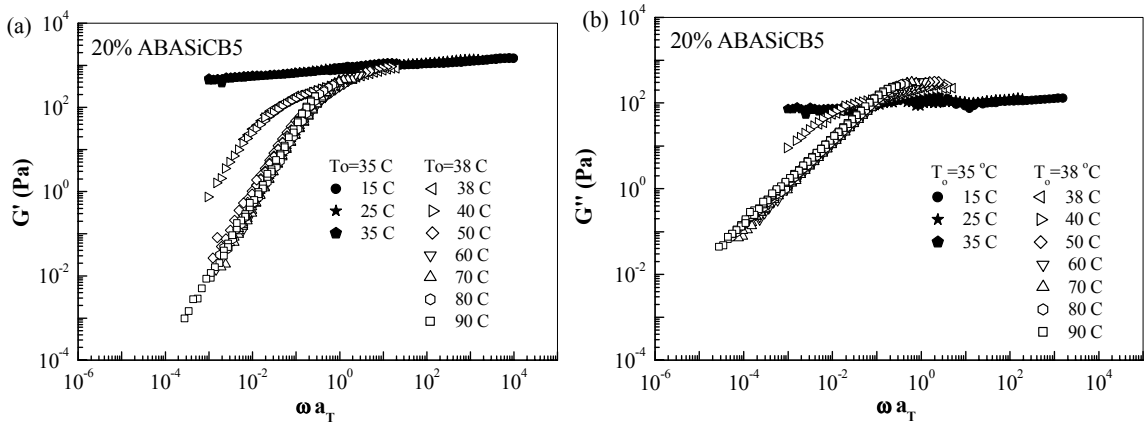

Figure 7.8. Time temperature superposition with dynamic moduli (a) G' and (b) G" of a nematic gel containing 20 wt % ABASiCB5 in 5CB at temperatures from 15 to 90 °C. For the isotropic phase $T \geq T_o$=38 °C. For the nematic phase $T \leq T_o$=35 °C.

Since the polymers ABASiCB4 and ABASiBB formed gels at a much lower concentration and did not form two-phase systems, several different polymer concentrations were tested to determine the threshold polymer concentration necessary to create a gel and produce moduli that are nearly independent of frequency. Similarly to ABASiCB5, when enough polymer is present to form a gel, a transition from fluid-like to solid-like behavior was seen as the materials were cooled through T_{ni}. One of the main differences between the ABASiCB5 gel and the ABASiCB4 and ABASiBB gels was that as the concentration of polymer was reduced, the latter gels slowly transitioned from solid-like behavior to more liquid-like behavior in the nematic phase, Figs. 7.9, 7.10, 7.11, 7.12, and 7.13. As these gels were cooled below T_{ni}, the nematic order increased, and the styrene end-blocks became less soluble, forming stronger physical cross-links and more solid-like behavior was seen, Fig. 7.10a.

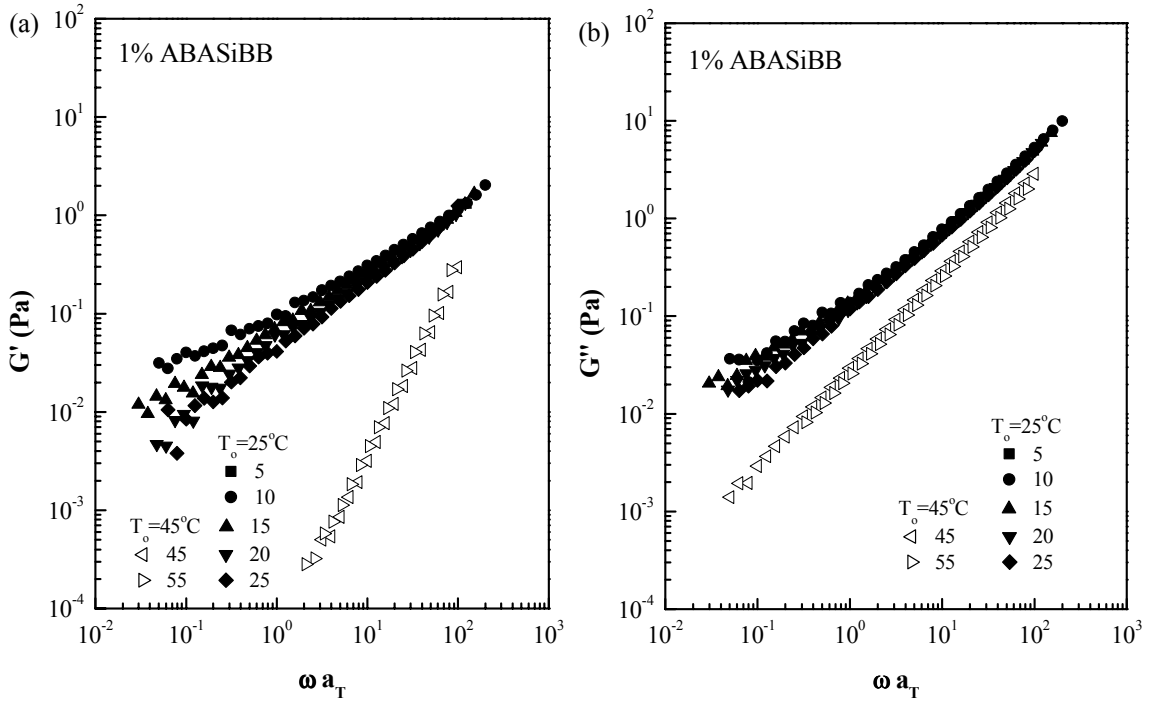

Figure 7.9. Time temperature superposition with dynamic moduli (a) G' and (b) G" of a nematic gel containing 1 wt % ABASiBB in 5CB at temperatures from 5 to 55 °C. For the isotropic phase $T \geq T_o$=45 °C. For the nematic phase $T \leq T_o$=25 °C.

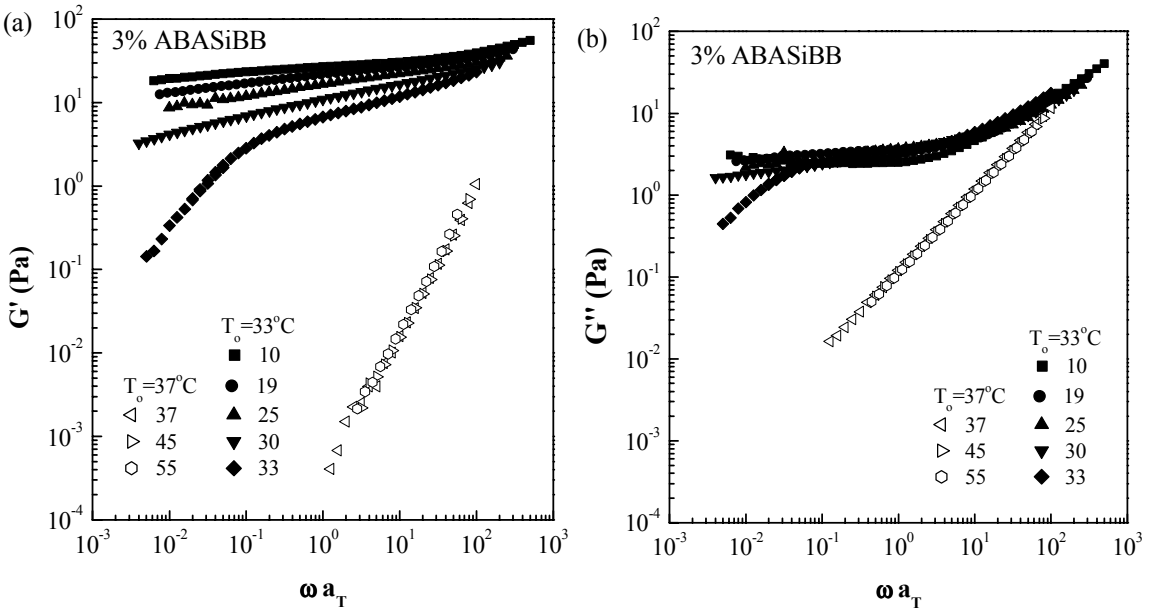

Figure 7.10. Time temperature superposition with dynamic moduli (a) G' and (b) G" of a nematic gel containing 3 wt % ABASiBB in 5CB at temperatures from 10 to 55 °C. For the isotropic phase $T \geq T_o$=37 °C. For the nematic phase $T \leq T_o$=33 °C.

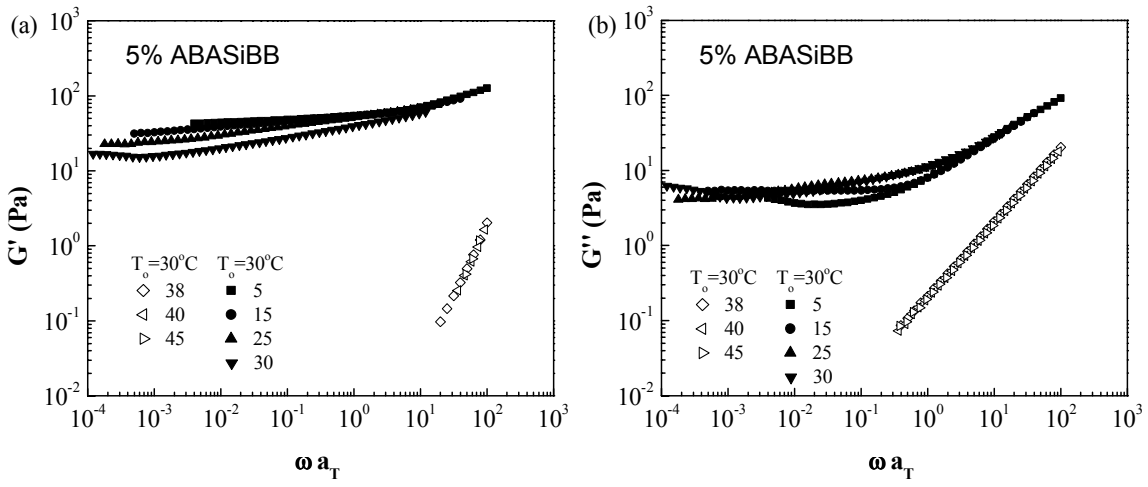

Figure 7.11. Time temperature superposition with dynamic moduli of ABASiBB (a) and (b) 5 wt % in 5CB at temperatures from 5 to 45 °C. For the isotropic phase $T \geq T_o$=38 °C. For the nematic phase $T \leq T_o$=30 °C

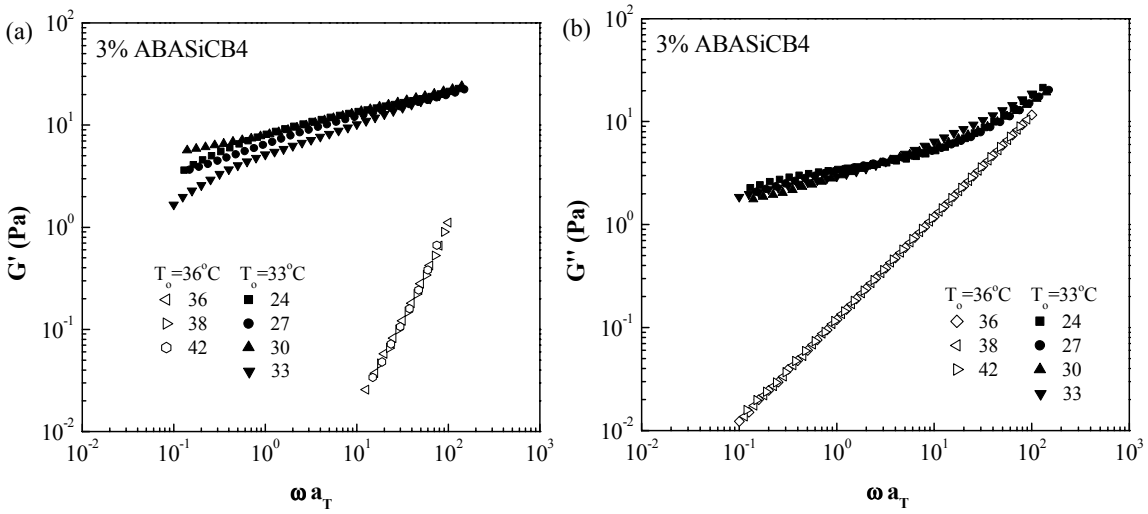

Figure 7.12. Time temperature superposition with dynamic moduli (a) G' and (b) G" of a nematic gel containing 3 wt % ABASiCB4 in 5CB at temperatures from 24 to 42 °C. For the isotropic phase $T \geq T_o$=36 °C. For the nematic phase $T \leq T_o$=33 °C.

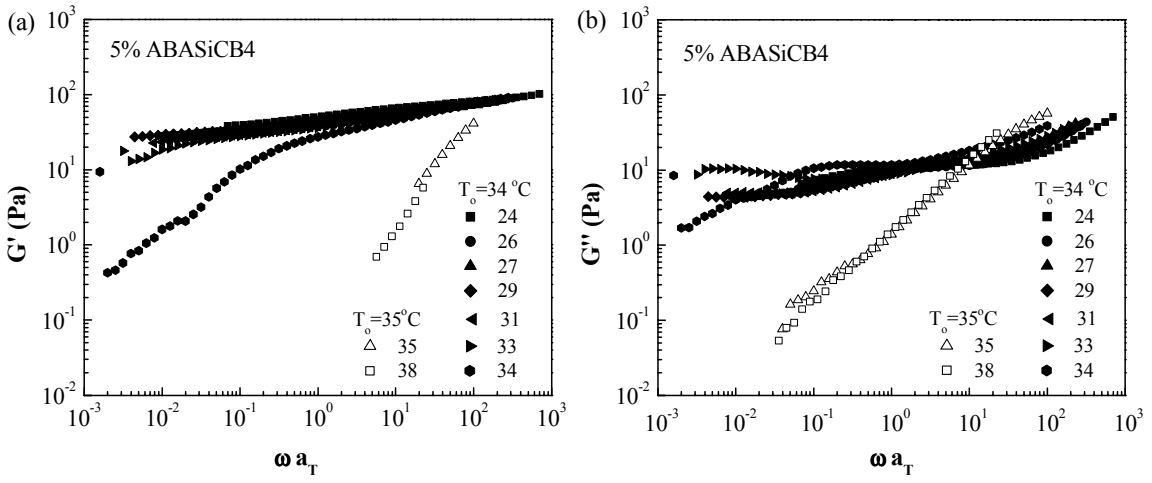

Figure 7.13. Time temperature superposition with dynamic moduli (a) G' and (b) G" of a nematic gel containing 5 wt % ABASiCB4 in 5CB at temperatures from 24 to 38 °C. For the isotropic phase $T \geq T_o$=35 °C. For the nematic phase $T \leq T_o$=34 °C.

If ABASiCB4 and ABASiBB are dilute enough, very little solid-like behavior is seen, Fig. 7.9. Here the polymer acts as an associative thickener causing a dramatic increase in viscosity in the nematic phase. At low enough polymer concentrations, micellar solutions, illustrated schematically in Fig. 7.3b, are most likely formed.

The solid-like properties of the gels are also affected by the fraction of loops and bridges. When a polymer chain forms a loop, it does not contribute to the strength of the polymer network. The reduced flexibility of ABASiBB should make it more difficult to form loops; therefore, if one wanted to create a very dilute gel a more highly anisotropic, rigid, and prolate polymer like ABASiBB is desired. At comparable temperatures and frequencies, slightly higher values for the storage modulus, G', are seen in ABASiBB as compared to ABASiCB4, 7.10 and 7.12, respectively. Similarly, ABASiBB also has a flatter plateau in $G'(\omega)$ at $T<T_i$, Fig.7.11, indicating a more solid-like behavior when compared to the same concentration of ABASiCB4, Fig. 7.13. Furthermore, one must also consider that ABASiBB had a molar mass that was 20% greater than ABASiCB4;

therefore, at the same wt % ABASiCB4 had a significantly greater molar concentration. This indicates that ABASiBB forms a stronger network with significantly fewer polymer chains. The greater dimension $(R_{//})$ and reduced flexibility of ABASiBB enable it to form gels at lower concentrations.

7.7 Gel Conoscopy and Orientational Response to Shear

Practical applications of LC systems require control over alignment. Typical small molecule LCs can be macroscopically aligned by surface treatment in either a parallel or a perpendicular orientation relative to a surface [33, 34]. Dilute physically cross-linked LC gels can be aligned by surface treatments as well as by shear or by electric and magnetic fields. However, the 20 wt % ABASiCB5 gel could not be aligned by surface treatment.

To evaluate the effect of an applied shear strain on the 20 wt % ABASiCB5 gel, the sample was examined using conoscopy as outlined in Appendix 5 [35, 36]. When the 20 wt % ABASiCB5 gel was heated into the isotropic state, above 38 ^{o}C, and then cooled to room temperature, a polydomain, light scattering structure was formed, Fig. 7.14a. After the application of a strain of 3.7 at a rate of 1.2 s^{-1}, an interference figure was observed, indicating that good alignment was achieved, Fig. 7.14b. Although the interference figure only lasted for a few minutes, its presence is a significant achievement since it required a defect-free monodomain over a thickness of 0.40 mm. Achieving a defect free monodomain of this quality is not observed in PDLCs or with PSLCs. Even the well-solvated nematic LC gels of Meyer et al. [9] had some director misorientations which resulted in a "fine speckle pattern."

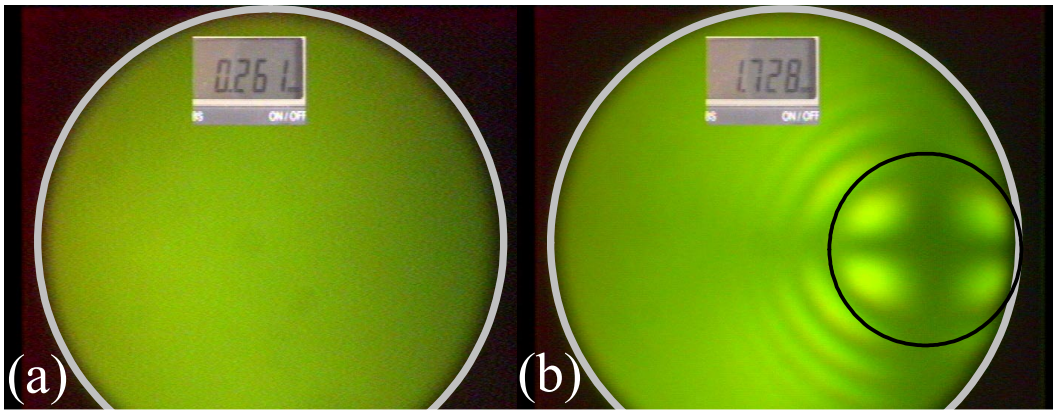

Figure 7.14. Conoscopic images of 20 wt % ABASiCB5 gel in 5CB at 25 °C (a) before shear and (a) after a shear strain. The black circle was drawn to emphasize the elliptical shape of the interference figure resulting from biaxiality. The inset images were used to synchronize the measurement of the stage translation with the recording of the conoscopic image. The sample thickness in this experiment was 0.40 mm.

The conoscopic experiments with 20 wt % ABASiCB5 indicated that the applied shear stress rotates the director counter to the vorticity direction and orients the gel at a steady-state angle of approximately –8 or –9 degrees with respect to the velocity gradient direction (surface normal). This situation is similar to what was seen in other experiments with an SGLCP homopolymer dissolved in 5CB [37] (Chapter 5). In these experiments, the addition of more than 7.5 wt % of a large, M_n = 420 kg/mol, SGLCP also caused the solution to flow align nearly perpendicular to the surface. In this way, our gel had an effect similar to what one would expect for an infinitely long polymer. The application of a shear stress caused the polymer backbone to orient in the velocity direction with a slight tilt toward the extensional axis. To maintain a preferred orientation perpendicular to the backbone, the mesogen would rotate counter to the vorticity direction, as observed.

Biaxiality was observed in the conoscopic image of 20 wt % ABASiCB5 at 25 °C, Fig. 7.14b. The overall shape of the image is circular, but the interference pattern has an

elliptical shape. Furthermore, the thickness of the Maltese cross pattern is different for the horizontal and the vertical directions. The appearance of biaxiality in an LC is unusual but not unprecedented [38, 39, 40]. The biaxial interference figure lasted only a few minutes and slowly faded away as the gel returned to a polydomain state. This indicated that stresses within the polymer matrix were responsible for the biaxiality.

At temperatures between 35 and 38 ^{o}C, the gel could be aligned by shear to produce a uniaxial conoscopic image. However, at lower temperatures, 25 ^{o}C, an aligned state near the surface normal could only be achieved if a very large amplitude, γ~20 to 30, oscillatory shear was applied to the sample while cooling rapidly. This demonstrates that 20 wt % ABASiCB5 can be macroscopically aligned by shearing forces in a nearly homeotropic orientation to yield an optically uniform gel.

The aligned state of the 20 wt % ABASiCB5 gel was unstable when oriented parallel to the surface. The gel was heated to the isotropic state and cooled to room temperature while in an 8.8 Tesla magnetic field oriented to give homogeneous, or parallel, alignment. The resulting aligned gel was sensitive to small disturbances caused by thermal expansion or by handling of the cell. Since the mesogen will align at an angle of about –8 degrees in response to a shear, the application of stresses can cause a director rotation of approximately 82 degrees which permanently alters the alignment of the LC. Changing the structure of the mid-block side group, e.g., ABASiBB, could allow for shear alignment in the parallel orientation [41]. Future experiments will address this issue.

In dilute gels, surface treatment, electric fields, and magnetic fields were all able to induce alignment. A 10 μm thick sample of the 3 wt % ABASiBB gel placed in a cell

having rubbed polyimide surface treatment achieved a monodomain after annealing for several days at room temperature. The gel could be aligned more quickly when cooled from the isotropic to nematic state in an 8.8 Tesla magnetic field. Furthermore, these gels can be immediately aligned from a polydomain structure in response to an electric field of 1.2 V/μm (i.e., 30 V_{rms} in a 25 μm gap). If the electric field is removed after a short period of time, <1 day, the LC relaxes back to a polydomain structure with a time constant of ~10 to 20 ms. More concentrated gels, e.g. 20% ABASiCB5, could not be aligned using surface anchoring alone but could be aligned by higher fields of ~8 V/μm; however, when the voltage was removed it took 1 to 2 seconds for the polydomain structure to return. This demonstrates the need for a very dilute gel.

7.8 Potential Applications of ABA Nematic Gels

This new type of nematic gel has many properties that could make it uniquely useful for electro-optic devices. The primary properties that distinguish it from other polymer gels, PDLCs, and PSLCs are its excellent optical uniformity and the ability to create dilute gels that are easily reoriented [7]. For example, these gels provide a means to produce a switchable electro-optic device that work in a light scattering mode in the voltage-off state with a haze-free, transmissive voltage-on state.

As a proof of concept, gels of ABASiCB4 and ABASiBB were placed between glass plates with indium tin oxide (ITO) electrodes and a gap of 25 μm. The samples were heated to the isotropic state and then cooled rapidly to produce a light scattering, polydomain structure, Fig. 7.15a. A 1000 Hz AC voltage applied across the cells reversibly generated monodomains, Fig. 7.15b. An electric field of 1.6 V/μm was

required to generate an optically clear monodomain of 5 wt % ABASiCB4 gel, and a field of 1.2 V/mm was required for a 4 wt % ABASiBB gel. Gray scale (analog response) was illustrated by applying field strengths less than 1.6 V/μm to the 5 wt % ABASiCB4 gel to slightly orient the gel, resulting in a state with an intermediate degree of light scattering.

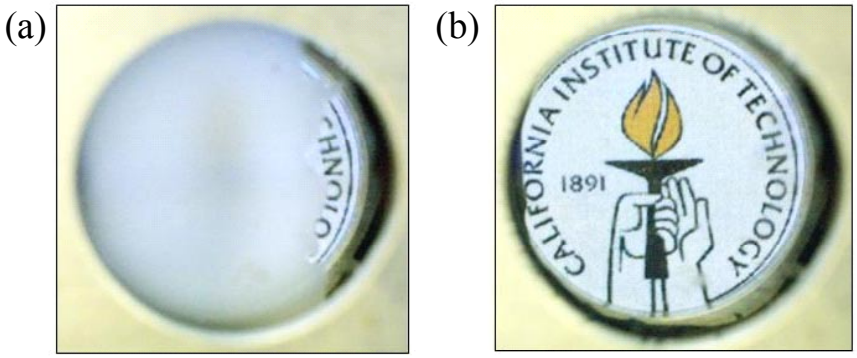

Figure 7.15. Photo showing the switching of an electro-optic device using 5 wt % ABASiCB4 block copolymer nematic gel in a 25 μm gap. (a) Light scattering voltage off state. The section of the image where part of the word "TECHNOLOGY" can be seen was intentionally kept free from gel to demonstrate the optical clarity of the cell. (b) Transmissive voltage on state switched at 40 V_{rms}. The diameter of the window in these pictures is 1.8 cm.

These gels exhibited a threshold field [9] for director rotation, rather than the threshold voltage typical of small molecule LCs. In a 5 μm gap the dilute gels produced a weakly light scattering state; however, the 5 wt % ABASiCB4 gel at this thickness required only 10 V_{rms} to achieve optical clarity. This phenomenon has been previously observed in chemically cross-linked LC gels [9, 42]. Future experiments will be performed to more quantitatively define and evaluate the threshold field effect.

These experiments indicate that an ABA nematic gel can be effectively used in a light scattering electro-optic device [4], Fig. 7.16. Without an applied voltage, incident light is scattered to produce a bright state. Application of a voltage induces the formation of an LC monodomain that allows the incident light to be transmitted and absorbed on the back

surface, yielding a dark state. At intermediate voltages, the ratio of absorbed to scattered light can be modulated.

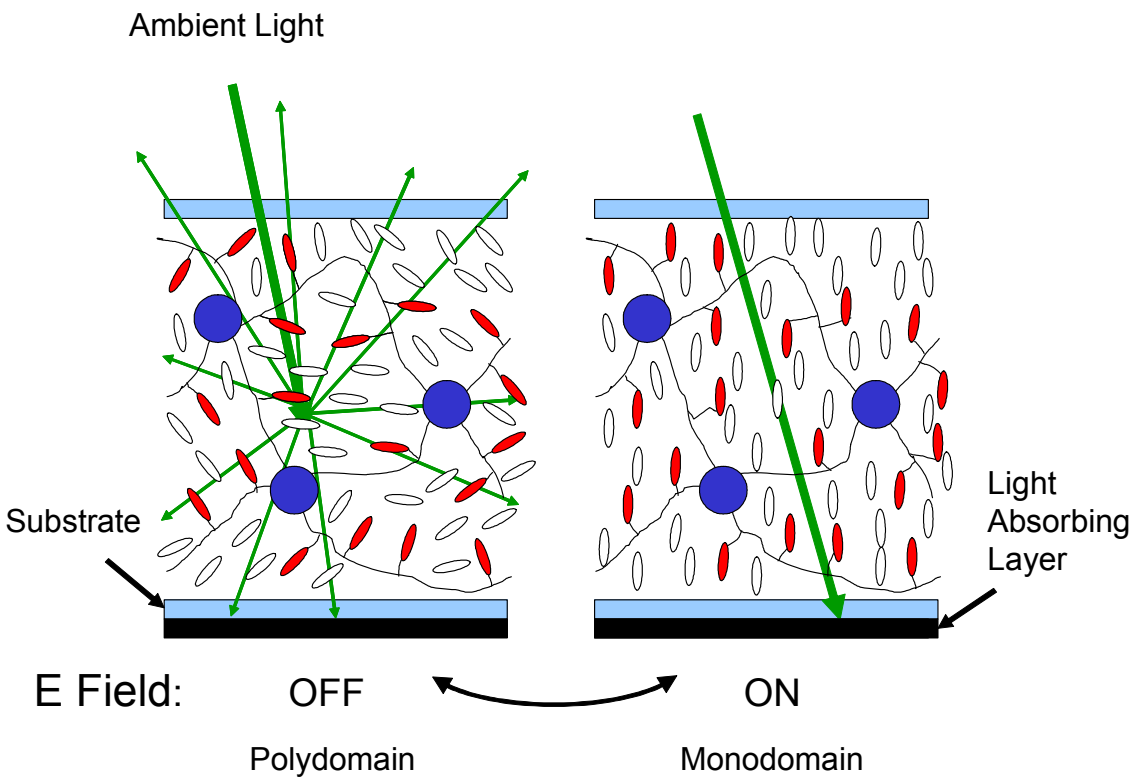

Figure 7.16. Schematic of an electro-optic device using an ABA block copolymer nematic gel. The LC domains are shown schematically with dimensions on the order of the polymer size even though they would actually be much larger than that and may slowly transition from one orientational direction to another. Similarly, the size of the polymers relative to the cell dimensions is greatly exaggerated.

This type of device has many advantages over current display technologies. Polarizers and alignment layers are not required, there is no viewing angle dependence because light is scattered in all directions, and the power requirements should be very small because it uses ambient light. Furthermore, the thermoreversibility of these gels makes them amenable to low cost processing techniques such as "printing" and "roll-to-roll" processing. Therefore, in addition to better optical properties, no viewing angle problem, these gel materials may be significantly cheaper to manufacture in a device

Because of the absence of the viewing angle problem and the formation of "haze", this gel material is positioned to replace most PDLCs applications such as electronically switchable windows [3,7]. Similarly, the rapid response time of these materials give them a dramatic advantage over materials such as E-ink [43].

Although the thermoreversibility of these gels is beneficial for some applications, this property can also be detrimental. Over time, and with the repeated application of a field, physical gels will reorganize unless the physical crosslinks are effectively permanent. Fore example, in a light scattering device, this would result in a transmissive voltage-off state. Currently, work is under way to create a gel that can be chemically cross-linked by a photo or thermally initiated reaction once the desired alignment is achieved by self-assembly. This crosslinking reaction will take advantage of a locally high concentration of reactive units in the end-block aggregates to achieve controlled covalent cross-linking. This would result in a well controlled and reliably produced permanent structure.

Preliminary results indicate that the director reorientation rates of these gels could be made comparable or possibly even faster than bulk 5CB. The presence of homopolymer in solutions of 5CB always slows down the director relaxation rate (Chapter 6). If the polymer backbones are not able to rotate with the director they can promote alignment from throughout the nematic gel. The relaxation time of a nematic is related to the reciprocal of a characteristic distance squared, $1/\xi^2$ [44]. In a standard cell ξ is equal to the gap thickness, but in a gel ξ is related to the distance between polymer chains. Since the distance between polymer chains is very small, the deleterious effects of the polymer can be overcome by locking the polymer in place as in a gel.

7.9 Conclusion

We have demonstrated a new method for creating nematic gels using a well-defined, high molecular weight ABA block copolymer. The polystyrene end-blocks are well dissolved in the isotropic state but microphase separate upon cooling into the nematic state. This produces nematic gels with a physically cross-linked, macroscopic polymer network. Since the end-blocks are not chemically cross-linked, the material can be reversibly heated into the isotropic state to produce a viscous fluid that is amenable for production of electro-optic devices. Because the microphase-separated end-block aggregates are smaller than the wavelength of light, gels with excellent optical uniformity are achievable.

While the ABASiCB5 polymer required a minimum of approximately 18 wt % polymer to form a single-phase gel, the ABASiCB4 and ABASiBB polymers did not have this limitation. The ABASiCB4 and ABASiBB gels slowly transitioned from a solid-like state to a micellar solution as the polymer concentration was reduced. Since the polymerization is done anionically in a controlled manner a very large and uniform distance between cross-links is possible. This allows the synthesis of an optically uniform gel is not limited to a concentration of approximately 8 wt % like photoinitiated systems [9]. Furthermore, this method does not produce free floating oligomers that slow the director reorientation in PSLC and PDLCS. Using this approach, gels with as little as 3 to 5 wt % polymer have been created and aligned by surface treatment, shear stresses, electric fields, and magnetic fields. Such gels were demonstrated to be suitable for a reflective electro-optic device. The use of larger molecular weight polymers should lead to even more dilute nematic gels with a faster director reorientational response.

Bibliography

[1] P.-G. de Gennes, *The Physics of Liquid Crystals*, Clarendon Press, Oxford, 2nd ed., (1993).
[2] L. Bouteiller and P. Le Barny, *Liq. Cryst.* **21**, 157 (1996).
[3] D. Coates, *J. Mater. Chem.* **5**, 2063 (1995).
[4] H. E. A. Huitema, G. H. Gelinck, J. B. P. H. van der Putten, K. E. Kuijk, C. M. Hart, E. Cantatore, P. T. Herwig, A. J. J. M. van Breemen, and D. M. de Leeuw, *Nature* **414**, 599 (2001).
[5] J. D. LeGrange, S. A. Carter, M. Fuentes, J. Boo, A. E. Freeny, W. Cleveland, and T. M. Miller, *J. Appl. Phys.* **81**, 5984 (1997).
[6] R. A. M. Hikmet, *J. Appl. Phys.* **68**, 4406 (1990).
[7] I. Dierking, *Adv. Mater.* **12**, 167 (2000).
[8] D. K. Yang, L. C. Chien, and J. W. Doane, *Appl. Phys. Lett*. **60**, 3102 (1992).
[9] C. C. Chang, L. C. Chien, and R. B. Meyer, *Phys. Rev. E* **56**, 595 (1997).
[10] L. Guan and Y. Zhao, *Chem. Mater.* **12**, 3667 (2000).
[11] C. A. Guymon, E. N. Hoggan, N. A. Clark, T. P. Rieker, D. M. Walba, C. N. Bowman, *Science* **275**, 57 (1997).
[12] B. R. Nair, M. A. R. Osbourne and P. T. Hammond, *Macromolecules* **31**, 8749 (1998).
[13] H. Kihara, R. Kishi, T. Miura, T. Kato, and H. Ichijo, *Polymer* **42**, 1177 (2001).
[14] M. C. Chang, H. W. Chiu, X. Y. Wang, T. Kyu, N. Leroux, S. Campbell, L. C. Chien, *Liq. Cryst.* **25**, 733 (1998).
[15] J. Sanger, C. Tefehne, R. Lay, and W. Gronski, *Polym. Bull.* **36**, 19 (1996).
[16] I. Ojima, M. Nihonyanagi, T. Kogure, M. Kumagai, S. Horiuchi, K. Nakatsugawa, Y. Nagai, *J. Organomet. Chem.* **94**, 449 (1975).
[17] M. A. Hempenius, R. G. H. Lammertink, and G. J. Vancso, *Macromol. Rapid Commun.* **17**, 299 (1996).
[18] A. Moment, R. Miranda, and P. T. Hammond, *Macromol. Rapid Commun.* **19**, 573 (1998).
[19] M. L. Auad, M. L., M. D. Kempe, J. A. Kornfield, S. Rendon, W. R. Burghardt, K Yoon, *Manuscript in Preparation* (2003).
[20] J. D. Laffitte, M. F. Achard, F. Hardouin, H. T. Nguyen, and G. Sigaud, *Liq. Cryst.* **17**, 487 (1994).
[21] J. D. Ferry, *Viscoelastic Properties of Polymers*, John Wiley and Sons, New York (1970).
[22] G. Y. Tae, J. A. Kornfield, J. A. Hubbell, and J. S. Lal, *Macromolecules* **35**, 4448 (2002).
[23] I. Haller, M. J. Freiser, and H. A. Huggins, *Mol. Cryst. Liq. Cryst*. **16**, 53 (1972).
[24] S. T. Wu, Q. H. Wang, M. D. Kempe and J. A. Kornfield, *J. Appl. Phys*. **92**, 7147 (2002).
[25] J. S. Higgins and H. C. Benoit, *Polymers and Neutron Scattering*; Oxford University Press, Oxford, (1996).
[26] M. H. Li, A. Brulet, P. Davidson, P. Keller, and J. P. Cotton, Phys. Rev. Lett. 70, 2297 (1993).
[27] P. Keller, B. Carvalho, J. P. Cotton, M. Lambert, F. Moussa, and G. Pepy, *J. Physique Lett*. **46,** L-1065 (1985).
[28] G. R. Mitchell, M. Coulter, F. J. Davis, and W. Gou, *J. Phys. II France* **2,** 1121 (1992).
[29] A. A. Craig and C. T. Imrie, *J. Mater. Chem*. **4**, 1705 (1994).
[30] N. Leroux, P. Keller, M. F. Achard, L. Noirez, and F. Hardouin, *J. Phys. II France* **3,** 1289 (1993).
[31] S. Lecommandoux, M. F. Achard, F. Hardouin, A. Brulet, and J. P. Cotton, *Liq. Cryst.* **22**, 549 (1997).
[32] R. G. Larson, *The Structure and Rheology of Complex Fluids*, Oxford University Press, New York (1999).
[33] M. Barmentlo, N. A. J. M. van Aerle, R. W. J. Hollering, J. P. M. Damen, *J. Appl. Phys.* **71**, 4799 (1992).
[34] N. A. J. M. van Aerle, M. Barmentlo, and R. W. J. Hollering, *J. Appl. Phys.* **74**, 3111 (1993).
[35] M. D. Kempe, M. L. Auad, J. A. Kornfield, W. J. Zhou, and S. T. Wu, *J. Rheol.* Manuscript in Preparation (2003).
[36] B. L. van Horn, and H. H. Winter, *Appl. Optics* **40**, 2089 (2001).
[37] M. D. Kempe and J. A. Kornfield, *Phys. Rev. Lett.* **90**, 115501 (2003).
[38] F. Hessel and H. Finkelmann, *Polym. Bull.* **15**, 349 (1986).
[39] P. A. Santoro, J. R. D. Pereira, and A. J. Palangana, *Phys. Rev. E* **65**, 057602 (2002).
[40] T. De'Neve, M. Kleman, and P. Navard, *J. Phys II France* **2**, 187 (1992).

[41] D. F. Gu and A. M. Jamieson, *Macromolecules* **27**, 337 (1994).
[42] E. M. Terentjev, M. Warner, R. B. Meyer, and J. Yamamoto, *Phys. Rev. E* **60**, 1872 (Aug, 1999).
[43] B. Comiskey, J. D. Albert, H. Yoshizawa, and J. Jacobson, *Nature* **394**, 253 (1998).
[44] I. C. Khoo and S. T. Wu, *Optics and Nonlinear Optics of Liquid Crystals*, World Scientific, New Jersey (1993).

Chapter 8 Concluding Remarks

In electro-optic devices, there is interest in using liquid crystalline polymers to control liquid crystal (LC) alignment, and to simplify the manufacturing of displays [1, 2, 3, 4, 5, 6] and compensating films [7, 8]. One concern with using polymers in an LC host is that the accompanying increase in viscosity adversely affects performance in an electro-optic device where rapid director reorientation is needed [9, 10, 11]. To minimize the viscosity increases and maintain rapid director reorientation, a low concentration of high molecular weight polymer is desired; therefore, this work has focused on the synthesis of well-defined high molecular weight side-group liquid crystalline polymers (SGLCPs) and their effects on a nematic host. High molecular weights were pursued as a pathway to create novel LC gels with low polymer concentration using self-assembly of an ABA block copolymer with an SGLCP center block.

The main obstacle to overcome was developing a method for synthesizing well-defined, high molecular weight polymers in a way that could also be used to create block copolymers. To do this, the polymer analogous approach was taken in which a functionalized mesogenic group was attached to a pendant vinyl group on 1,2-polybutadiene. Two methods to accomplish this were investigated. The first used hydroboration followed by oxidation to produce a polyalcohol, to which an acid chloride functionalized mesogen was then attached (Appendix 2). The second method used direct mesogen attachment to the vinyl group by hydrosilylation (Appendix 3). Since the second method converted the prepolymer to the desired SGLCP in one step (compared to three for the hydroboration method), it provided a superior route to low polydispersity

polymers. The hydrosilylation method was therefore used to create ABA block copolymers for use in nematic gels.

The effect of these SGLCPs on the rheological properties of a nematic solvent revealed a novel director reorientational phenomenon. Strong effects of the SGLCPs on the viscous parameters of a nematic host were found at relatively low polymer concentration compared to prior systems [12].

The information gained from homopolymer experiments was used to design high molecular weight ABA SGLCPs. These block copolymers produced gels when swollen with a nematic solvent. Prior researchers focused on methods to produce phase-separated "gels" using photo- or thermally-initiated polymerization of reactive monomers in a nematic solvent. Problems, such as the lack of control over cross-link density, restricted the concentration regimes of these systems and/or resulted in significant director misorientations manifested in deleterious turbidity. In our systems, the chain length between cross-links is uniform and known. In contrast to covalent gelation, spontaneous association of the end blocks allowed us to produce dilute nematic gels. Since the microphase-separated end-block domains were smaller than the wavelength of light, an optically uniform gel was obtained.

Since a gel controls the alignment of the director from throughout the material, rather than just at the surfaces, there is the potential for faster director reorientation relative to bulk small molecule LCs. When the director orientation is changed it can create elastic stress in the polymer network that may increase the rate of director relaxation. Preliminary results support this hypothesis. The success of this endeavor is a significant accomplishment and could have a profound effect on the display industry.

Modern electro-optic devices are demanding faster and faster response times from liquid crystals [13]. Despite many years of research, the basic twisted nematic cell with a response time ≥2 ms [14], has remained the dominant choice for display applications. Some polymer-dispersed LC (PDLC) and polymer-stabilized LC (PSLC) systems have shown fast director reorientation rates; however, problems with haze from unmatched refractive indices and director misorientations have limited their use. Because ABA nematic gel systems do not suffer from unwanted light scattering and poor contrast ratios, they have great potential in many types of electro-optic devices. Furthermore, this class of nematic gels holds the potential for improving the response time for director reorientation.

This approach to creating LC gels may be extended in the future to higher-order LC phases (cholesteric, ferroelectric, smectic, and "bownana" phases). Due to the reduced symmetry of a cholesteric material, alignment is more difficult, which can be used to advantage in a reflective display by facilitating the formation of a strongly light scattering "field off" state. Stronger light scattering would reduce the required thickness of an LC material and, consequently, lower driving voltages could be used to obtain fast electro-optic responses [15].

In recent years ferroelectric liquid crystals, with reorientational dynamics 100 to 1000 times faster than nematic LCs, have been investigated. Problems associated with alignment instabilities have limited their use. Future efforts to create a ferroelectric ABA gel hold the potential to overcome the mechanical instability of these LCs enabling them to be used in large displays [14, 16].

This work has opened new possibilities in an established field of study with a broad array of scientific directions and technological opportunities to explore.

Bibliography

[1] D. Coates, *J. Mater. Chem.* **5**, 2063 (1995).
[2] H. E. A. Huitema, G. H. Gelinck, J. B. P. H. van der Putten, K. E. Kuijk, C. M. Hart, E. Cantatore, P. T. Herwig, A. J. J. M. van Breemen, and D. M. de Leeuw, *Nature* **414**, 599 (2001).
[3] J. D. LeGrange, S. A. Carter, M. Fuentes, J. Boo, A. E. Freeny, W. Cleveland, and T. M. Miller, *J. Appl. Phys.* **81**, 5984 (1997).
[4] R. A. M. Hikmet, *J. Appl. Phys.* **68**, 4406 (1990).
[5] I. Dierking, *Adv. Mater.* **12**, 167 (2000).
[6] D. K. Yang, L. C. Chien, and J. W. Doane, *Appl. Phys. Lett*. **60**, 3102 (1992).
[7] M. C. W. van Boxtel, R. H. C. Janssen, C. W. M. Bastiaansen, and D. J. Broer, *J. Appl. Phys*. 89, 838 (2001).
[8] H. Mori, *Jpn. J. Appl. Phys*. **36**, 1068 (1997).
[9] R. Simon and H. J. Coles, *Polymer* 27, 812 (1986).
[10] A. I. Hopwood and H. J. Coles, *Polymer* 26, 1312 (1985).
[11] H. Ringsdorf and A. Schneller, *Makromol. Chem., Rapid Commun*. **3**, 557 (1982).
[12] A. M. Jamieson, D. F. Gu, F. L. Chen, and S. Smith, *Prog. Polym. Sci*. **21**, 981 (1996).
[13] S. Kobayashi and H. Furue, *Proc. SPIE* **3421**, 2 (1998).
[14] H. Furue, H. Yokoyama, and S. Kobayashi, *Jpn. J. Appl. Phys*. **40**, 5790 (2001).
[15] Z. J. Lu and D. K. Yang, *Appl. Phys. Lett*. **65**, 505 (1994).
[16] M. Shikada, Y. Tanaka, J. Xu, K. Furuichi, H. Hasebe, H. Takatsu, and S. Kobayashi, *Jpn. J. Appl. Phys.* **40**, 5008 (2001).

Appendix 1 Polymer Backbone Synthesis

There are two ways to use anionic polymerization to get a high 1,2-content in poly butadiene. One involves running the reaction in the polar solvent tetrahydrofuran (THF) at a low temperature. This technique takes advantage of conditions where the kinetics of formation of 1,4-repeat units are slowed down relative to the formation of 1,2-repeat units [1, 2] when the reaction temperature is reduced to approximately -40 ^{o}C. The other technique uses a non-polar solvent like cyclohexane in the presence of 1,2-dipiperidoethane (DIPIP) [3]. The DIPIP forms an complex with the Li ion that increases the overall polymerization rate and produces ~99% 1,2-repeat units [4, 5, 6, 7] at room temperature.

The DIPIP method in non-polar solvents can destabilize the growing polymer of other monomeric units, such as styrene [3], making the formation of block copolymers very difficult. This problem can be overcome by adding about 10% THF to the solution when switching from a butadiene to a styrene monomer. The THF method, however, is more sensitive to impurities and can only produce polymers with approximately 80 to 95% 1,2-repeat units.

A1.1 Synthesis of 1,2-Polybutadiene

The 1,2-polybutadiene polymers used in these experiments were synthesized at Procter & Gamble under the direction of Dr. Steven D. Smith. This was done using anionic polymerization in cyclohexane with t-butyl lithium as an initiator at 16 ^{o}C and a pressure of ~25 psig [4, 5, 6, 7]. Approximately 5 moles of DIPIP [8, 9], purchased

through ACROS chemicals, were added per mole of initiator as a reaction modifier to favor the production of 1,2- over 1,4-repeat units. This reaction ran for several hours and was quenched by the addition of methanol. The polymer was precipitated from the solution by the addition of methanol and dried in a vacuum oven at room temperature. For long-term storage the polymers were kept at -20 ^{o}C with ~1 wt % Irganox or with Octadecyl-3-(3,5-di-tert-butyl-4-hydroxphenyl)propionate, an antioxidant. All the 1,2-polybutadiene samples used in these experiments had ~98% 1,2-repeat units as detected by NMR and polydispersity indices (PDI) of ~1.04 as detected by GPC with multi-angle laser light scattering (MALLS).

A1.2 Synthesis of ABA Triblock Backbone

The poly[styrene-block-(1,2-butadiene)-block-styrene] SBS triblock copolymer backbone was synthesized by Polymer Source by sequential addition of each block in the presence of DIPIP [1, 4, 5, 6]. Since DIPIP destabilizes a growing chain of polystyrene [3], the DIPIP was not added until the styrene monomer was spent and the butadiene had been added. THF was added prior to the addition of styrene for the last block making the solution more polar. This maintains stability of the growing polystyrene block in the presence of DIPIP but results in the formation of some 1,4-units from small amounts of residual butadiene.

This technique enabled the synthesis of well-defined blocks with a low polydispersity of 1.26, a total molar mass of M_n=270 kg/mol (57, 146, and 67 kg/mol for the respective SBS blocks), and 88% 1,2-polybutadiene units in the center block. The molecular weights of the different blocks were calculated by Polymer Source using multi-angle laser light scattering (MALLS). Our own MALLS measurements gave slightly different

numbers so the values from Polymer Source were adjusted keeping the same ratios for the respective blocks.

Bibliography

[1] T. A. Antkowiak, A. E. Oberster, A. F. Halasa, and D. P. Tate, *J. Polym. Sci., Part A-1* **10**, 1319 (1972).
[2] C. A. Uraneck, *J. Polym. Sci., Part A-1*, **9**, 2273 (1971).
[3] J. Sanger, C. Tefehne, R. Lay, and W. Gronski, *Polym. Bull*., **36**, 19 (1996).
[4] J. Roovers and P. M. Toporowski, *Rubber Chem. Technol.* **63,** 734 (1990).
[5] A. F. Halasa, D. F. Lohr, and J. E. Hall, *J. Polym. Sci., Polym. Chem. Ed*. **19,** 1537 (1981).
[6] S. Bywater, D. H. MacKerron, D. J. Worsfold, and F. Schue, *J. Polym. Chem. Ed*. **23**, 1997 (1985).
[7] A. F. Halasa, D. N. Schultz, D. P. Tate, and V. D. Mochel, *Adv. Organomet. Chem*. **18,** 55 (1980).
[8] A. Gero, *J. Amer. Chem. Soc*. **76**, 5158 (1954).
[9] F. F. Blicke and E. B. Hotelling, *J. Amer. Chem. Soc*. **76** , 2422 (1954).

Appendix 2 Hydroboration Method for Polymer Synthesis

A2.1 Hydroboration/Oxidation of 1,2-Polybutadiene

The 1,2-polybutadiene prepolymer was converted to the polyalcohol poly(2-hydroxyethyl)ethylene (PBOH), using a procedure similar to that of Chung et al. [1], Adams and Gronski [2], and Mao et al. [3, 4]. Hydroboration with 9-borabicyclo[3.3.1]nonane (9-BBN) was followed by oxidation under basic conditions, Fig A2.1. In the first step, a 50% excess of 9-BBN under argon was added to the polybutadiene solution in anhydrous tetrahydrofuran (THF) and the reaction was run at room temperature for two to three days.

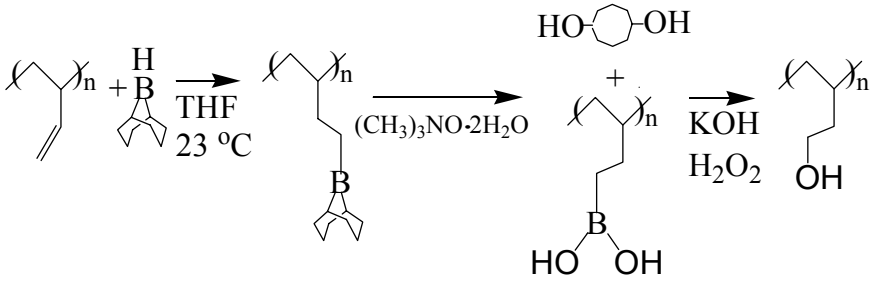

Figure A2.1. Conversion of 1,2-polybutadiene to a polyalcohol (PBOH) using hydroboration/oxidation.

To minimize cross-linking reactions, a mild oxidizing agent trimethyamine N-oxide dihydrate (TMAO) was used to avoid the presence of oxygen molecules from the decomposition of hydrogen peroxide. Since TMAO can only cleave the two secondary organoborane bonds on 9-BBN, it does not eliminate the need for hydrogen peroxide but it reduces the requirement by a third [5]. A 3:1 mole ratio of TMAO to 9-BBN was used for a relatively long reaction time (one day) due to both the low reactivity of TMAO

relative to hydrogen peroxide and the separation of the reaction mixture into two phases with the aqueous phase containing much of the TMAO.

A solution with a molar equivalent of KOH and a 20% excess of hydrogen peroxide was used to complete the oxidation of the polymer [2, 3, 4]. Other researchers [2] using smaller molecular weight starting polymers found that the product PBOH was soluble in THF with small quantities of water. At our high molecular weight, the poly-organoborane was soluble in THF, but the PBOH product was not. Therefore, to avoid precipitation, the H_2O_2 and KOH were dissolved in methanol and the polymer solution, in THF, was added slowly (over 30 minutes) to this methanol solution at 0 ^oC.

After the reaction, the solution turned cloudy due to the precipitation of a water-soluble borate salt. These salts were removed by dissolving the polymer in methanol at ~20 wt% along with a small amount of KOH, and precipitating the polymer three times by the direct addition of H_2O while stirring. Starting with 1,2-polybutadiene with a PDI of about 1.04, a final polymer with a PDI between 1.08 and 1.15 could be obtained at a yield of 85%. The disappearance of peaks between 4.8 and 5.6 ppm in the ^1H NMR spectrum of 1,2-polybutadiene and the appearance of a peak at 3.6 ppm in PBOH confirmed >99% vinyl group conversion to alcohol, Fig. A2.2.

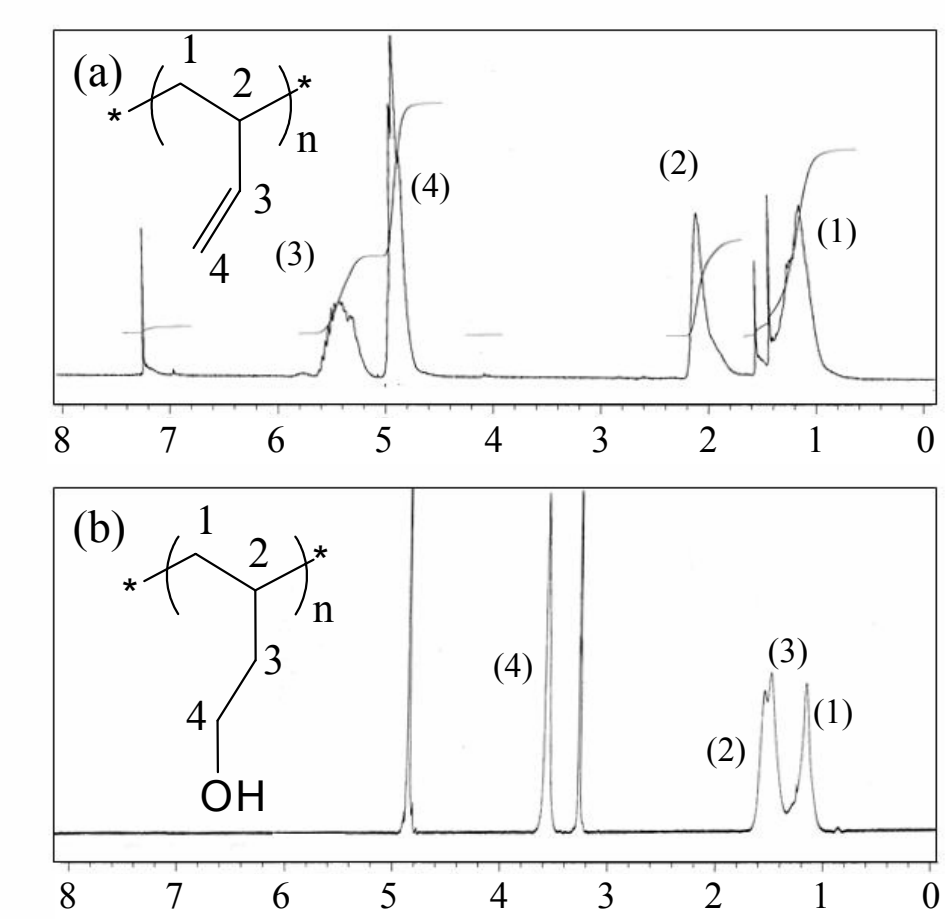

Figure A2.2. NMR spectrum of (a) 1,2-Polybutadiene in $CDCl_3$ (b) PBOH in CD_3OD. The signal from the vinyl groups between 4.8 and 5.6 ppm are absent indicating that all vinyl groups had been hydrated. The Peaks at 3.3 and 4.9 ppm are due to the solvent CD_3OD.

A2.3 Cyanobiphenyl Mesogen Synthesis

A cyanobiphenyl mesogen was chosen for this study to confer SGLCP solubility in extensively characterized cyanobiphenyl-based small molecule LCs, Fig. A2.3. The spacer was made from an ethyl-ω-bromine ester with different numbers of carbons atoms. Esters with 4, 5, and 6 carbon atoms were purchased from Aldrich and esters with 7 and 8 carbon atoms were purchased from TCI America and Narchem Corporation, respectively. The esters were attached to the mesogen 4-cyano-4'-hydroxybiphenyl (purchased from TCI America) by a Williamson ether synthesis reaction in anhydrous DMF with one

molar equivalent of anhydrous K_2CO_3 at 90 ^oC for 3 hours and the reaction was monitored by TLC. The product was purified by fractionation on a silica gel column using 30% ethyl acetate in hexane and was recrystallized in ethanol providing a 90% yield.

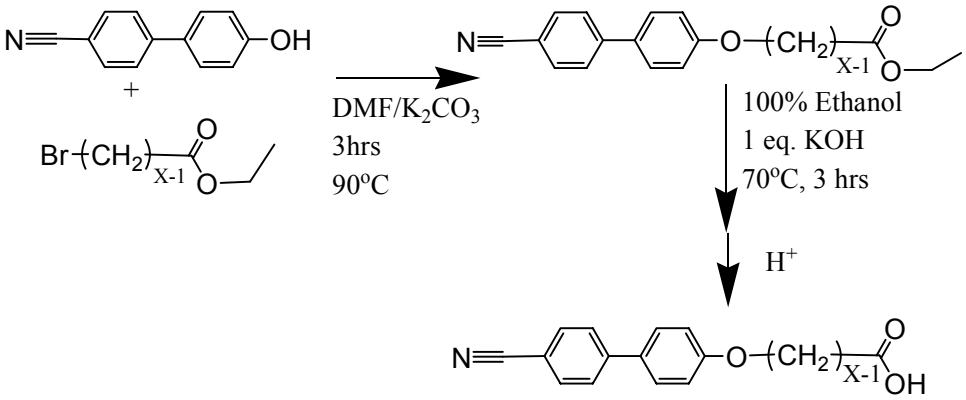

Figure A2.3. Cyanobiphenyl mesogen synthesis, CBAx.

The ethyl protecting group was removed by reaction with 1 molar equivalent KOH in anhydrous ethanol at 70 ^oC for 3 hours. The reaction mixture was poured into a dilute aqueous $NaHCO_3$ solution and the pH was adjusted to 6 using acetic acid to precipitate the mesogenic unit in its acid form. The product, CBAx, was further purified by dissolution in an acetone/H_2O solution followed by filtration to remove insoluble byproducts. The yield of this step was 90%.

A2.4 Attachment of Mesogen to Polyalcohol

The final step in the polymer synthesis was the attachment of the mesogen to the polymer backbone following a procedure similar to Adams and Gronski [2] and Coleman et al. [6], Fig. A2.4. Two grams of the mesogen were dissolved in 20 ml anhydrous THF with a molar equivalent of anhydrous K_2CO_3. A large excess of thionyl chloride was

added to produce the acid chloride. The reaction was allowed to progress at room temperature for three hours. The $SOCl_2$ and THF were removed under vacuum at room temperature, and the mesogen was redissolved in anhydrous toluene which was also removed under vacuum. The remaining solids were hot filtered in a solution of anhydrous hexane at 70 ^oC. Upon cooling to ~0 ^oC, the acid chloride product precipitated; then the solvent was decanted, and the precipitate was washed with additional cold anhydrous hexane.

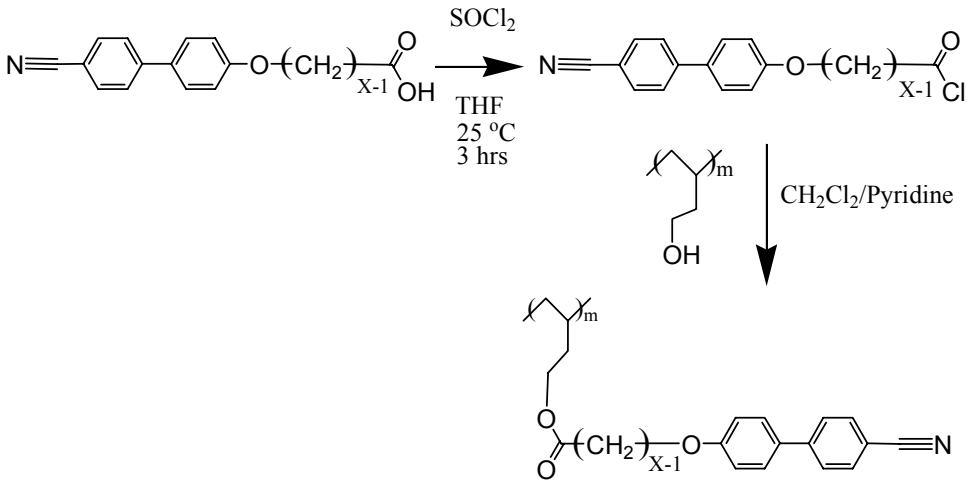

Figure A2.4. Procedure for attaching the cyanobiphenyl-based mesogen to the polymer backbone. PBCBx denotes a 1,2-polybutadiene backbone, with a cyanobiphenyl mesogen. The "X" in the polymer name indicates the size of the spacer where X+4 is the number of atoms between the mesogen and the polymer backbone. In these experiments X=4 to 8.

Once purified, a 50% excess of the acid chloride (~2 grams) was dissolved in 20 ml CH_2Cl_2 and the PBOH was dissolved in 5 ml pyridine, which serves as the reaction catalyst. Since PBOH was not soluble in CH_2Cl_2 but the product SGLCP was, the attachment of the mesogen could not be accomplished in a single solvent without precipitation. Therefore, the PBOH/pyridine solution was added slowly (5 min) to the acid chloride/CH_2Cl_2 solution allowing mesogenic units to rapidly attach to the polymer rendering it soluble in the reaction mixture. The reaction was allowed to progress for

several hours before the polymer was precipitated twice from a solution of dichloromethane by the addition of methanol, removing any unattached mesogen, giving a final yield of 95%. The final polymers were designated PBCBx where "x" indicates the number of carbon atoms in the ester group used to form the spacer.

The extent of the attachment reaction was monitored by NMR and FTIR. The chemical shifts of the hydrogens in the α position relative to the hydroxyl group changes from 3.6 ppm to 4.1 ppm upon addition of mesogen, Figs. A2.2b and A2.5. FTIR further confirmed that the reaction proceeded to completion by the disappearance of a broad hydroxyl peak at 3300 cm^{-1} and the appearance of a sharp peak at 2125 cm^{-1} corresponding to a -C≡N group [1, 3], Fig. A2.6. This confirmed that greater than 99% of the available hydroxyl groups had reacted.

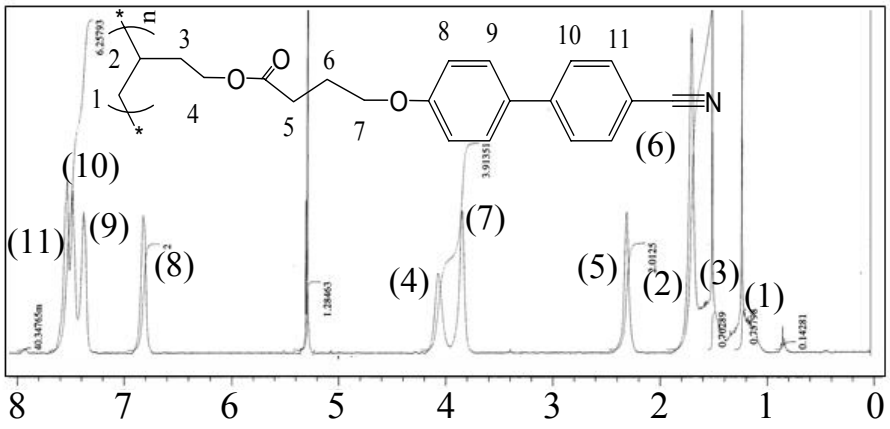

Figure A2.5 NMR spectra of PBCB4 in CD_2Cl_2. The peak at 3.6 ppm in PBOH was replaced by a peak at 4.04 ppm indicating complete attachment of the mesogen.

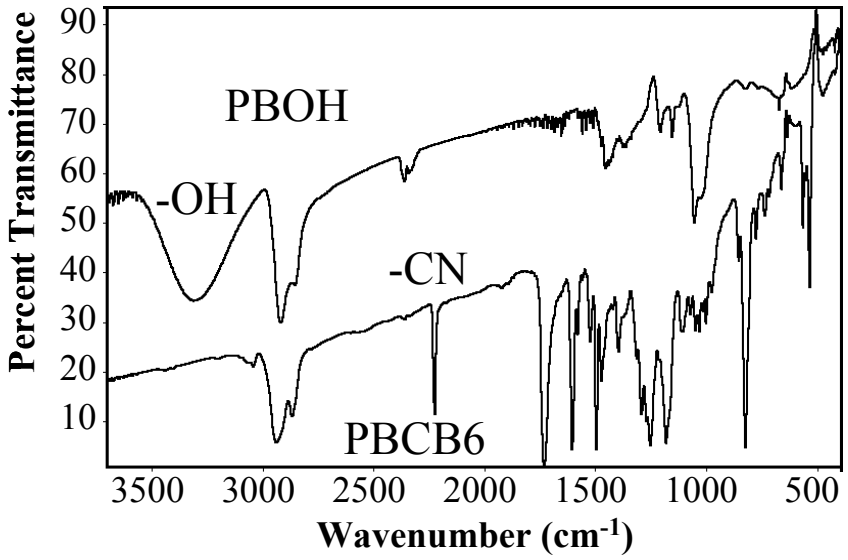

Figure A2.6. FTIR spectrum comparing PBOH to PBCB6. The loss of the broad peak at 3300 cm^{-1} and the addition of the peak at 2224 cm^{-1} indicated complete attachment of mesogen to the hydroxyl groups.

A2.5 Discussion

Some of the first attempts at hydroboration/oxidation of polybutadienes were carried out by Yamaguchi et al. [7] and Ikeda et al. [8]. One of the largest problems they encountered was with gelling of the polymer. Yamaguchi et al. traced this gelling to a reaction between the organoborane polymer and oxygen to produce borate cross-links. In similar experiment, Pinazzi et al. [9, 10] were also plagued by gelation side reactions. The first reported successful modification of a polydiene that maintained a low polydispersity was accomplished by Chung et al. [1].

Prior to this study, M_n=51,000 g/mol was the highest molar mass 1,2-polybutadiene that had been reportedly converted to PBOH [11]. Making high molar mass polymers was difficult since the kinetics of the reaction were greatly reduced, the polymers were

less soluble at all stages of the reaction, and most importantly, cross-linking reactions were not eliminated they were only minimized.

The slow kinetics of large polymers was easily compensated for by long reaction times and higher excesses of reactants. The problems associated with solubility were overcome by using dilute conditions and careful control of solvent conditions. The cross-linking problems were much more difficult to solve. Little cross-linking was observed during the hydroboration step; however, during the oxidative work-up of the organoborane polymer with hydrogen peroxide and KOH, the polymer was prone to cross-linking and precipitating rapidly. This could have been due to two mechanisms: borate cross-links, or the removal of H_2O to form ether cross-links. Problems with borate cross-linking could be eliminated by increasing solution basicity to break these bonds, however increased basicity resulted in the formation of additional ether cross-links. To minimize ether cross-linking reactions, a milder oxidizing agent, TMAO, was used. Although the use of TMAO reduced the formation of cross-links, its lower reactivity limited it to reacting with the secondary organoborane bonds associated with the 9-BBN molecule; therefore, the use of hydrogen peroxide was still necessary.

Even though an 85% yield could be achieved by this method, the resultant polymer often had an unacceptably large PDI. After repeated attempts a PDI of 1.08 for PBOH was achieved at molar masses as high as M_n=89,000 g/mol. Similarly to Chung et al. [1], Adams and Gronski [2], and Mao et al. [4], this method allowed us to maintain a PDI of 1.1 to 1.15 for the final PBCBx polymers even at high molar masses and to systematically vary both the molar mass and the spacer length.

Bibliography

[1] T. C. Chung, M. Raate, E. Berlunche, and D. N. Schulz, *Macromolecules* **21**, 1903 (1988).
[2] J. Adams and W. Gronski, *Makromol. Chem., Rapid Commun.* **10**, 553 (1989).
[3] G. Mao, J. Wang, S. R. Clingman, and C. K. Ober, *Macromolecules*, **30**, 2556 (1997).
[4] G. Mao, J. Want, and C. K. Ober, *Chem. Mater*. **10**, 1538 (1998).
[5] G. W. Kabalkam and H. C. Kedgecock *J. Org. Chem,* **40**, 1776 (1975).
[6] G. H. Coleman, G. Nichols, C. M. McCloskey, and H. D. Anspon, *Org. Synth*. **3**, 712 (1955).
[7] H. Yamaguchi, K. Azuma, and Y. Minoura, Y., *Polymer Journal* **3**, 12 (1972).
[8] H. Ikeda, A. Kogure, K. Shiina, and Y. Minoura, *J. Chem. Soc., Japan, Chem. Ind. Sect*. **68**, 1103 (1965).
[9] C. Pinazzi, J. Vassort, and D. Reyx, *Eur. Polym. J.* **13**, 395 (1977).
[10] C. Pinazzi, P. Guillaume, and D. Reyx, *Eur. Polym. J.* **13,** 711 (1977).
[11] J. Sanger and W. Gronski, *Macromol. Chem. Phys*. **199**, 555 (1998).

Appendix 3 Synthesis of Polymers with a Siloxane-based Spacer

In this approach to polymer synthesis, it much easier to avoid side reactions that might cause cross-links since only one step involves the polymer. Similar to the PBCBx series of polymers, a cyanobiphenyl-based mesogen was chosen to confer solubility on the polymer in many well characterized cyanobiphenyl-based small molecule LCs.

Unless otherwise stated, all chemicals were purchased from Aldrich Chemical Company and used without further purification. The synthetic methods for using 1,1,3,3-tetramethylydisiloxane (TMDS) to attach a mesogenic group to a polymer backbone were similar to the work by other researchers [1, 2, 3, 4], but the relatively high molar mass of our polymers required more effort to purify our products.

The details of the synthesis of the mesogenic group SiCB4 were worked out jointly by Neal Scruggs and Michael Kempe, and the details of the synthesis of SiBB were worked out jointly by Rafael Verduzco and Michael Kempe.

A3.1 SiCB4 Mesogen

The 4'-cyano-4-hydroxybiphenyl (CHB), purchased from TCI America, ~95%, was purified on a silica gel column using 33% ethylacetate in hexane. The spacer was prepared by the reaction of 3-butene-1-ol with one molar equivalent pyridine as a catalyst and a 2X excess of tosylchloride in CH_2Cl_2 [5], Fig. A.3.1. The reagents were mixed at 0 ^oC, but the reaction was allowed to run at room temperature for 10 hours. An excess of pyridine was added to form a salt with the remaining tosylchloride and then combined

with a 5% solution of HCl in water. The product 3-butenyl-1-tosylate was removed by liquid-liquid extraction with CH_2Cl_2. Then trace amounts of tosylchloride in the product were removed by liquid-liquid extraction with a fresh 5% solution of HCl in water. The organic layer was dried using $MgSO_4$, and the solvent was removed using a rotovac, giving an 83% yield. The spacer was attached to CHB with 2X excess 3-butenyl-1-tosylate in DMF with 1 molar equivalent anhydrous K_2CO_3 at a temperature of 90 ^oC for 8 hours. The tosic acid byproduct was precipitated by the addition of CH_2Cl_2, and the product 4-cyano-4′-(3-buteneoxy)-biphenyl, CBV4, was purified on a silica gel column using 10% ethylacetate in hexane followed by recrystallization from hexane, for a yield of 63%.

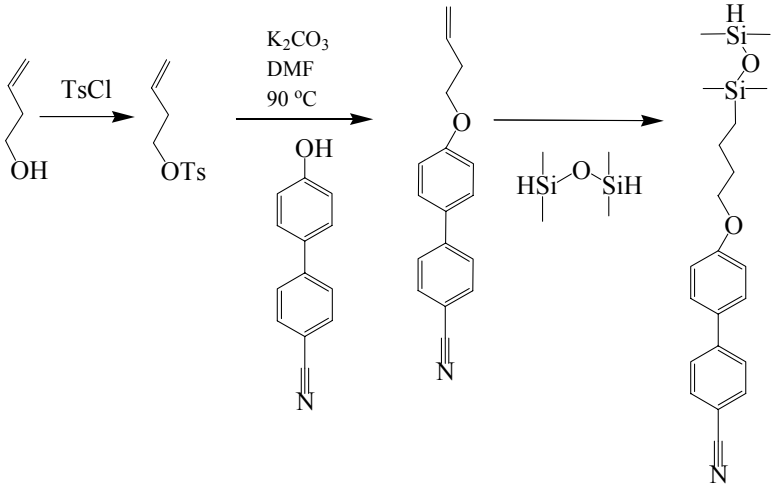

Figure A3.1. Schematic for synthesis of SiCB4.

TMDS (10X excess) was attached to the CBV4 in anhydrous toluene using a few drops of the catalyst PC085, platinum-cyclovinyl-methylsiloxane complex, or PC072, platinum-divinyltetramethyldisiloxane complex in xylene, both of which were purchased from United Chemical Technology. This reaction ran overnight at room temperature producing 4-cyano-4′-(5-(1,1,3,3-tetramethyldisiloxane)butoxy)biphenyl (CBSi4).

Since only a small amount of disiloxane byproducts was necessary to cross-link a high molecular weight polymer, the CBSi4 must be highly purified prior to attachment to the 1,2-polybutadiene backbone. The excess TMDS, bp 71 ^{o}C, was removed by boiling under vacuum at 50 ^{o}C. Then the product was dissolved in anhydrous toluene, bp 110 ^{o}C, which was also removed by boiling under vacuum at 50 ^{o}C, producing a product that should have been completely free of TMDS. Any trace amounts of water in the system have the potential to form 1,1,3,3,5,5,7,7-octamethyltetrasiloxane (OMTS) which would have a significantly higher boiling point than TMDS and consequently not be removed by boiling. Therefore, a silica gel column was used to remove this and other byproducts of the reaction. The column was dried by blowing argon through the column while heating it with a propane torch and then loaded with anhydrous hexane as the solvent. The mesogen was added to the column in an anhydrous solution of toluene/hexane and a generous amount of hexane was run through the column until the mesogen nearly stopped moving, as seen with a UV lamp, removing the OMTS. Since the mesogen barely moves down the column with hexane, an anhydrous solution of 5% ethylacetate in hexane was used to remove it from the column and to fractionate out other byproducts. This last step was sometimes repeated until no yellow color was seen in the product CBSi4.

A3.2 SiCB5 Mesogen

Since 5-bromopentene, unlike 4-bromobutene, does not undergo a β elimination reaction to form 1,4-pentadiene at significant rates, a Williamson ether synthesis reaction could be used to attach the vinyl spacer to CHB, Fig. A3.2. This was done using a 30% excess of 5-bromopentene in DMF with 1 molar equivalent anhydrous K_2CO_3 at a

temperature of 90 °C for 3 hours. Other than this detail, the synthesis of 4-cyano-4′-(5-(1,1,3,3-tetramethyldisiloxane)pentoxy)biphenyl (SiCB5) was similar to that of SiCB4.

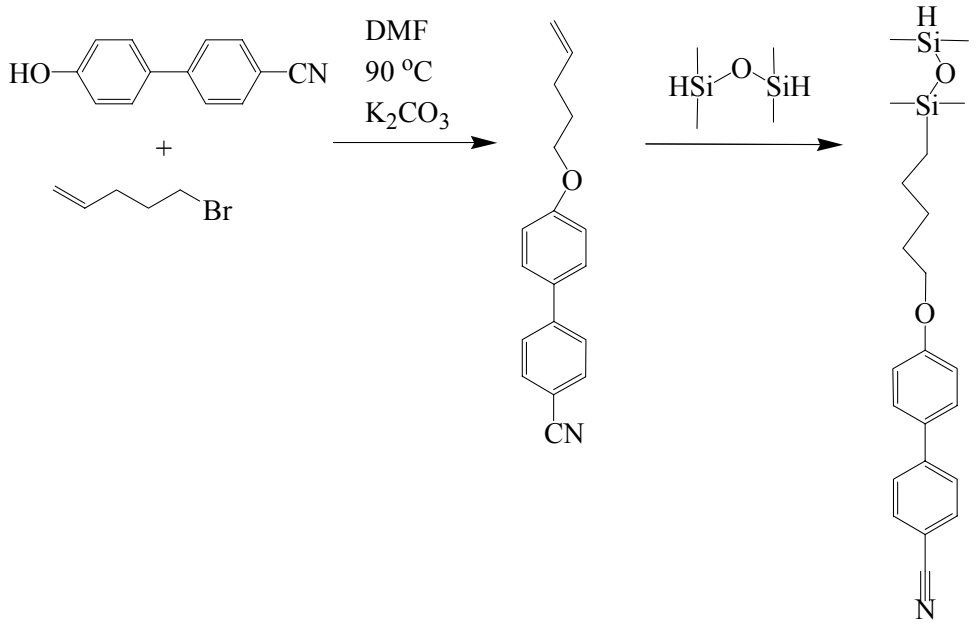

Figure A3.2. Schematic for synthesis of SiCB5 mesogen.

A3.3 SiBB Mesogen

The synthesis of this mesogenic unit was similar to that used by researchers making polyacrylates [6, 7]. 4-Butoxybenzoic acid was converted into 4-butoxybenzoyl chloride using a large excess of $SOCl_2$ as the solvent at room temperature for several hours, Fig. A3.3. The $SOCl_2$ was removed by evaporation under vacuum at 50 °C. A 30% excess of 4-butoxybenzoyl chloride was added to 2,5-dihydroxybenzaldehyde (purchased from Lancaster Chemical) in a CH_2Cl_2 solution with some pyridine as a catalyst, and the reaction was allowed to proceed at room temperature for several hours. The product 2,5-di(4-butoxybenzoate)-benzaldehyde was purified by liquid-liquid extraction using CH_2Cl_2 and a 0.1 N solution of HCl followed by another extraction using CH_2Cl_2 and an

aqueous solution of $NaHCO_3$. The product was further purified by crystallization from 15% ethanol in H_2O.

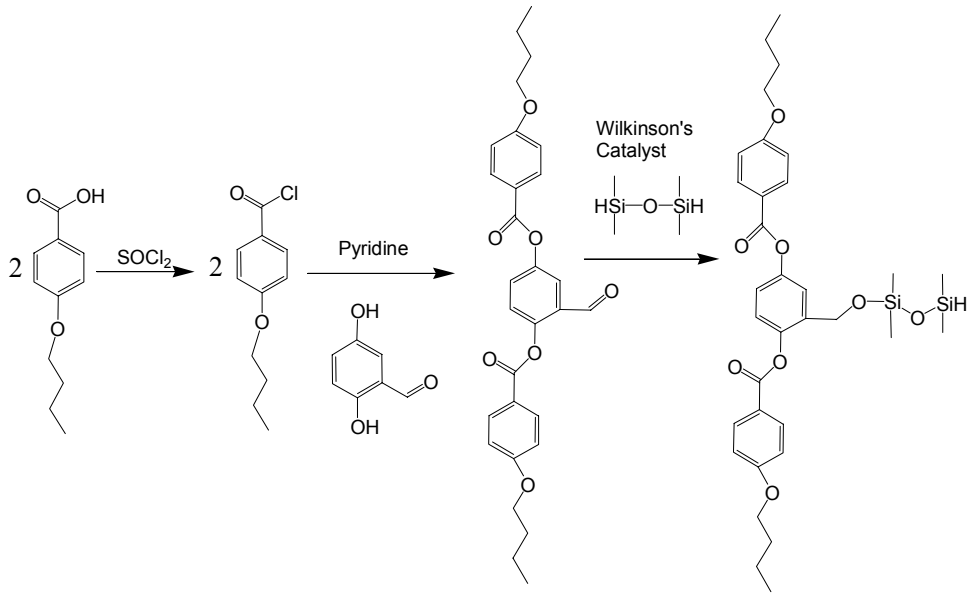

Figure A3.3. Schematic for synthesis of SiBB mesogen.

The spacer was attached to the aldehyde using Wilkinson's Catalyst [8] [chlorotris(triphenylphospine)-rhodium(I)] with a 10X excess TMDS in Toluene. The reaction was allowed to progress for 30 minutes at 60 ^{o}C. The product 1,4-bis(4-butoxybenzoate)-2-methyl[(1,1,3,3-tetramethyl-disiloxane)oxy]-benzene (SiBB) was purified on a silica gel column in a manner similar to that used for CBSi4.

A3.4 Attachment of Siloxane-Based Mesogens to 1,2-Butadienes

Once purified, the SiH functionalized mesogens SiCB5, SiCB4, and SiBB were attached to the pendant vinyl groups of 1,2-polybutadiene homopolymer or SBS triblock copolymer backbone. The CBSiX (X=4,5) mesogens were added at 3 times excess relative to the initial amount of mesogen used to account for losses in the last column

purification and to push the reaction closer to completion in a reasonable amount of time. Due to the either low yields and/or lower reactivity of the SiBB mesogenic unit, a 5 times excess, relative to the initial amount of vinyl of aldehyde functionalized mesogen, was necessary to get a high attachment of vinyl groups. The SiH functionalized mesogens and the polymer backbone were dissolved in anhydrous THF with a few drops of the catalyst PCO85. The reaction was allowed to progress for 3 or 4 days with 80 to 90% attachment of the mesogen typically achieved in 2 days, Fig. A3.4. The reaction was quenched by the addition of an excess of a vinyl containing compound, such as styrene, to neutralize the reactive end of any disiloxane byproducts that may have been partially attached to the polymer backbone. After a day of quenching the reaction, the product polymer was precipitated two to three times by addition of methanol to a THF solution, resulting in an overall yield of 90%.

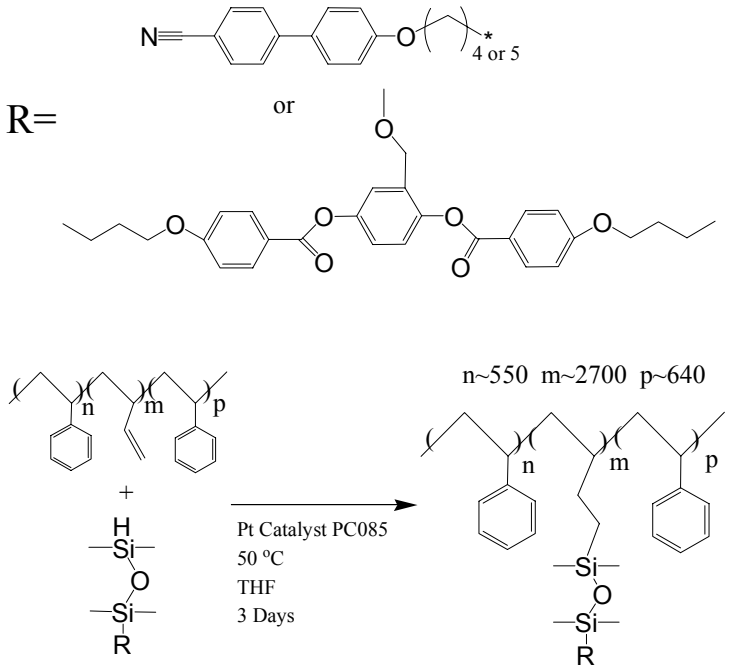

Figure A3.4. Schematic for attachment of mesogens to a polymer backbone.

The fractional attachment of the mesogen was found using NMR by comparing the integrated area for the peaks corresponding to the alkene at 4.9 and 5.3 ppm with the peak at 3.9 ppm corresponding to a methylene group next to an ether link, Fig. A2.5. In SiCB4 and SiCB5 the methylene was next to the cyanobiphenyl and in SiBB it was next to the benzoate. Comparison of the areas of the two peaks of the vinyl groups allowed the determination of the relative number of 1,4-and 1,2-repeat units allowing us to verify that, within the experimental uncertainty, all the vinyl groups had been accounted for. Typically we found that between 87 and 94% of the available vinyl groups had reacted, but for ABASiBB we were only able to achieve 80% attachment of the available vinyl groups.

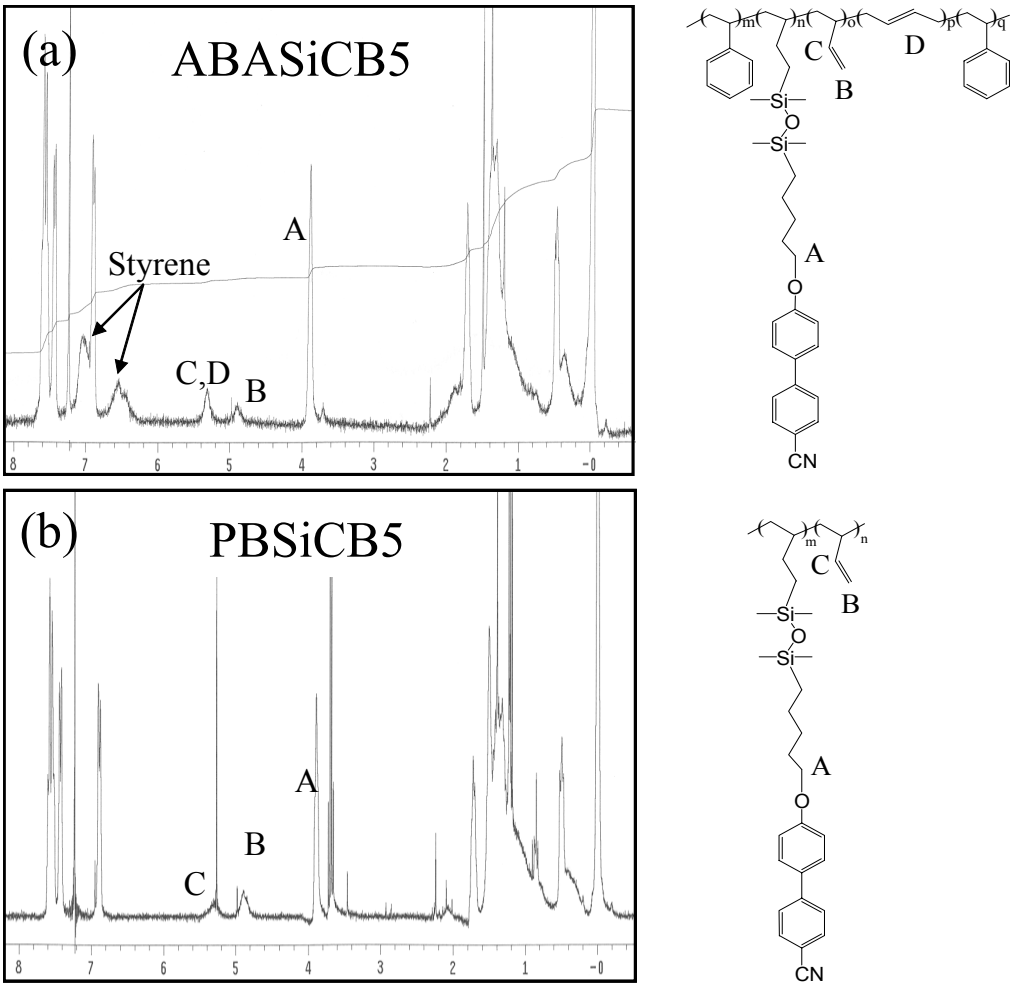

Figure A3.5. NMR spectrum of (a) ABASiCB5 and (b) PBSICB5 used to calculate the fractional attachment of mesogen to the pendant vinyl groups. The mole fraction of the components of the LC block can be calculated from the peak areas A, B, and C as: $f_{mesogen}=(2A)/(2A+B+2C)$, $f_{1,2}=(2B)/(2A+B+2C)$ and $f_{1,4}=(2C-B)/(2A+B+2C)$.

Some broadening of the molecular weight distribution occurred the first day after the polymer was precipitated out of solution. After that point, the polymer had long-term stability, and was stored with ~1% inhibitor, Octadecyl 3-(3,5-di-tert-butyl-4-hydroxphenyl)propionate. The polydispersity, computed using polystyrene standards, was between 1.3 and 1.8 for the triblock copolymers and 1.1 and 1.2 for the homopolymers. The molecular weights of these polymers were computed based on the backbone pre-polymer molecular weight and the fractional attachment of mesogenic

units. In the cases where a large polydispersity was found and the GPC showed a large bump in the higher molecular weight end of the peak, a preparative column, Polymer Labs, PLgel 10 μm 10E5Å, was used to fractionate out these chemically cross-linked chains.

Bibliography

[1] M. A. Hempenius, R. G. H. Lammertink, and G. J. Vancso, *Macromolecules*, **30**, 266 (1997).
[2] M. A. Hempenius, R. G. H. Lammertink, and G. J. Vancso, *Macromol. Rapid Commun.,* **17**, 299 (1996).
[3]A. Moment, R. Miranda, and P. T. Hammond, *Macromol. Rapid Commun*., **19**, 573 (1998).
[4] A. Moment and P. T. Hammond, *Polymer*, **42**, 6945 (2001).
[5] X. F. Ren, E. Turos, C. H. Lake, and M. R. Churchill, *J. Org. Chem.* **60,** 6468 (1995).
[6] M. C. Chang, H. W. Chiu, X. Y. Wang. T. Kyu, N. Leroux, S. Campbell, and L. C. Chien, *Liq. Cryst*. **25**, 733 (1998).
[7] Q. F. Zhou, H. M. Li, and X. De Feng, *Macromolecules* **20**, 233 (1987).
[8] I. Ojima, M. N. Anagi, T. Kogure, M. Kumagai, S. Horiuchi, K. Nakatsugawa, and Y. Nagai, *J. Organomet. Chem*. **94**, 449 (1975).

Appendix 4 Synthesis of Perdeuterated 4'-Pentyl-4-cyanobiphenyl

Perdeuterated 4'-pentyl-4-cyanobiphenyl (D5CB) was synthesized following a procedure similar to that used to produce selectively deuterated 5CB [1, 2, 3, 4] Fig. A4.1. Unless otherwise stated, all chemicals were purchased from Aldrich and used without further purification. The hydrogen atoms on 15 ml 4-pentylbiphenyl (5B), purchased from TCI America, were exchanged with deuterium from 99.9% D_2O, purchased from Cambridge Isotope Laboratories, using 0.3 g platinum black. This exchange reaction was conducted in a Teflon-lined Parr Autoclave reaction vessel at autogenous pressure. The vessel was placed in a convection oven at a temperature between 150 and 200 ^oC and was mixed by rotation at ~60 rpm [5]. Prior to sealing the reaction vessel, argon was bubbled through the reaction mixture to remove oxygen which may react with 5B and poison the catalyst. To further remove oxygen and keep the catalyst active, a 1 cm^2 piece of aluminum foil was added to the mixture. After three or more days of proton exchange, the D_2O/H_2O was removed by pipette and replaced with 20 ml of fresh D_2O. A new piece of aluminum and occasionally more platinum black could be added at this time. This deuterium exchange was repeated eight times to get the desired degree of deuteration. The degree of deuterium/hydrogen exchange was monitored throughout the process by measuring the density of the H_2O/D_2O removed and by using NMR. In the NMR method, a known weight of deuterated 5B (D5B) and hydrogenated dichloromethane were mixed in deuterated chloroform and a ^1H NMR spectrum was made. The fractional deuteration of each hydrogen could be calculated by

comparing the ratio of the CH_2Cl_2 peak to the D5B peaks. After 3 days of hydrogen exchange, the aromatic hydrogens were at equilibrium with the H_2O/D_2O. However, the amount of deuterium on alkyl carbons only achieved 25 to 50% of the predicted increase if equilibrium was achieved.

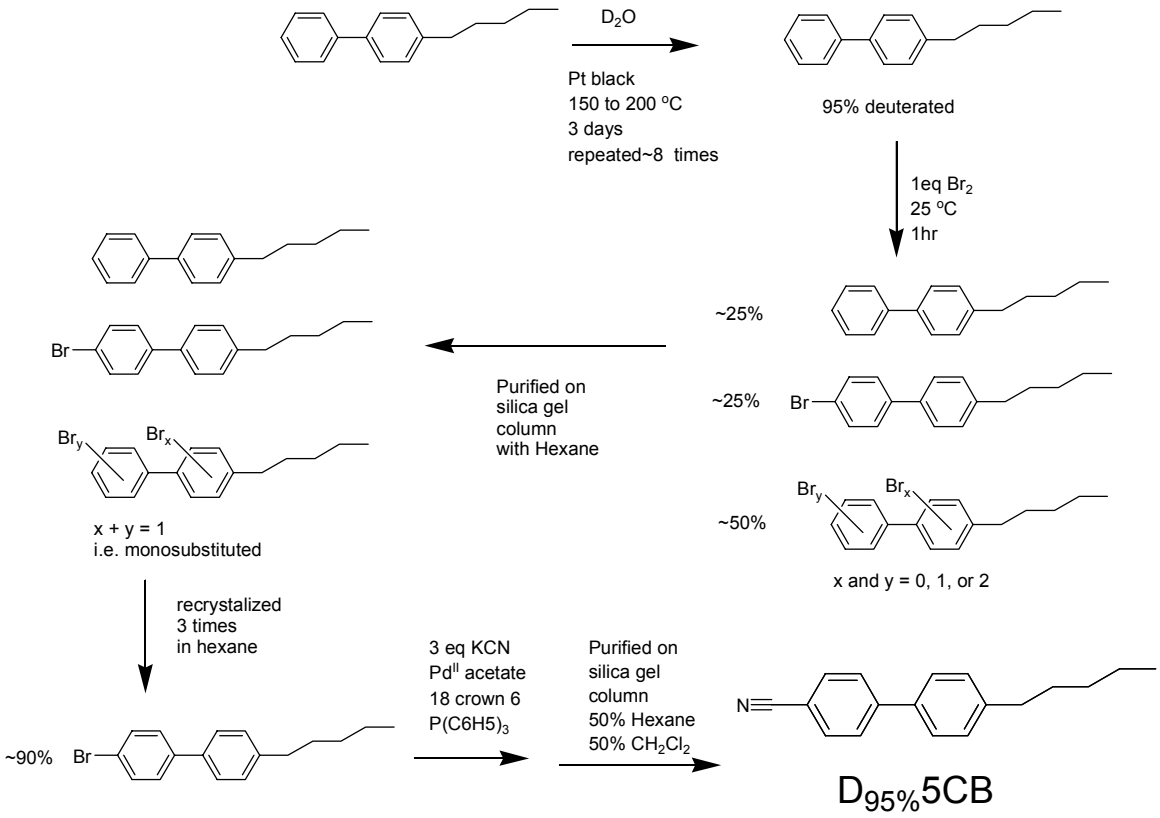

Figure A4.1. Schematic diagram for the synthesis of deuterated 5CB.

At 25 °C 5 grams of D5B was dissolved in 20 ml $CHCl_3$ to which 3 ml of Bromine was added. After one hour, the reaction was stopped by boiling off the bromine and $CHCl_3$ at room temperature under vacuum. The resulting mixture was approximately 25% D5B, 25% perdeuterated 4'-Bromo-4-pentylbiphenyl (DBr5B) and 50% other mono, di, and tri-substituted D5B.

The di and tri-substituted D5B was easily removed using hexane in a silica gel column, but the randomly mono-substituted D5B was not easily separated from its

isomer, DBr5B. The remaining unsubstituted D5B could have been removed using hexane on a silica gel column with moderate difficulty, but was left since it would not react further and was very easily separated from the product D5CB.

Crystallization in hexane further purified this reaction mixture. Since large losses were incurred with each crystallization, this could only be repeated three times. The resulting product was 90% DBr5B. The byproducts and unreacted D5B were recycled for reaction with more bromine.

The bromine atoms on 3.75 g DBr5B were substituted with –CN from 1.52 g KCN in the presence of a palladium catalyst and 1.23 g 18-crown-6. The catalyst was prepared by dissolving 0.4 g Pd^{II} acetate and 0.92 g triphenylphospine in 35 ml toluene and heating to 80 ^{o}C prior to addition of DBr5B [6, 7]. The reaction mixture was monitored by TLC for 20 hours until all the DBr5B had reacted.

Since only a few percent of impurities in the liquid crystal D5CB will cause significant deviation in the nematic to isotropic transition temperature (T_{ni}), purification of the final product was very important. This was carried out on a silica gel column using 50% hexane in CH_2Cl_2. One gram of impure product was placed on a 50 mm diameter 30 cm long column and the elution product was collected into three or four fractions. The first fraction had isomeric impurities that caused it to have a low or no T_{ni}, and later fractions had a dimeric impurity that resulted in an extremely high T_{ni}. Fractions from different runs were recombined based on their T_{ni} until fractions were collected which had a T_{ni} between 34.5 and 35.5 ^{o}C and TLC showed no sign of byproducts.

NMR results of the final product showed 95% perdeuterated of D5CB, Fig. A4.2. The overall yield from D5B to D5CB was 25%.

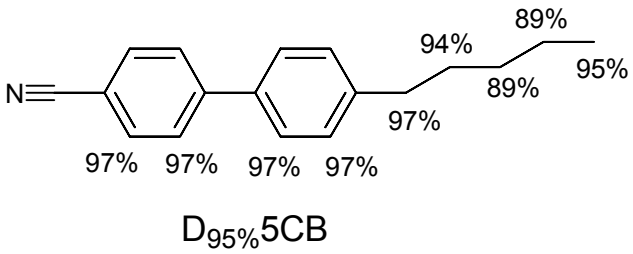

Figure A4.2. Fractional deuteration of D5CB.

Bibliography

[1] G. Gray and A. Mosley, *Mol. Cryst. Liq. Cryst.* **35**, 71 (1976).
[2] G. Gray and A. Mosley, *Mol. Cryst, Liq. Cryst*. **48**, 233 (1978).
[3] J. Emsley, G. Luca, G. Celebre, and M. Longeri, *Liq. Cryst.*, **20**, 569 (1996).
[4] H. Zimmermann, *Liq. Cryst*., **4**, 591 (1989).
[5] A. F. Thomas, *Deuterium Labeling in Organic Chemistry*, (Appleton-Century-Crofts, New York, 1971).
[6] M. Prochazka and M. Siroky, *Collect. Czech. Chem. Commun*. **48**, 1765 (1983).
[7] K. Nakatani, C. Dohno, T. Nakamura, and I Saito, *Tetrahedron Lett*. **39**, 2779 (1998).

Appendix 5 Conoscopy

Conoscopy has been used for years by geologists to measure the refractive indices of small crystals [1]. Recently [2, 3, 4, 5, 6, 7, 8, 9] similar methods have been applied to monodomains of liquid crystals to directly measure the effect of shear strains on the director orientation. Then application of the Leslie [10] Ericksen [11] transversely isotropic fluid model yields a measurement of the tumbling parameter.

A5.1 Instrument Setup

The apparatus used in these experiments was built by Dr. Weijun Zhou [12] and was modified to provide more accurate strain measurement and to record video rather than still images. Two optically smooth ($\lambda/5$), 3.2 mm thick, glass windows with a diameter of 25 mm were positioned parallel to each other at between 0.25 and 0.75 mm. Prior to being positioned in the instrument, the surfaces of the glass windows were treated with L-α-lecithin type XI-E (Aldrich chemical company) to promote perpendicular alignment of the LC sample. The lecithin was applied using a spin coater with a 1% lecithin solution in chloroform. The glass pieces were dried at 140 ^{o}C for 30 minutes. The two glass windows were independently heated using a mica heater (Minco, Inc.) and, at ~25 ^{o}C, were controlled with temperature stability to within $\pm$0.2 ^{o}C.

The top plate was held in place by three micrometers which also served to measure the gap. The lower of these two plates was mounted onto a spring-loaded translating stage. The position of this stage was determined using a Mitutoyo digimatic indicator in contact with the moving stage capable of measuring $\pm$1 μm. The shear strain was applied

to the bottom stage by rotating an off-center cam which was machined to apply a constant strain rate when rotated at a constant angular velocity. The rotation of the cam was controlled by a microstepping motor (6104 Compumotor, Inc.) connected to a computer.

The microscope was focused on the back focal plane of the objective lens using a Bertrand lens. A bandpass filter (λ=520 nm) was used to make the image easier to analyze. Conoscopic images were recorded using a Javelin Electronics video camera mounted on the microscope. To determine the angle of the director as a function of the applied shear strain the output of the Mitutoyo indicator must be synchronized with the conoscopic images. This was accomplished by recording a video image of the Mitutoyo indicator with a JVC VHS video camcorder and combining it with the conoscopic video image using an Emerson picture in picture TV tuner. This picture in picture image was then recorded digitally using an Iomega Buz video capture system installed on a Macintosh G3. By observing the instant the image began to move, as compared to when the indicator output changed, it was found that the indicator lagged by about 1/6 of a second. This time lag was found to be due primarily to the relatively slow response time of the indicator and was easily compensated for.

This configuration allows the orientation of the liquid crystal solution to be measured as a function of the applied shear strain. From the shift in the position *(Δ)* of the interference figure, Fig. A5.1, the tilt of the director *(θ)* relative to the velocity gradient direction can be estimated for small-angles as [8]

$$\theta \cong \sin^{-1}\left(\frac{\Delta\, NA}{R\, n_o}\right). \quad \text{(A5.1)}$$

The numerical aperture *(NA)* of our objective lens was equal to 0.40. Since refractive index measurements, Section 2.2.4, indicate that the addition of polymer does not significantly affect the birefringence, a value for the ordinary refractive index (n_o=1.53 for λ=520 nm) was obtained for bulk 5CB from Khoo and Wu [13].

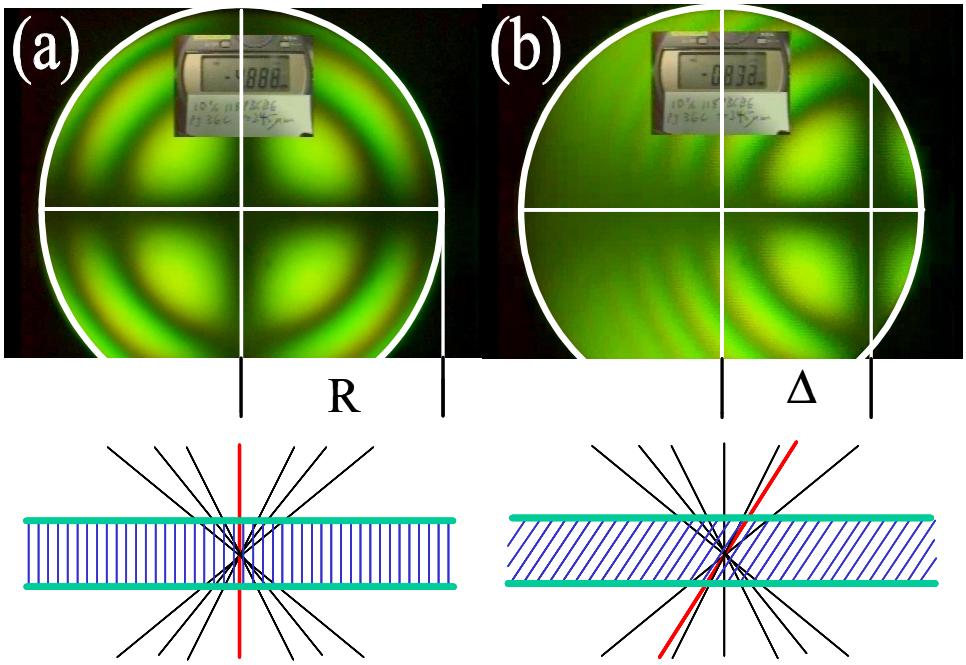

Figure A5.1. Conoscopic method for determining the response of the director to a shear strain. (a) before shear strain (b) after a shear strain of -3.4. Photos are for a 10% solution of M_n=420 kg/mol PBCB6 dissolved in 5CB at 25 °C. The inset is a picture of a digital indicator measuring the translation of the stage.

A5.2 Conoscopic Determination of the Tumbling Parameter.

In the limit of rapid deformation, the director does not have time to relax in response to distortional elasticity and the reorientation of the director is governed by viscous effects allowing the Leslie-Ericksen theory to be applied. If θ is small and the shear strain *(γ)* was applied starting from the homeotropic condition (i.e., θ=0), then by using the 2-D version of the Leslie-Ericksen equations

$$(\alpha_3 - \alpha_2)\frac{\partial \theta}{\partial t} = \left(\alpha_3 \sin^2 \theta - \alpha_2 \cos^2 \theta\right)\frac{\partial \gamma}{\partial t}, \quad \text{(A5.2)}$$

the ratio of θ to the shear strain is determined by the viscosity coefficients α_2 and α_3

$$\frac{\theta}{\gamma} = \frac{\alpha_2}{\alpha_2 - \alpha_3}, \quad \text{(A5.3)}$$

which leads to

$$\lambda = \frac{\alpha_2 + \alpha_3}{\alpha_2 - \alpha_3} = 2\frac{\theta}{\gamma} - 1 = 2\frac{\partial \theta}{\partial \gamma} - 1. \quad \text{(A5.4)}$$

In this way λ can be conveniently determined from conoscopic measurement of the change in the director angle under the influence of an applied strain in the limit of rapid, small amplitude deformation.

A5.3 Experimental Considerations

The most common experimental way to use Eq. A5.4 is to apply a known shear strain and then record an image to measure λ. The difficulty with this method is in knowing if the strain rate is high enough [6]. In Fig A5.2a it can be seen that for the 7.5% solution of 420 kg/mol PBCB6 in 5CB after the application of a large rapid strain the form of the conoscopic image is unperturbed. Then after 3 minutes, Fig A5.2b, the conoscopic image is much more distorted. For bulk 5CB the response is much quicker and the image is distorted almost instantly, Fig A5.2c. Work by Boudreau et al. [7] and G. Waton et al. [2] have shown that this distortion is due to the formation of a sinusoidal director profile. Since this type of distortion will lead to incorrect values of λ, care must be taken to be sure the strain rate is fast enough.

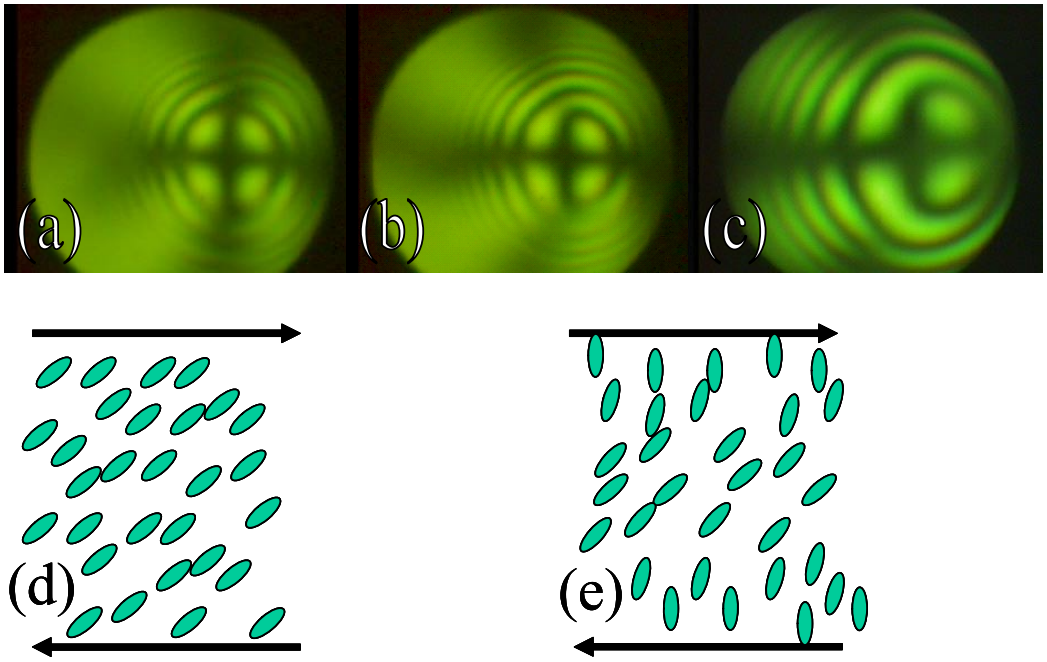

Figure A5.2. Conoscopic images demonstrating the effects of director relaxation and the formation of a sinusoidal director profile. (a) and (b) are for a 7.5% solution of 420 kg/mol PBCB6 dissolved in 5CB and sheared at a strain rate of 10 (1/s) for 0.816 seconds with a sample thickness of 600 (μm) at 29 ^{o}C. (a) 2.7 seconds after the application of a shear strain and (b) 180 seconds after application of a shear strain. (c) Bulk 5CB at 25 ^{o}C with a sample thickness of 250 μm during application of strain at 0.1 1/s. (d) Schematic representation of the director profile for part a. (e) Schematic representation for the director profile for parts b and c.

Since the equipment used in these experiments can record 30 images per second along with the applied shear strain, the slope, $\partial\theta/\partial\gamma$, can be measured in the limit of small θ, Fig. A5.3. The advantages with this method are that more data points are taken for a given measurement, which improves our statistics, and it is easy to ensure that the measurements are the linear region where director relaxation is not important. In Fig. A5.3 the effect of different strain rates on the director response is shown. Similar to work by Muller et al. [14], for all strain rates the slope of the line at small strains is the same but as the strain rate is reduced the size of this small strain linear regime diminishes and greater deviations from theory

$$\tan(\theta) = \pm\left(\frac{1+\lambda}{\lambda-1}\right)^{1/2} \tanh\left(\frac{\gamma}{2}\sqrt{\lambda^2-1}\right), \quad \text{(A5.5)}$$

are seen due to relaxation of the director in response to frank elasticity.

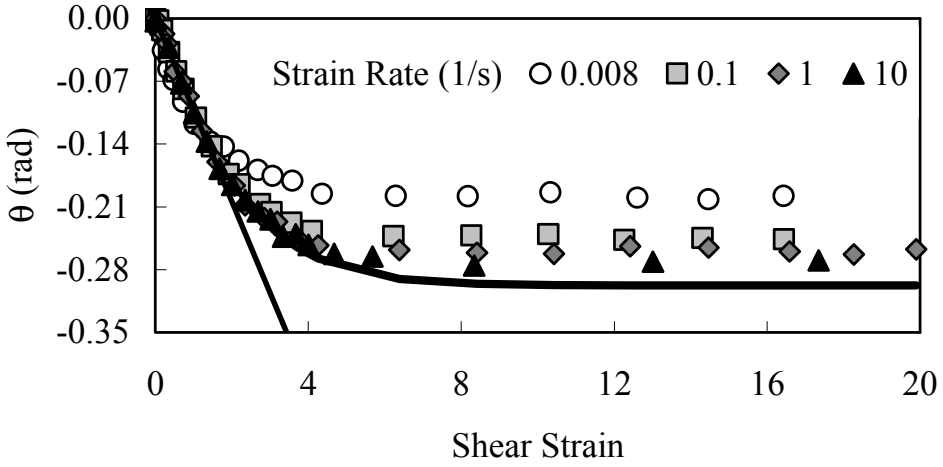

Figure A5.3. Method for determining the tumbling parameter from the director tilt as a function of applied strain. Linear initial response provides consistent value of λ over wide range of $\dot{\gamma}$. 10% 420 kg/mol PBCB6 in 5CB at 30 ^{o}C. The curved line is the theoretical fit using Eq. A5.5. The deviations from the theoretical fit are primarily due to frank elasticity.

In addition to using the small strain deflection of the conoscopic image to determine the tumbling parameter, the steady-state angle, θ_{ss}, of a flow-aligning LC can also be used to measure the tumbling parameter

$$\lambda = \frac{-1}{\cos(2\theta_{ss})}. \quad \text{(A5.6)}$$

Since this requires the steady-state angle to be with in the field of view of the microscope, ~14^{o}, an initially homeotropic cell only allows Eq. A5.6 to be used for λ<-1. In Fig. A.5.3 it can be seen that the steady-state angle is not quite as large as is expected based on λ calculated from initial slope and Eq. A5.5. As the strain rate is increased the agreement with theory is better, but even at 10 1/s, the fastest strain rate possible with this instrument, the steady-state angle is still increasing with strain rate. It is not possible to conclusively determine if the remaining uncertainty is due to director relaxation caused by frank elasticity or to experimental uncertainty. Even if this method is used, the

difference between λ calculated with Eq. A5.4 and Eq. A5.6 is barely larger than the experimental uncertainty, for the 10 wt % solutions of 420 kg/mol PBCB6 in 5CB, making this method valid for the determination of λ.

In our experiments conditions were found which gave measurements of λ for bulk 5CB which were consistent with measurements by Ternet et al. [8]. Since the addition of a small amount of polymer generally increases the viscosity and leaves the Frank elasticity relatively unchanged [15], the viscous forces will be even more dominant as polymer is added. Therefore the conditions for accurate measurement of λ in 5CB will be good for the polymer solutions also.

Bibliography

[1] F. D. Bloss, *An Introduction to the Methods of Optical Crystallography*, Holt, Rheinhart & Winston (1961).
[2] G. Waton, A. Ferre, S. Candau, J. N. Perbet, and M. Hareng, *Mol. Cryst. Liq. Cryst*., **78**, 237 (1981).
[3] M. Srinivasarao and G. C. Berry, *J. Rheol*, **35(3)**, 379, (1991).
[4] H. Mattoussi, M. Srinivasarao, P. Kaatz, and G. C. Berry, *Macromolecules,* **25,** 2860 (1992).
[5] J. A. Muller, R. S. Stein, and H. H. Winter, *Rheologica Acta*, **33**, 473 (1994).
[6] P. T. Mather, D. S. Pearson, and W. R. Burghardt, *J. Rheol,* **39**, 627 (1995).
[7] D. M. Boudreau, H. H. Winter, C. P. Lillya, and R. S. Stein, *Rheol. Acta*, **38**, 503, (1999).
[8] D. J. Ternet, R. G. Larson, and L. G. Leal, *Rheol Acta,* **38**, 183 (1999).
[9] B. L. Van Horn and H. H. Winter, *Appl. Opt.,* **40,** 2089 (2001).
[10] F. M. Leslie, *Quart. Journ. Mech. And Applied Math.,* Vol. **19**, Pt. 3, (1966).
[11] J. L. Ericksen, *Arch. Rational Mech. Anal.,* **4**, 231-237 (1960).
[12] W. Zhou, J. A. Kornfield, and W. R. Burghardt, *Macromolecules*, **34**, 3654 (2001).
[13] I. C. Khoo and S. T. Wu, *Optics and Nonlinear Optics of Liquid Crystals*, World Scientific, New Jersey, pg 83 (1993).
[14] J. A. Muller, R. S. Stein, and H. H. Winter, *Rheologica Acta*, **33**, 473 (1994).
[15] A. M. Jamieson, D. Gu, F. L. Chen, and S. Smith, *Prog. Polym. Sci*. **21**, 981 (1996).

Appendix 6 Refractive Index Measurement

The refractive indices and birefringence were measured in an Abbe refractometer equipped with a bandpass filter at 632.8 nm with temperature control of ±0.1 ^{o}C using circulated water from a Fisher Scientific Isotemp Refrigerated Circulator Model 900. Since the refractometer is large and contained ferromagnetic parts, a magnetic field could not be used to align the sample. Dilute gels, <5 wt % polymer, and homopolymer solutions can be homeotropically aligned by washing the glass prisms with a 1% solution of lecithin in chloroform prior to use. Since the lecithin surfactant layer was deposited by allowing the solvent to evaporate without heating the surface, it is easily removed after the experiment by washing the instrument in chloroform.

The birefringence of the an LC monodomain causes light with different polarizations to be bent at different angles; therefore, instead of a single line separating a light and dark area, as is seen with an isotropic fluid, a change from a bright to a dimmer region is seen at the ordinary refractive index, n_o, and a transition from a dim to a dark region is seen at the extraordinary refractive index, n_e.

With the 20 wt % gel of ABASiCB5 in 5CB, alignment with surface treatment was not possible. Conoscopic experiments (Chapter 7) demonstrated that the application of a shear stress caused the gel to align at an angle of between 0 and 8^{o} to the perpendicular direction. Therefore the sample was aligned by placing it on the prisms and squishing them together creating shear stresses large enough to create some macroscopic order. This results in a director aligned locally at between ±8^{o} in all directions relative to the surface normal on the prism.

An Abbe refractometer functions on the principle of total internal reflection with n_o corresponding to the largest critical angle and n_e to the smallest critical angle at which this occurs. When the instrument is set up to measure n_o, even with some director miss-alignment, there is always an angle of light polarization that will experience total internal reflection enabling the correct value for n_o to be measured [1]. To measure a correct value for n_e light must be polarized parallel to the director and traveling parallel to the surface, the critical condition for total internal reflection. These two conditions can only be met when the director tilt is not in the direction of light propagation. Therefore, for a large portion of the director tilt angles, no polarization angles of the incident light will correspond to n_e resulting in a slightly lower value being measured. With the imperfections in the orientation of our gel this results in a more gradual transition to a completely dark state. The condition for the correct measurement of n_e corresponds to the smallest angle at which any light can pass. Therefore, the measurement of n_e was repeated several times and the highest values observed were recorded.

Estimates of the maximum uncertainty possible for n_e in the 20 wt % gel of ABASiCB5 were made by considering the case of a monodomain tilted at an angle, relative to the surface normal, toward the direction of light propagation. If a liquid crystal is viewed with light polarized at an angle θ relative to the director, it will experience a refractive index that varies with theta according to

$$n(\theta) = \frac{n_o n_e}{\sqrt{n_e^{\,2} \sin^2 \theta + n_o^{\,2} \cos^2 \theta}}. \quad (5)$$

For a worst-case scenario, the director will be tilted by 8 degrees from the perpendicular. Using typical literature values of n_e=1.7091 and Δn=0.1820, for 5CB at 25 ^{o}C, the n_e and

Δn measured for a tilt angle of 8 degrees would be 1.7050 and 0.1778 resulting in a 0.24% and 2.3% uncertainty, respectively. Since the Abbe refractometer can measure up to 4 decimal places, this uncertainty is within experimental detection. By measuring at the high side of the fuzzy line for n_e, this systematic uncertainty in Δn is smaller than 2.3%.

Bibliography

[1] I. Haller, M. J. Freiser, H. A. Huggins, *Mol. Cryst. Liq. Cryst*. **16**, 53 (1972).

Appendix 7 Rheology

A7.1 Reorientational Response Time

In typical electro-optic devices, the reorientation of a liquid crystal (LC) is usually accomplished through the application of a voltage across a thin gap containing an LC material. When the voltage is removed, the distortion of the director creates an elastic stress which causes the director to relax back to a macroscopically uniform aligned state. It is this voltage off relaxation process that limits the speed of an electro-optic device. Relaxation of the director is governed by two competing forces, splay elasticity (K_{11}) and the director rotational viscosity $(\gamma_1=\alpha_3-\alpha_2)$. The ratio γ_1/K_{11} can be used to describe the reorientational response time of an LC.

A7.1.1 Instrument Setup

The ratio γ_1/K_{11} was measured using a technique outlined by Khoo and Wu (1993) [1]. Two optically smooth (λ/10) glass plates were coated with a layer of indium tin oxide (ITO) and a rubbed polyimide film (SE-150, Nissan Chemical, Inc.) to confer homogeneous (parallel) alignment of the LC, Fig. A7.1. The LC sample cell was also equipped with two Minco flexible heating elements and an Omega CN76000 temperature controller. The glass pieces were assembled so that the rubbing direction of the two plates were anti-parallel giving the liquid crystal a uniform pretilt angle across the cell gap. A Teflon spacer was used to produce a gap of approximately 8 to 10 μm. The plates were made parallel by tightening screws on the aluminum housing holding the glass pieces until the interference fringes are minimized and the plates are parallel.

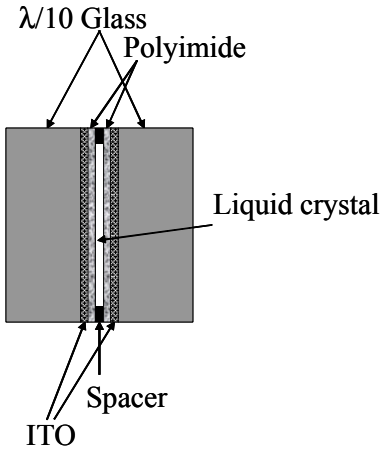

Figure A7.1. Glass cell used for LC reorientational response time experiments.

Once assembled the final gap thickness was measured using a Beckman DU640 UV-Vis spectrophotometer. A spectrum is taken over the range of 350 to 1100 nm showing a series of peaks associated with interference from light reflected in the inner cavity, Fig. A7.2. The gap thickness *(d)* can be calculated using

$$d = \frac{m\lambda_1\lambda_2}{2(\lambda_1 - \lambda_2)}, \quad \text{(A7.1)}$$

where m is the number of cycles between two peaks and λ_1 and λ_2 are the wavelengths of these two peaks. After the gap is measured, the liquid crystal solution is loaded into the cell by capillary action in a vacuum at a temperature of 40 ^{o}C.

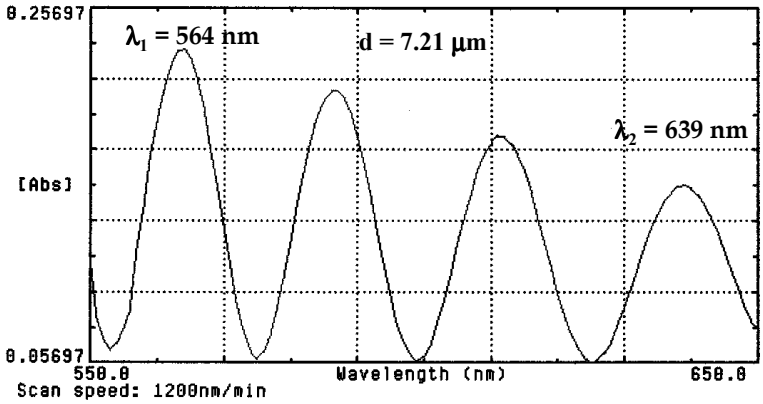

Figure A7.2. UV/Vis spectrophotometer output used to calculate the gap thickness.

The phase shift (δ) of the laser passing through the sample was measured in reflective mode to track the relaxation of the director, Fig. A7.3. A polarized laser beam was sent through the sample which is at 45 degrees to the polarization of the light. The beam was reflected off a mirror at a small-angle so that it returns through the LC sample at nearly the same spot. This reflected beam was reflected again with a second mirror sending it through an analyzer at 90 degrees to the initial polarizer and detected with a photodetector.

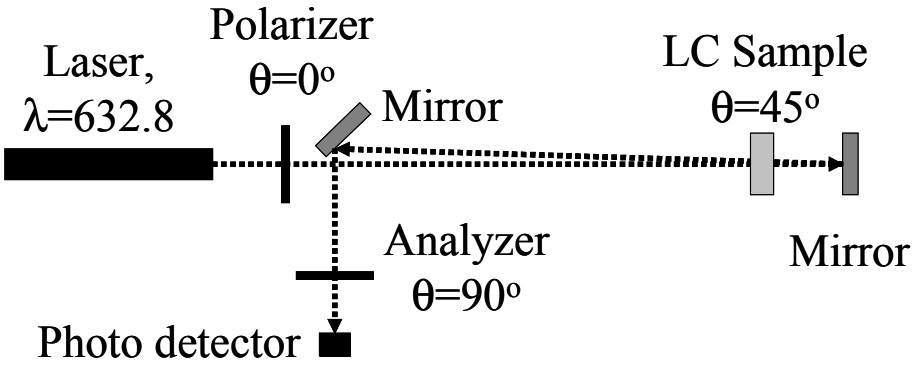

Figure A7.3. Apparatus used to measure the reorientational response times of liquid crystal solutions.

For the optical experiments, a Macintosh computer was equipped with a National Instruments data acquisition board and the Labview data acquisition software. Using a Stanford Research Systems Model DS340 function generator, a 1000 Hz AC voltage was amplified in external circuitry, Fig. A7.4, using a 0 to 10 volt DC control voltage from the computer. This allows a computer-controlled, 1000 Hz, 0 to 6 V_{rms} signal to be applied across the LC gap while measuring the optical transmittance.

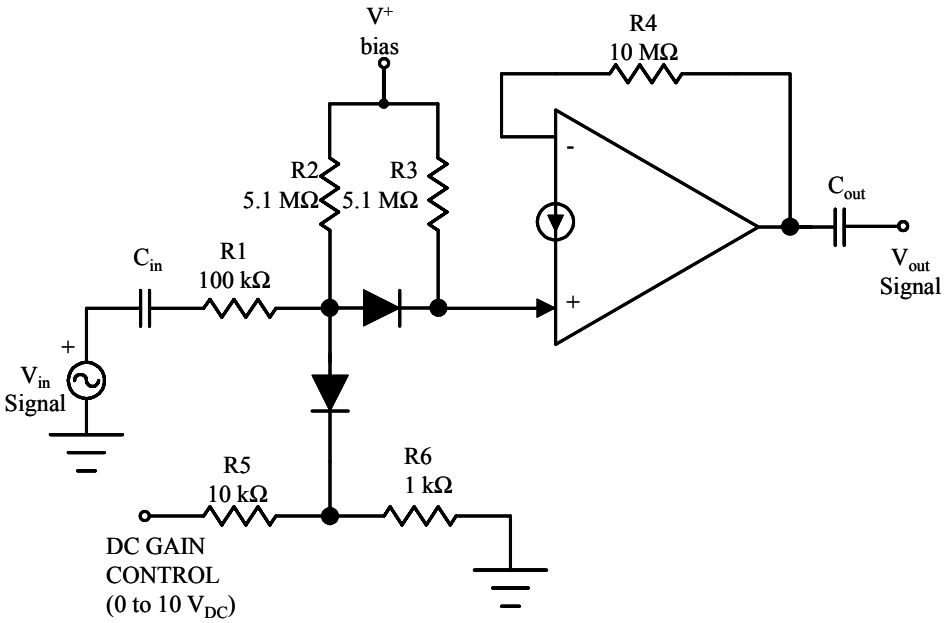

Figure A7.4. Schematic diagram of circuit used for computerized gain control. V_{in} is the signal from a function generator that will be amplified. DC gain is a 0 to 10 V_{DC} from the computer that controls the amount of amplification of the signal. V_{bias} is a small voltage necessary for the electronics to work. V_{out} is the amplified output signal.

As the voltage is decreased from 6 to 0 V, the transmitted beam intensity goes through a series of *m* peaks and valleys, Fig. A7.5. This can be used to calculate the phase shift (δ) for m=0,2,4…

$$\delta = m\pi + 2\sin^{-1}\sqrt{\frac{I_{\perp}}{I_{max}}}, \quad \text{(A7.2)}$$

or for m=1,3,5…

$$\delta = m\pi + 2\cos^{-1}\sqrt{\frac{I_{\perp}}{I_{max}}}. \quad \text{(A7.3)}$$

Using the phase shift measured without an applied voltage (δ_o) another measurement of the gap thickness can be made using the LC's birefringence (Δn), which was previously obtained using an Abbe refractometer

$$d = \frac{\delta_o \lambda}{2\Delta n}. \quad \text{(A7.4)}$$

The factor of "2" is present because the laser goes through the sample twice. Having two independent measurements of the gap thickness improves accuracy and enables one to detect and avoid changes in gap thickness due to thermal expansion differences.

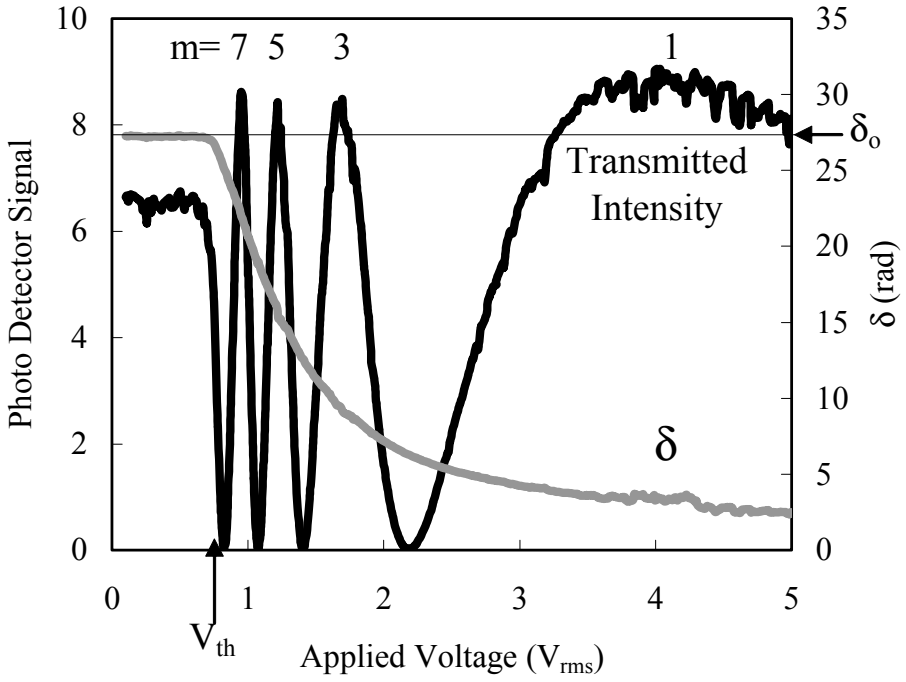

Figure A7.5. Representative output for measurement of birefringence and phase shift. 1% 420 kg/mol PBCB6 in 5CB. "*m*" is the number of peaks and valleys in the voltage vs. transmission curve. δ_o is the maximum in the phase shift for no applied voltage. V_{th} is the threshold voltage corresponding to the minimum voltage necessary to cause rotation of the director.

A7.1.2 Twist Viscosity Measurement

Once the voltage versus transmission curve is known, the reorientational response time can be calculated by applying a small voltage (~1 V) just above the threshold voltage (V_{th}) and instantly removing it allowing the director to relax in response to Frank elasticity [2, 3, 4], according to

$$\frac{\partial}{\partial y}\left[\left(K_{11}\cos^2\phi + K_{33}\sin^2\theta\right)\frac{\partial\phi}{\partial y}\right] + \left(K_{33}-K_{11}\right)\sin\phi\cos\phi\left(\frac{\partial\phi}{\partial y}\right)^2 = \gamma_1\frac{\partial\phi}{\partial t}, \quad \text{(A7.5)}$$

where ϕ is the angle of the director relative to the surface, K_{11} and K_{33} are the splay and bend elastic constants, γ_1 is the twist viscosity, and y is the distance above the bottom surface. The director profile, between plates separated by a distance d, can be modeled as a superposition of spatial modes with a time-dependent amplitude

$$\phi(y,t) = \sum_{m=0}^{\infty} C_m(t)\sin\left[\frac{(2m+1)\pi y}{d}\right]. \quad \text{(A7.6)}$$

By substituting this into Eq. A7.5 and making a small-angle approximation, the director profile as a function of time is

$$\phi(y,t) = \sum_{m=0}^{\infty} K_m e^{\left[\frac{-(2m+1)^2 K_{11}\pi^2 t}{\gamma_1 d^2}\right]}\sin\left[\frac{(2m+1)\pi y}{d}\right]. \quad \text{(A7.6)}$$

For long times, the only mode that is important corresponds to m=0, which produces a sinusoidal director profile [5] that will decay exponentially in time with a time constant equal to

$$\tau_o = \frac{\gamma_1 d^2}{K_{11}\pi^2}. \quad \text{(A7.6)}$$

When the measured phase shift is plotted as

$$\ln\left[\frac{\delta_o - \delta(0)}{\delta_o - \delta(t)}\right], \quad \text{(A7.7)}$$

versus time (t), a line corresponding to an exponential decay time constant (τ_o) can be found and used with Eq. A7.6 to measure γ_1/K_{11}. The dependence of τ_o on d^2 demonstrates the need to get an accurate measurement of the cell gap.

A7.2 Transient Rheology

The transient viscous response of a homeotropically (perpendicularly) aligned nematic was measured to determine the tumbling parameter, and to measure the Leslie-Ericksen viscous parameters α_1, α_2, and α_3 and the Miesowicz viscosity η_b. Samples were placed in a Rheometrics Fluids Spectrometer (RFS II) rheometer equipped with a shear cell made of a 50 mm diameter titanium cone and plate having a 0.0202 cone angle. To promote homeotropic alignment of the liquid crystals, the surfaces were washed with a 1% solution of L-α-lecithin type XI-E (Aldrich chemical company) in chloroform and placed in an oven at 140 ^{o}C for 30 minutes. The temperature of the shear cell was controlled using a Neslab RTE-130 refrigerated circulator to within ±0.2 ^{o}C. The LC was given between 30 min, for bulk 5CB, and one day, for a 10 wt % polymer solution, before the application of a shear stress so that a homeotropic monodomain could form [6].

In these experiments instrumental inertia caused a small time lag, ~0.04 s [7], between when the instrument started taking data and when the strain rate reached its set point. This time lag was constant for all strain rates and was compensated for by shifting the time of the data points accordingly.

For the tumbling case, the period of oscillation (γ_p) can be used to determine the tumbling parameter utilizing

$$\lambda = \pm\sqrt{1-\frac{4\pi^2}{\gamma_p^{\,2}}}\,. \quad \text{(A7.8)}$$

In this equation the sign of the tumbling parameter must be determined by looking at the character of the rheological response.

Since the twist viscosity ($\gamma_1=\alpha_3-\alpha_2$) can only have positive values and α_3 and α_2 must have opposite signs for an LC to tumble, $\alpha_3>0$ and $\alpha_2<0$. The definition of the tumbling parameter

$$\lambda = \frac{\alpha_2 + \alpha_3}{\alpha_2 - \alpha_3} = \frac{\alpha_2 + \alpha_3}{-\gamma_1} \qquad \text{(A7.9)}$$

indicates that for $\lambda>0$, $|\alpha_2| > |\alpha_3|$ and for $\lambda<0$, $|\alpha_2| < |\alpha_3|$. The rate of rotation of the director is related to its angle (θ) relative to the surface normal by

$$\gamma_1 \frac{\partial \theta}{\partial t} = \left(\alpha_3 \sin^2 \theta - \alpha_2 \cos^2 \theta\right) \frac{\partial \gamma}{\partial t}, \qquad \text{(A7.10)}$$

which demonstrates that if $|\alpha_2| > |\alpha_3|$ then $\lambda>0$ and the director will rotate faster when $\theta=0$ than when $\theta=\pm 90$ causing the transient response to show a single peak followed by successive pairs of peaks close together, Fig. 5.3b and A7.6a. If $|\alpha_2| < |\alpha_3|$, then $\lambda<0$ and the opposite is true causing the transient response to start with pairs of peaks, Fig. 5.3c and A7.6b.

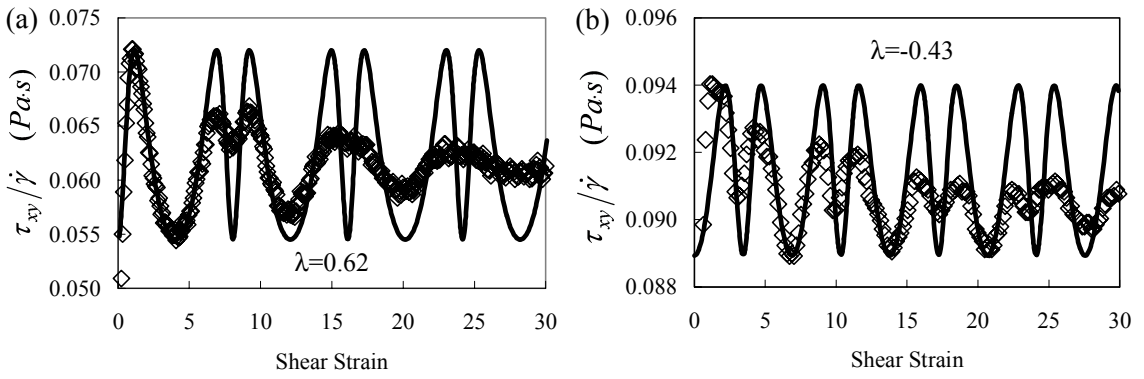

Figure A7.6. Representative rheological response, diamond symbols, of solutions showing theoretical fit, black line, to data. (a) 3% 78 kg/mol PBCB6 at 30 °C $\dot{\gamma}$=16 1/s. (b) 3% 420 kg/mol PBCB6 at 30 °C $\dot{\gamma}$=32 1/s. This figure is a copy of Fig. 6.3.

For the flow-aligning case, Figs. 6.3a,d and A7.7, values for the viscous parameters must be fit to the transient response in order to determine the tumbling parameter. Since θ is related to λ and the applied shear strain by

$$\tan(\theta) = \pm\left(\frac{1+\lambda}{\lambda-1}\right)^{1/2} \tanh\left(\frac{\gamma}{2}\sqrt{\lambda^2-1}\right), \quad \text{(A7.11)}$$

the rate at which the steady-state angle is reached is determined entirely by λ. Therefore, a fit of the 2-D transient stress response to the theoretical response

$$\tau_{xy} = \dot{\gamma}\left\{\left[\alpha_1 + \frac{(\alpha_2+\alpha_3)^2}{\alpha_3-\alpha_2}\right]\sin^2\theta\cos^2\theta + \eta_b - \frac{\alpha_3^2}{\alpha_3-\alpha_2}\right\}, \quad \text{(A7.12)}$$

does not need to have all the correct values of the viscous parameters to extract a value for λ.

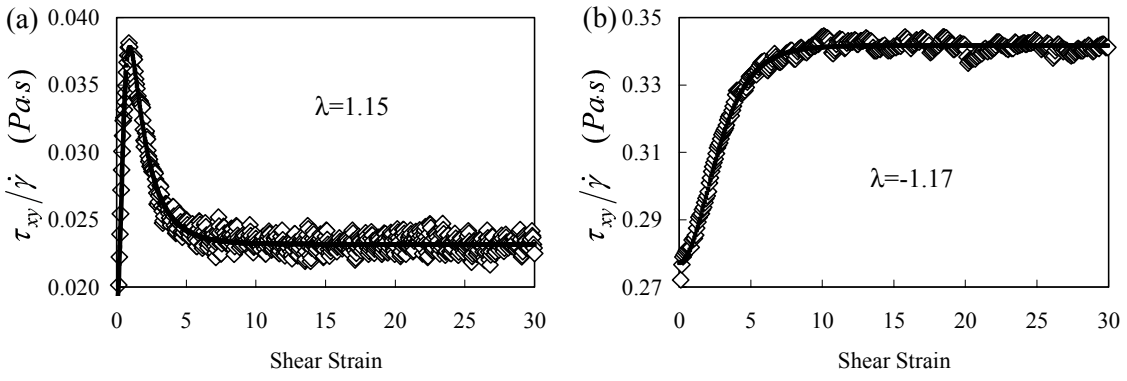

Figure A7.7. Representative rheological response flow-aligning solutions showing theoretical fit to data, Eqs. A7.11 and A7.12. (a) Bulk 5CB at 30 ^{o}C (b) 10% 420 kg/mol PBCB6 at 33 ^{o}C $\dot{\gamma}$=16 1/s.

Inspection of Eqs. A7.9, A7.11 and A7.12 indicates that the transient response is determined by the four parameters α_1, α_2, α_3, and η_b, but a fit of the transient response can only be used to solve for three variables. The extra variable is supplied by the reorientational response time experiments where the ratio γ_1/K_{11} was obtained. Dynamic light scattering experiments [8] have shown that polymers can have elastic constants of the same magnitude as small molecule liquid crystals, and that addition of polymer changes γ_1 much more than K_{11} [9 10]. Furthermore, refractive index measurements, section 2.2.4, have shown that addition of up to 10 wt % PBCB6 to 5CB caused negligible change to Δn. Since changes in the birefringence and in the order parameter are highly correlated, one can assume that K_{11} remains constant and that changes in the ratio γ_1/K_{11} are primarily due to changes in γ_1. By multiplying the ratio γ_1/K_{11} by values of K_{11} for bulk 5CB obtained by Skarp et al. [11], a measurement of the twist viscosity ($\gamma_1=\alpha_3-\alpha_2$) can be made for our solutions. This allows all the viscous parameters α_1, α_2, α_3, and η_b to be determined by a fit of the transient response to Eq. A7.12.

After the period of the oscillations and γ_1 are used to determine α_2 and α_3, it can be seen from Eq. A7.12 that for a tumbling nematic α_1 is determined from the peak to peak amplitude of the oscillations in the viscous response, and η_b is determined by the value of the minimum in the oscillations. Since the period of the oscillations and the values of the minima in the viscous response are less dependent on the alignment quality than the peak to peak amplitude, less uncertainty is expected in α_2, α_3, and η_b than in α_1. In our experiments, this results in an uncertainty in α_1 roughly equal to its magnitude. Similar arguments hold for α_1 in flow-aligning solutions.

Bibliography

[1]I. C. Khoo and S. T. Wu, *Optics and Nonlinear Optics of Liquid Crystals*, World Scientific, New Jersey, (1993).
[2] F. M. Leslie, *Arch. Ration. Mechan. Anal*., **28**, 265 (1968).
[3] J. L. Ericksen, *Trans. Soc. Rheol*., **5**, 23 (1961).
[4] F. Brochard, P. Pieranski, and E. Guyon, *J. Phys. (Paris),* **34**, 35 (1973).
[5] D. M. Boudreau, H. H. Winter, C. P. Lillya, and R. S. Stein, *Rheol. Acta*, **38**, 503, (1999).
[6] D. F. Gu, A. M. Jamieson, and S. Q. Wang, *J. Rheol*. **37,** 985 (1993).
[7] D. F. Gu and A. M. Jamieson, *J. Rheol*. 38, 555 (1994).
[8] J. Schmidtke, W. Stille, and G. Strobl, *Macromolecules* **33**, 2922 (2000).
[9] P. Y. Liu, N. Yao, and A. M. Jamieson, *Macromolecules* 32, 6587 (1999).
[10] H. Mattoussi, Veyssie, C. Casagrande, and M. A. Guedeau, *Mol. Cryst Liq. Cryst*., **144**, 211 (1987).
[11] K. Skarp, S. T. Lagerwall and B. Stebler, *Mol. Cryst. Liq. Cryst*., **60**, 215 (1980).